Design and Validation of Active Trailer Steering Systems for Articulated Heavy Vehicles Using Driver-Hardware-in-the-Loop Real-Time Simulation

By

Qiushi Wang

Thesis Presented to the University of Ontario Institute of Technology

in Fulfillment of

Thesis Requirement for Degree of Master of Applied Science

in the Faculty of Engineering and Applied Science

Mechanical Engineering Program

Oshawa, Ontario, Canada, 2015

Dedicated to

my mother Guie Liu, my father Hui Wang, and

my sister Qiujin Wang

Thanks for their great support, understanding, and love.

Abstract

To improve the low-speed maneuverability and high-speed lateral stability of Double Trailer Articulated Heavy Vehicles (DTAHVs), an Active Trailer Steering (ATS) system has been designed. To date, investigations on ATS systems are mainly focused on numerical simulations. To advance this research towards real-world applications, a Driver-Hardware-In-the-Loop (DHIL) real-time simulation platform is developed for the design and validation of ATS system for DTAHVs. The real-time simulation results derived under the emulated low-speed path-following test maneuvers demonstrate the effectiveness of the DHIL platform and the distinguished features of the ATS system. This thesis examines the applicability of two single lane-change test maneuvers specified in ISO-14791 for acquiring rearward amplification, which is an important indicator for the high-speed lateral stability. Simulation results indicate that the closed-loop test is more applicable for DTAHVs with ATS systems. This thesis also proposes a new ATS controller using the model reference adaptive control technique. Numerical simulations illustrate that the proposed MRAC controller can achieve robust performance under the variations of vehicle forward speed and trailer payload.

Acknowledgements

I would like to take this opportunity to express my sincere appreciation to my supervisor Dr. Yuping He for his support, guidance and encouragement during the past two years. Thank him to give me this valuable opportunity to work on the vehicle simulator located in the multidisciplinary vehicle systems design laboratory. I am grateful to him for his inspiration and motivation on the completion of my thesis. Without him, it would be impossible for me to finish this thesis.

Meanwhile, I would like to thank Stephen Singh and Kai Boettcher for their amazing hands-on experience on the development of driver-hardware-in-the-loop real-time simulation platform. I am also immensely grateful to Shenjin Zhu and Eungkil Lee for their help and collaboration on my research. Last but not least, I appreciate the lovely cat, Leo, for accompanying me through the hard time.

Table of Contents

List of Figures

List of Tables

Nomenclature

a_{11}	Longitudinal distance between tractor front axle and tractor total mass center of gravity
ASS	Active safety system
ATS	Active trailer steering
AHV	Articulated heavy vehicle
b_{12}	Longitudinal distance between tractor rear axle and tractor total mass center of gravity
b_{23}	Longitudinal distance between trailer total mass center of gravity and trailer middle axle
CAN	Controller area network
C_{f11}	Cornering stiffness of tractor front tire
C_{r12}	Cornering stiffness of tractor rear tire
C_{r23}	Cornering stiffness of semitrailer tire
CG	Center of gravity
DAQ	Data acquisition
DHIL	Driver-hardware-in-the-loop
DOF	Degree of freedom
DSIL	Driver-software-in-the-loop
DTAHV	Double-trailer articulated heavy vehicle
ESC	Electronic stability control

FTP	File transfer protocol
F_{y1}	Tractor's lateral tire force
F_{y2}	1st semitrailer's lateral tire force
F_{y3}	2nd semitrailer's lateral tire force
GDP	Gross domestic production
h_{cr1}	Height of the coupling point on the tractor, measured upwards from roll center of tractor sprung mass
h_{cr2}	Height of the coupling point on 1st semitrailer, measured upwards from roll center of semitrailer sprung mass
h_{cr3}	Height of the coupling point on 2nd semitrailer, measured upwards from roll center of semitrailer sprung mass
h_{r1}	Height of roll center of tractor sprung mass, measured upwards from ground
h_{r2}	Height of roll center of 1st semitrailer sprung mass, measured upwards from ground
h_{r3}	Height of roll center of 2nd semitrailer sprung mass, measured upwards from ground
h_{s1}	Height of CG of tractor sprung mass, measured upwards from ground
h_{s2}	Height of CG of 1st semitrailer sprung mass, measured upwards from ground
h_{s3}	Height of CG of 2nd semitrailer sprung mass, measured upwards from ground
HSTO	High-speed transient off-tracking

HSTO_0	High-speed transient off-tracking of the center of the rear axle of the first semitrailer or the second semitrailer with respect to the center of the front axle of the tractor in the case of the double trailer articulated heavy vehicle without active trailer steering
HSTO_1	High-speed transient off-tracking of the center of the rear axle of the first semitrailer or the second semitrailer with respect to the center of the front axle of the tractor in the case of the double trailer articulated heavy vehicle with active trailer steering
ISO	International organization for Standardization
I_{xx1}	Roll moment of inertia of tractor sprung mass, measured form CG of sprung
I_{xx2}	Roll moment of inertia of 1st semitrailer sprung mass, measured from CG of sprung mass
I_{xx3}	Roll moment of inertia of 2nd semitrailer sprung mass, measured from CG of sprung mass
I_{xz1}	Roll/yaw product of inertia of tractor sprung mass, measured from the CG of sprung mass
I_{xz2}	Roll/yaw product of inertia of 1st semitrailer sprung mass, measured from the CG of sprung mass
I_{xz3}	Roll/yaw product of inertia of 2nd semitrailer sprung mass, measured from the CG of sprung mass
I_{zz1}	Yaw moment of inertia of whole mass of the tractor
I_{zz2}	Yaw moment of inertia of whole mass of the 1st semitrailer
I_{zz3}	Yaw moment of inertia of whole mass of the 2nd semitrailer

K_{f1}	Roll stiffness of front suspension of the tractor, adjusted with the tire vertical stiffness
K_{r1}	Roll stiffness of rear suspension of the tractor, adjusted with the tire vertical stiffness
K_{r2}	Roll stiffness of rear suspension of the 1st semitrailer, adjusted with the tire vertical stiffness
K_{r3}	Roll stiffness of rear suspension of the 2nd semitrailer, adjusted with the tire vertical stiffness
K_{tf1}	Tire roll stiffness of front axle of tractor
K_{tr1}	Tire roll stiffness of rear axle set of tractor
K_{tr2}	Tire roll stiffness of rear axle set of 1st semitrailer
K_{tr3}	Tire roll stiffness of rear axle set of 2nd semitrailer
K_{12}	Roll stiffness of coupling point of tractor and 1st semitrailer
K_{23}	Roll stiffness of coupling point of tractor and 2nd semitrailer
l_{c1}	Longitudinal distance between the whole mass CG of the tractor and the coupling point
l_{c21}	Longitudinal distance between the whole mass CG of the 1st semitrailer and the 1st coupling joint
l_{c22}	Longitudinal distance between the whole mass CG of the 1st semitrailer and the 2nd coupling joint
l_{c3}	Longitudinal distance between the whole mass CG of the 2nd semitrailer and the 2nd coupling joint

LCV	Long combination vehicle
L_{f1}	Roll damping of front suspension of tractor
L_{r1}	Roll damping of rear suspension of tractor
LQR	Linear quadratic regulator
L_{r2}	Roll damping of rear suspension of 1st semitrailer
L_{r3}	Roll damping of rear suspension of 2nd semitrailer
m_1	Tractor's total mass
m_2	1st semitrailer's total mass
m_3	2nd semitrailer's total mass
m_{s1}	Tractor's sprung mass
m_{s2}	1st semitrailer's sprung mass
m_{s3}	2nd semitrailer's sprung mass
MRAC	Model reference adaptive control
MTAHV	Multi-trailer articulated heavy vehicle
MTO	Ontario Ministry of Transportation
MVSD	Multi-disciplinary vehicle systems design
N_{β_1}	Partial derivative of tractor's net tire yaw moment with respect to its side-slip angle
N_{β_2}	Partial derivative of 1st semitrailer's net tire yaw moment with respect to its side-slip angle
N_{β_3}	Partial derivative of 2nd semitrailer's net tire yaw moment with respect to its side-slip angle

$N_{\dot{\psi}_1}$	Partial derivative of tractor's net tire yaw moment with respect to its yaw rate
$N_{\dot{\psi}_2}$	Partial derivative of 1st semitrailer's net tire yaw moment with respect to its yaw rate
$N_{\dot{\psi}_3}$	Partial derivative of 2nd semitrailer's net tire yaw moment with respect to its yaw rate
$N_{\delta_{1f}}$	Partial derivative of tractor's net tire yaw moment with respect to its front wheel steering angle
ODE	Ordinary differential equation
PCI	Peripheral component interconnect
PFOT	Path-following off-tracking
PID	Proportional integral derivative
RA	Rearward amplification
RA_Acc_0	The rearward amplification of the lateral acceleration between the first or second semitrailer and the tractor without active trailer steering
RA_Acc_1	The rearward amplification of the lateral acceleration between the first or second semitrailer and the tractor with active trailer steering
RA_Yaw_0	The rearward amplification of the yaw rate between the first or second semitrailer and the tractor without active trailer steering
RA_Yaw_1	The rearward amplification of the yaw rate between the first or second semitrailer and the tractor with active trailer steering
SAE	Society of Automotive Engineers

SLC	Single lane change
STAHV	Single-trailer articulated heavy vehicle
UOIT	University of Ontario Institute of Technology
U_1	Tractor's forward speed
U_2	1st semitrailer's forward speed
U_3	2nd semitrailer's forward speed
VS	VehicleSim
VSE	Vehicle Systems Engineering
Y_{β_1}	Partial derivative of tractor's net tire lateral force with respect to its side-slip angle
Y_{β_2}	Partial derivative of 1st semitrailer's net tire lateral force with respect to its side-slip angle
Y_{β_3}	Partial derivative of 2nd semitrailer's net tire lateral force with respect to its side-slip angle
$Y_{\dot{\psi}_1}$	Partial derivative of tractor's net tire lateral force with respect to its yaw rate
$Y_{\dot{\psi}_2}$	Partial derivative of 1st semitrailer's net tire lateral force with respect to its yaw rate
$Y_{\dot{\psi}_3}$	Partial derivative of 2nd semitrailer's net tire lateral force with respect to its yaw rate
$Y_{\delta_{1f}}$	Partial derivative of tractor's net tire lateral force with respect to its front wheel steering angle
α_1	Side-slip angle of tires on the 1st axle

α_2	Side-slip angle of tires on the 2nd axle
α_3	Side-slip angle of tires on the 3rd axle (group)
β_1	Tractor's side-slip angle
β_2	1st semitrailer's side-slip angle
β_3	2nd semitrailer's side-slip angle
ψ_1	Tractor's yaw angle
$\dot{\psi_1}$	Tractor's yaw rate
ψ_2	1st semitrailer's yaw angle
$\dot{\psi_2}$	1st semitrailer's yaw rate
$\dot{\psi_3}$	2nd semitrailer's yaw rate
ϕ_1	Roll angle of tractor's sprung mass
ϕ_2	Roll angle of 1st semitrailer's sprung mass
ϕ_3	Roll angle of 2nd semitrailer's sprung mass
δ_{1f}	Tractor front wheel steering angle
δ_3	Semitrailer rear wheel steering angle
ϕ_{t1}	Roll angle of tractor's un-sprung mass
ϕ_{t2}	Roll angle of 1st semitrailer's un-sprung mass
ϕ_{t3}	Roll angle of 2nd semitrailer's un-sprung mass

1 Introduction

1.1 Articulated Heavy Vehicles

The main vehicles researched in this thesis are Double Trailer Articulated Heavy Vehicles (DTAHVs), which are the most commonly used across Canada for goods transportation. The DTAHV examined in this thesis consist of a tractor and two semitrailers. The tractor has one front steerable axle and two rear solid axles, and each of the two semitrailers each has three solid axles. The adjacent units of the DTAHV are connected by a fifth wheel. Note that in this thesis, a Single Trailer Articulated Heavy Vehicle (STAHV) is also explored. Figs. 1-1 and 1-2 show the configuration of the DTAHV and the STAHV researched in this thesis, respectively.

Figure 1-1. The configuration of the DTAHV.

Figure 1-2. The configuration of the STAHV.

Articulated Heavy Vehicles (AHVs) exhibit three typical unstable motion modes, i.e., jack-knifing, trailer sway, and rollover. Jack-knifing is caused by a large relative angle between the leading unit and its trailing unit. In the case of trailer sway, the trailing unit moves side to side behind the leading unit. It could be elicited by external or internal factors. Regarding the external factors, side wind gust or aggressive steering from the driver are the main causes of disturbances; for the internal factors, the vehicle structure design parameters are the main reasons [1]. When an AHV rollovers, the vehicle unit tips over to the other side, which can also be triggered by external and internal factors, e.g. collision with adjacent vehicles, aggressive steering input or high turning speed.

1.2 Motivations and Objectives

Compared with STAHVs, the application of DTAHVs in Alberta, Canada, can save 29% in shipping costs, reduce mileage by 44% and decrease road wear by 40% [2]. Despite these

benefits, DTAHVs exhibit poor low-speed maneuverability and low high-speed lateral stability because of their complex structure, large size, heavy payloads and high center of gravity. In addition to this, most North American highway ramps and interchanges were designed between the 1950s and 1970s without adequately considering the unique geometric features of DTAHVs. This may partially contribute to the high accident rates of DTAHVs [3]. Moreover, Canada's long and severe winter weather patterns further degrade the directional performance of DTAHVs. Therefore, it is imperative to design and develop embedded control systems to improve the low-speed maneuverability and high-speed stability of DTAHVs.

Computer modelling and simulations provide an effective method to design Active Safety Systems (ASSs) for DTAHVs to achieve desired dynamic responses [4, 5]. For the purpose of improving the directional performance of DTAHVs, control algorithms for Active Trailer Steering (ATS) systems based on linear vehicle models are investigated [6, 7]. To test the functionality of the designed ATS systems, numerical simulations on desktop computers have been widely accepted. Nevertheless, it is undeniable that to validate and improve the overall performance of these control systems, field and road tests of real physical prototypes are indispensable [8]. However, at initial design stages these tests can be time-consuming, dangerous and costly to accomplish. Also, the overall directional performance of a vehicle is not only dependent on an ASS designed, but also on the interaction between the driver and the vehicle system. Therefore, Driver-Hardware-In-the-Loop (DHIL) real-time simulations have been proposed to evaluate the performance of newly developed control systems prior to in-vehicle road tests [9]. This motivates the Multidisciplinary Vehicle System Design (MVSD) laboratory at the University of Ontario

Institute of Technology (UOIT) to design and build the DHIL real-time simulation platform based on the existing vehicle driving simulator.

Numerical simulations indicate that under an open-loop Single Lane Change (SLC) maneuver with a given single sine-wave steering angle input, the trajectory of the leading unit of an AHV without ATS is different from that of vehicles with ATS [10]. On the other hand, the closed-loop SLC maneuver specified by ISO-14791 was successfully applied to the design optimization of an AHV with an ATS system [11]. The above observation of the difference between the open-loop and closed-loop maneuvers raises a question: between the two SLC test maneuvers, which one is applicable for determining the Rearward Amplification (RA) measures of DTAHVs with and without ATS? This motivates our research on the applicability of the SLC test maneuvers for acquiring RA measurements of DTAHVs with and without ATS system.

To date, the Linear Quadratic Regulator (LQR) technique has mainly been applied to design controllers for ATS systems of AHVs. However, these LQR controllers were designed under the assumption that the vehicle model parameters and operating conditions were given and they remained as constants. In reality, the vehicle system parameters, operating conditions, as well as external disturbances caused by wind and other factors may vary. To address and tackle the problem of vehicle system parametric variation, this thesis proposes a Model Reference Adaptive Control (MRAC) strategy for ATS system controller design for STAHVs. The objective of proposing the MRAC strategy in this research is to examine whether a semitrailer's lateral acceleration controlled by the ATS system to be designed can track that of the reference model. To examine the performance of the MRAC technique for the ATS system, numerical simulation is conducted under an emulated SLC maneuver.

All in all, the objectives of this thesis can be summarized as:

1) Design and develop DHIL real-time simulation platform based on the existing vehicle simulator;
2) Test the functionality of the resulting DHIL real-time simulation platform and validate the functionality of the ATS system reported in Ref. [4];
3) Evaluate the applicability of the SLC test maneuvers recommended by ISO-14791 on acquiring the RA measurements of DTAHVs with ATS system;
4) Apply MRAC technique to the ATS system design of STAHVs.

1.3 Methodology

The methodology for this thesis can be outlined as follows:

First, built upon the existing driving simulator, a DHIL real-time simulation platform is developed in the MVSD laboratory at UOIT. To achieve this goal, two self-steering axles by Ingersoll Axles, an Ontario-based company, are modified, and then microcontrollers designed at the MVSD laboratory are loaded to control the steering of the two axles. The degrees of angles and the directions that the axles will turn is calculated by the ATS controller, which is written into LabVIEW Real-Time (hereafter called LabVIEW-RT) computer. Therefore, using serial communication between the LabVIEW-RT computer and the two active steering axles the DHIL real-time simulation platform could be established.

Second, this thesis examines the applicability of the two SLC test maneuvers recommended by ISO-14791 for acquiring RA measurements of DTAHVs with ATS systems using DHIL real-time simulations. Comparing the RA measurements of DTAHVs without an ATS system with those of DTAHVs with an ATS system under the open-loop and closed-loop

tests, we can determine which test methods specified in ISO-14791 are applicable for acquiring RA measurements of DTAHVs with the ATS system.

Third, the MRAC controller is designed using linear yaw-plane model developed in the MVSD laboratory. The objective is to enable the semitrailer's lateral acceleration of the nonlinear STAHV model developed under TruckSim to track that of the reference model. The reference model is derived from the linear yaw-plane STAHV model. To track the lateral acceleration of the reference model, a proper controller structure and adaptive law for MRAC shall be chosen and deduced.

1.4 Thesis Contributions

The thesis contributions can be summarized as follows:

First, development of the DHIL real-time simulation platform based on our existing driving simulator in the MVSD laboratory, and application of wireless communication between the LabVIEW-RT computer and microcontrollers for ATS axles which represents the wireless communication between the tractors and trailers in the real world. With this DHIL real-time simulation platform, the AHV model and its ATS design could be more realistically tested. It bridges the lab research work and the industry's road test. At the same time, we are stepping towards real world application. This is pioneer work in ASSs for commercial vehicles to equip ATS systems on AHVs based on real-time dynamic simulations.

Second, examining the applicability of the two SLC test maneuvers recommended by ISO-14791 for determining the RA measures of DTAHVs with and without ATS. With the emerging ATS system for AHVs, whether the two SLC test maneuvers specified by ISO-14791 can both properly acquire the RA measurements is of interest to researchers and

industries. According to our simulation results and analysis, we actually found that the closed-loop SLC test is more applicable compared with the open-loop test for acquiring RA when the DTAHV is equipped with an ATS system.

Third, applying the MRAC technique to improve the robustness of the ATS system to address vehicles' parametric variation and varied operating conditions in the real world. The LQR technique has been long used to design controllers for ASS. It is convenient to get the controller designed under MATLAB/SIMULINK simulation environment using the LQR technique and then enhance the AHVs dynamic performance. However, the deficiencies of LQR controllers impede their real world applications. With this background, a robust control technique called the MARC technique is proposed to design the ATS controller for AHVs.

1.5 Thesis Organization

This thesis is composed of six chapters. In the first chapter, the configuration of vehicles are presented and their corresponding problems are introduced; motivation for the research is discussed and thesis contribution is briefly introduced. The second chapter reviews recent year's work on the ATS system for AHVs by introducing vehicle modelling, ATS system design, test procedures for evaluating the directional performance of AHVs, and the necessities for developing a DHIL real-time simulation platform. The third chapter describes the DHIL real-time simulation platform, the linear and nonlinear models for DTAHVs, and the ATS controller design in details. The fourth chapter provides the simulation results and data analysis under low-speed and high-speed testing scenarios. The emphasis is placed on the high-speed case by analyzing whether both of the two SLC test

maneuvers recommended by ISO-14791 are suitable for determining RA measures of DTAHV with ATS. To date, the controllers designed for ATS systems are based on the LQR technique. However, the LQR-based controllers may be problematic in real world applications considering vehicles' varied operating conditions, loading conditions, etc. Therefore, the fifth chapter will investigate the MRAC technique for controller design of the ATS system of STAHV. Chapter 6 summarizes the insightful findings derived from this research and provides valuable suggestions for future work.

2 Literature Review

2.1 Introduction

This chapter presents a comprehensive literature review on ATS technology for AHVs. MTAHVs, especially DTAHVs, are increasingly used on highways in North America for freight and goods transportation. In the past seven years, the MVSD laboratory at UOIT has been working on innovative ATS technologies including vehicle system modelling, controller design, numerical simulations, vehicle system design optimization, and validation using DHIL real-time simulations. When designing ATS systems for DTAHVs, attention should be paid to the vehicles' low-speed maneuverability and high-speed stability. To test and quantify the directional performance of DTAHVs, various path-following testing maneuvers and high-speed stability testing procedures have been recommended by relevant standards or regulations.

2.2 Background

Regarding Canada's economy, the trucking industry plays a significant role. In 2011, Canada's Gross Domestic Production (GDP) obtained from truck transportation alone was $ 16.96 billion, while the revenue from air, rail, transit, and ground passenger transportation in total was $ 19.01 billion [12]. Truck transportation is mainly dependent on AHVs which follow a rule that transport goods and freights should be cost-effectively as much as possible [13]. In commercial trucking, cost-effectiveness is often realized by using the-bigger-the-better method. In modern trucking operations, the fare spent on driver and fuel

are costly. To achieve the cost-effectiveness goal, industries are inclined to use bigger and longer AHVs which can transport much more goods at a time. In this case, less drivers could be deployed and less fuel could be consumed. Actually, DTAHVs have been running in Quebec and more than 20 American states for decades. To promote the free traffic movement of goods transportation between Ontario and Quebec, the Ontario Ministry of Transportation (MTO) launched the Long Combination Vehicle (LCV) program in 2011 to permit LCVs to travel on designated highways in Ontario [14]. Recently, New Brunswick and Nova Scotia governments also launched similar programs [15, 16].

Despite of all the benefits of DTAHVs, this vehicle combination exhibits unstable motion modes at high speeds, e.g. jack-knifing, trailer sway, and rollover. Each year in North America, over 450,000 commercial trucks are involved in crashes resulting in 140,000 injuries and approximately 5,000 fatalities [17]. The poor low-speed maneuverability of DTAHVs is also problematic. Furthermore, the un-steerable trailer axles make the tires tend to scrub against road surfaces during curve negotiations, which damages both tires and road infrastructure. The ramps and interchanges designed in North America in the 1950s and 1960s were designed without adequately considering the operation of LCVs, making this situation even worse [18].

To tackle these problems and run DTAHVs more safely on highways, the poor low-speed maneuverability and poor high-speed stability of DTAHVs have to be ameliorated. The existing advanced trailer steering technologies include the trailer steerable axles produced by Ingersoll Axles [19], Trackaxle Pty Ltd [20], and Vehicle Systems Engineering (VSE) [21]. The steerable axles produced by Ingersoll Axles and Trackaxle are mechanical self-steering axles. These axles can only operate at low speed and have to be locked at high

speeds. The steerable axles produced by VSE are computer-controlled, which is executed by manipulating the kinematic relationship between the articulation angle of the fifth wheel and the trailer steering angle. Also, this system can only operate under a speed of 55km/h. Therefore, the existing trailer steerable axles cannot guarantee high-speed stability. To ensure highway traffic safety, the Ontario LCV program indicates that the ASSs, such as Electronic Stability Control (ESC) system, are required for LCVs. To tackle the defects of existing trailer steerable axles, MVSD laboratory at UOIT has been working on alternative solutions by using dynamic ATS system.

2.3 AHV Configurations and Modelling

2.3.1 AHV Configurations

Generally, an AHV is an assembly of two or more rigid vehicle units. Between adjacent units, there is one mechanical mechanism called hitch for the connection of both units. Fig. 2-1 shows the common leading units of AHVs, namely a truck and a tractor. Leading unit means the first unit of the whole vehicle combination. If the first unit bears cargo by itself, it is generally called a truck. It is commonly named as tractor if it is only for trailing the trailers. Fig. 2-2 shows commonly used semitrailers of B-train in which (a) shows the one which can connect both front and rear units and (b) shows the one for the very last unit. Fig. 2-3 shows the common hitches for connecting adjacent units. Fig. 2-3(a) and Fig. 2-3(b) shows the pintal hitch and fifth wheel which are mainly used for AHVs. Their functionality differs by which pintal hitch provides three DOF, i.e. yaw, roll, pitch, while fifth wheel allows yaw and pitch motions. Pintal hitch cannot bear large vertical loads so it is normally used for towing full trailers, and fifth wheel is a connector for semitrailers therefore it needs

to bear huge vertical load at the rear of towing unit. Fig. 2-3(c) illustrates a ball hitch. Semitrailer has the only rear running axles as shown in Fig. 2-2. Full trailer has both front and rear running axles but it can also be constituted by a semitrailer and a converter dolly as shown in Fig. 2-4. MTAHVs can be classified into A-train and B-train. A-train consists of a tractor-semitrailer towing one or more full trailers, and B-train is composed of tractor towing at least two semitrailers [13]. Fig. 2-5 shows the structure of a B-train double and an A-train double using a converter dolly.

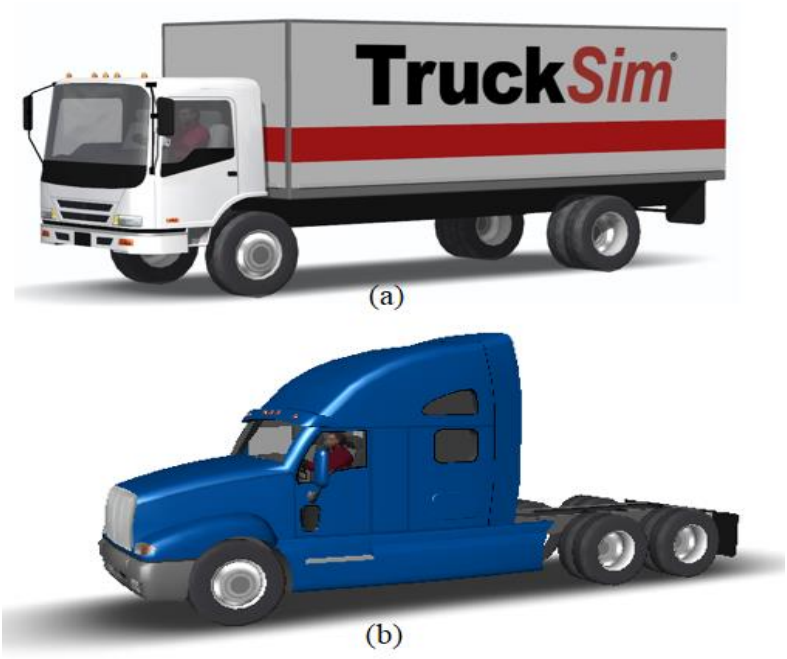

Figure 2-1. Common vehicle leading unit structures, (a): truck; (b): tractor.

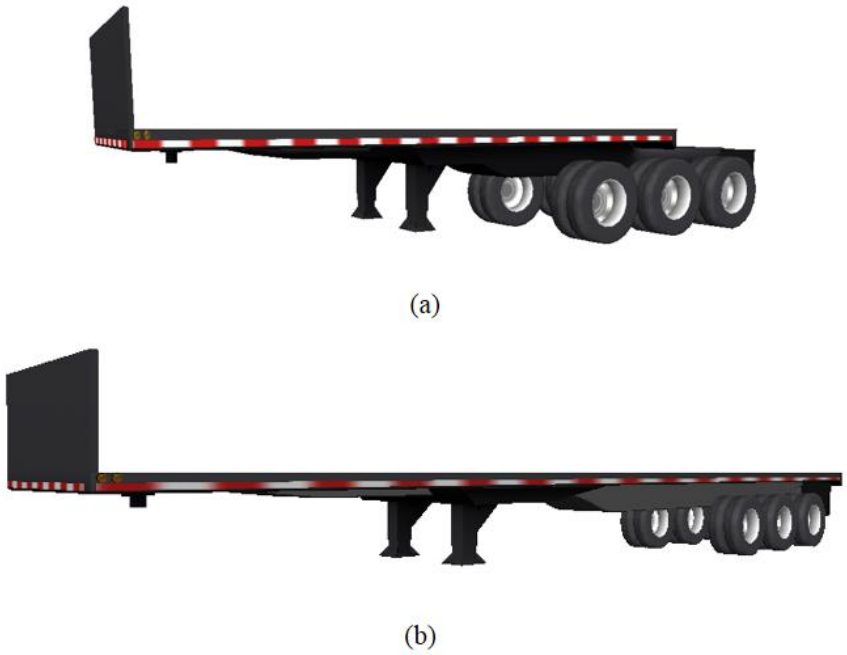

Figure 2-2. Semitrailer types for B-train, (a): semitrailer for connecting front and rear units; (b): last semitrailer.

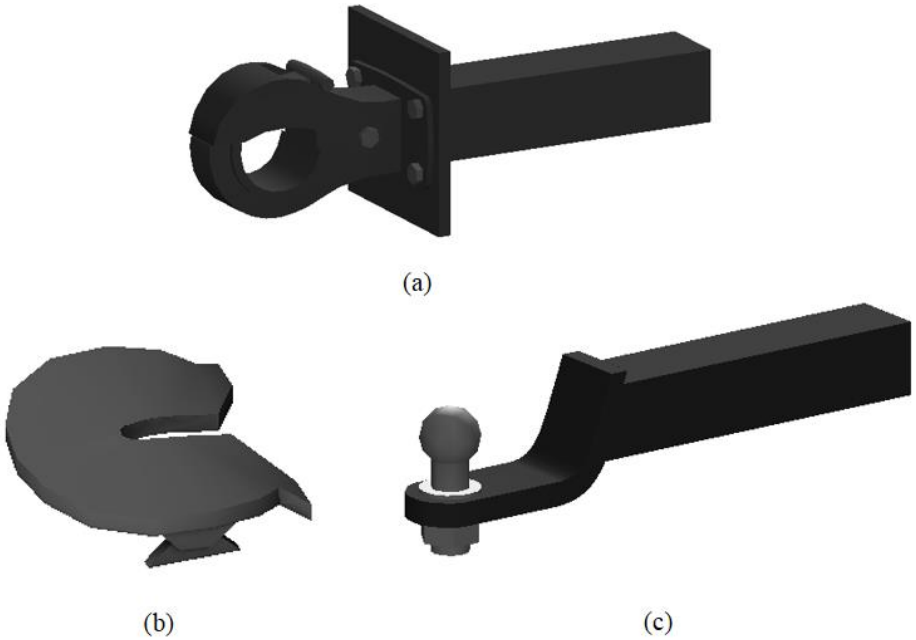

Figure 2-3. Common hitches for connecting two adjacent units, (a): pintal hitch; (b): fifth wheel; (c): ball hitch.

Converter Dolly

Figure 2-4. Converter Dolly which can be used to transform B-train into A-train type.

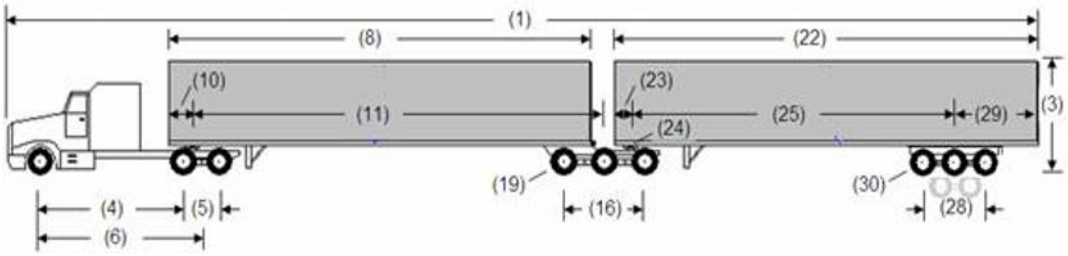

(a)

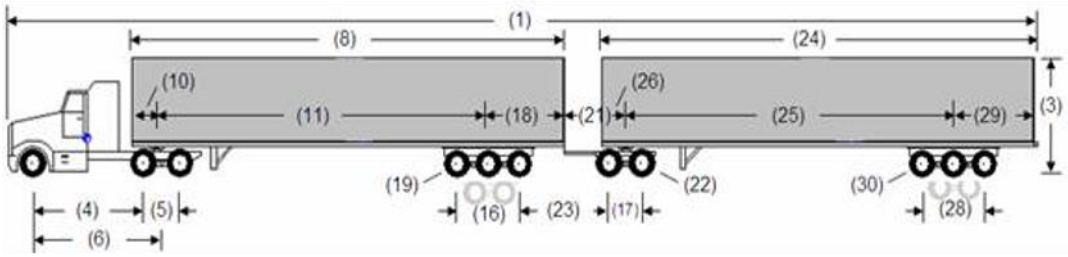

(b)

Figure 2-5. (a): the structure of B-train double; (b): the structure of A-train double [14].

2.3.2 AHV Modelling

As mentioned in the first chapter, the vehicle combination researched in this thesis includes two types of AHVs. One type is DTAHV and the other one is STAHV.

Ref. [22] provides valuable guidance on the selection of dynamic vehicle models for control algorithm development, design optimization and linear stability analysis for DTAHVs with ASSs. Vehicle modelling is of particular importance for computer simulations and controller design for DTAHVs. Whether a linear model or a non-linear model is selected to design a controller for DTAHVs, a few recommendations reported in the literature can be considered. In reality, DTAHV is highly nonlinear; the more complex and highly nonlinear the mathematical model is, the closer the dynamics of the model to the real system becomes. Using commercial multi-body software packages, e.g. SIMPACK, TruckSim, ADAMS, DADS, etc., we can generate highly nonlinear vehicle models with large numbers of DOF [23]. By means of a multi-body formulation, the equations of motion for a complex vehicle system with rigid and flexible bodies connected by kinematic and dynamic components may be generated automatically. These models are comprehensive, reliable and able to predict the vehicle dynamics with a high fidelity [24, 25]. However, these multi-body vehicle models can be large (e.g. they can have up to 100 DOF) and complex. The size and the complexity of a vehicle model are factors that tend to reduce physical insight, to increase the development costs of computer programs, and to decrease the computational efficiency of simulations. If a complex nonlinear model is simplified, e.g. a linear state space model, it becomes easier to design a controller for an ASS. Thus, less complex and linear models may be preferable, but necessary precautions should be made to ensure that the important dynamic features are not lost [23].

In Ref. [22], two linear mathematic models and one TruckSim nonlinear model are generated to represent a DTAHV. The four DOF linear yaw-plane model and TruckSim nonlinear model have been used to design and test a controller for the ATS system [26],

while the 7 DOF model has been employed to develop an anti-roll controller [4,5]. Previous studies conclude that the lateral tire forces are in the linear region if the lateral acceleration is below 0.3g (g is the gravity acceleration) under specified maneuvers [27-32]. The conclusions are drawn from the comparisons of dynamic models for light and single-unit vehicles. It has not been adequately validated whether simplified linear DTAHV models are applicable for model-based design optimization of vehicles under high-speed maneuvers, such as the SLC test maneuver specified by SAE [33] or ISO-14791 [34], if the lateral acceleration does not exceed 0.3g. The fidelity and the accuracy of the linear stability analysis are also evaluated by means of comparing the linear DTAHV models with TruckSim nonlinear model. Moreover, a frequency-response analysis based on the linear models is conducted in order to identify the unique dynamic features of DTAHV in the frequency domain. Later, a ten DOF yaw-roll model for DTAHV is developed in Ref. [35], which will be referred as the model for designing the ATS system in high-speed case.

In this thesis, a nonlinear vehicle model is developed under TruckSim software package. The TruckSim software package is based on a symbolic multi-body program, namely VehicleSim (VS) Lisp, which is used to generate equations of motion for three-dimensional (3D) multi-body vehicle systems [36]. In the case of the DTAHV shown in Fig. 1-1, the configuration of the vehicle can be defined as S_SS + SSS + SSS, where S indicates a solid axle, and underline (_) represents a separation of axle groups and a plus sign (+) denotes a fifth wheel connecting two vehicle units. Thus, as the configuration indicated, the DTAHV consists of a three-solid-axle tractor having one front steerable axle and two rear solid axles, and two semitrailers each having three solid axles. VS Lisp takes an input as the description of the AHV configuration mostly in geometric terms, e.g. the body DOF, the body point

locations and directions of the force vectors [37]. With the configuration information, VS Lisp derives equations of motion in terms of the Ordinary Differential Equations (ODEs) and generates a computer source code (C or Fortran) to solve them.

The TruckSim software package involves the following three relevant elements:

(a) The VS browser;

(b) The TruckSim databases;

(c) The VS solver.

The VS browser is a graphical user interface, which serves as the primary interface to TruckSim. The TruckSim databases are used to select vehicle configuration templates (e.g. S_SS + SSS + SSS, for which the ODEs are generated by VS Lisp) and to define the system parameters, the tire-road interactions, the test maneuvers, etc. The VS solver is utilized to solve the relevant governing equations of motion of the vehicle model and to execute the defined dynamic simulations. The VS browser can be used to allow other applications, e.g. design optimization defined in MATLAB and access to the TruckSim databases via interface.

In the course of developing performance-based standards for DTAHVs by the National Road Transport Commission of Australia, one DTAHV with the configuration S_SS + SSS + SSS was modelled using three software packages [38]: ADAMS [39], UMTRI's Constant Velocity Yaw/Roll Program [40] and TruckSim (originally under the name AutoSim) [36]. For the DTAHV modelling, the time histories from the pulse steer simulations and the step steer simulations were almost indistinguishable, showing excellent agreement between all three software packages. In the case of the step steer simulations, there is exceptionally good agreement across all three models, and the maximum differences in the steady-state

values are 3.0%, 2.0% and 2.1% for the roll angle, the yaw rate and the lateral acceleration respectively [38]. The TruckSim package has also been validated using experimental data [41-43].

2.4 ATS Systems

AHVs exhibit poor low-speed maneuverability and low high-speed lateral stability due to their complex structures, large sizes, and high center of gravity, which may lead to traffic accidents [44]. Trailers of AHVs are fitted with multi-axle groups that do not steer. This causes the tires to scrub against the road during a curve negotiation, damaging both the tires and road surface [45, 46].

In order to safely negotiate highway ramps and interchanges, AHVs should improve their low-speed maneuverability and high-speed stability. Steerable trailer axles, such as self-steering axles, are effective to improve the low-speed maneuverability, reduce tire scrubbing and road wearing [47]. However, AHVs with passive trailer steering systems exhibit poor high-speed lateral stability.

To overcome the drawbacks of the passive trailer steering axles, ATS systems have been proposed. Different from passive trailer steering axles, the steering angle of each trailer axle of an ATS system is computed based on the vehicle's current state rather than simple geometric relationships. The past two decades have witnessed the application of LQR technique to the controller design for ATS systems of AHVs mainly at research level [26, 48-50]. Recently, a real physical prototype of ATS system has been developed at the UOIT [51]. It is shown that the LQR technique provides a compact analytical solution with relatively low design and computational time, and the stability of the system designed is

guaranteed. Moreover, the result of an optimization process is a controller that considers and feeds back all system states with constant gains, while any classical controller structure may not be ensured to be optimal. Therefore, LQR technique is used at the beginning to develop ATS system of DTAHVs.

However, these LQR controllers are designed under the assumption that the vehicle model parameters, operating conditions are given and they remain as constants. In reality, the vehicle system parameters, operating conditions, as well as external disturbances caused by wind and other factors may vary. For example, the payload of a trailer and vehicle forward speed may vary within a large range. Conventional controllers, e.g. LQR controllers, have difficulty ensuring robust performance and stability over a wide range of parameter variation. In contrast, MRAC technique can guarantee robust performance and stability over a wide range of parameter change as long as relevant conditions are satisfied [52]. It is reported that MRAC technique may introduce additional flexibility under the situation of varied vehicle loading conditions [53].

2.5 Directional Performance of AHVs and Test Procedures

2.5.1 Directional Performance of AHVs

It is well known that AHVs exhibit the poor low-speed maneuverability and low high-speed stability. For the convenience of quantifying these two problems, Path-Following Off-Tracking (PFOT) was proposed as the performance measurements for low-speed maneuverability, meanwhile RA and High-Speed Transient Off-tracking (HSTO) were

brought up as the indicators of performance measurement for high-speed stability. PFOT is defined as the maximum radial offset between the path of the tractor's front-axle center and that of the designated trailer's rear axle center during a specified test maneuver [4, 13, 49]. RA is generally defined as a ratio of the lateral motion of the last trailer divided by that of leading unit of the AHVs [54]. HSTO is a measure of the lateral offset between the path of the center of rearmost trailer axle and that of front axle center of leading unit at the maneuvering section [55].

2.5.2 Test Procedures

To acquire the above three indicators for the measurement of directional performance of AHVs, the test procedures that 90-degree turn maneuver for low-speed maneuverability test [56] and SLC maneuver for high-speed stability test [57] are proposed. Fig. 2-6 and Fig. 2-7 show the maneuvers, 90-degree turn and SLC, for acquiring those test indicators listed above under TruckSim simulation environment. Fig. 2-8 shows the detailed information for the SLC test maneuver. As shown in Fig. 2-8, the test course has a 91.5m straight section, one 61m dynamic maneuvering section with 1.46m lateral displacement, and one exit section contains 61m which is parallel to the straight section. During the test, the heavy vehicle runs at 88km/h for about 2.5s to finish the dynamic maneuvering section. Regarding the low-speed maneuverability and high-speed stability, the latter one is of more interest in this thesis.

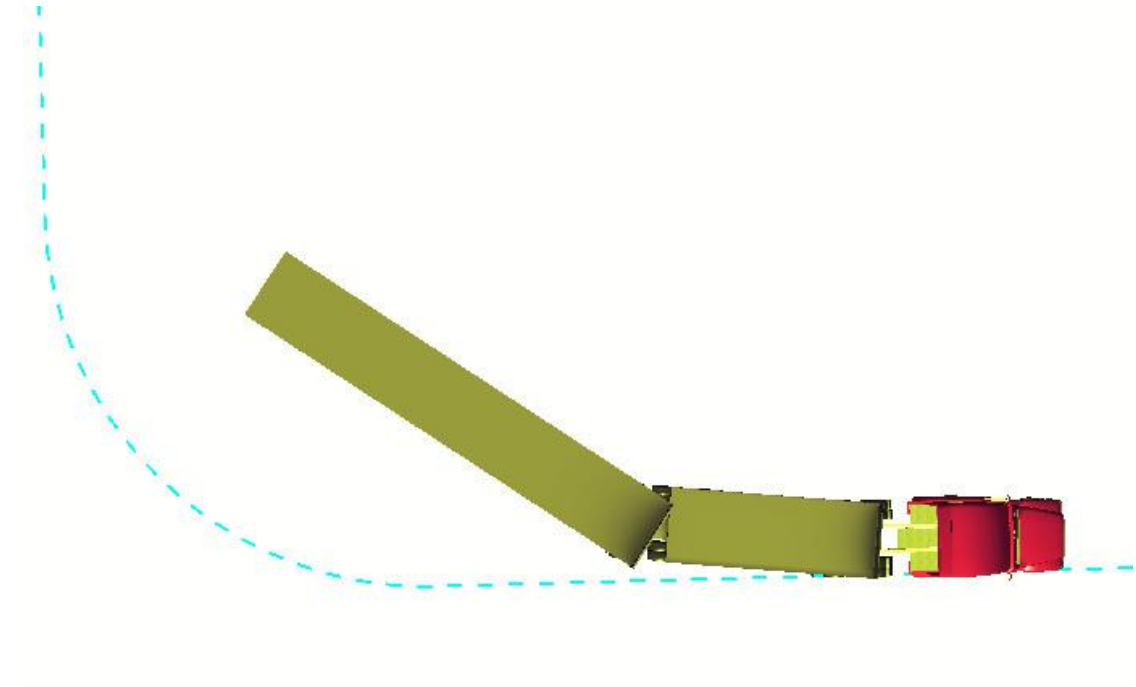

Figure 2-6. 90-degree turn maneuver for PFOT measurement.

Figure 2-7. SLC change test maneuver for RA and HSTO measurement.

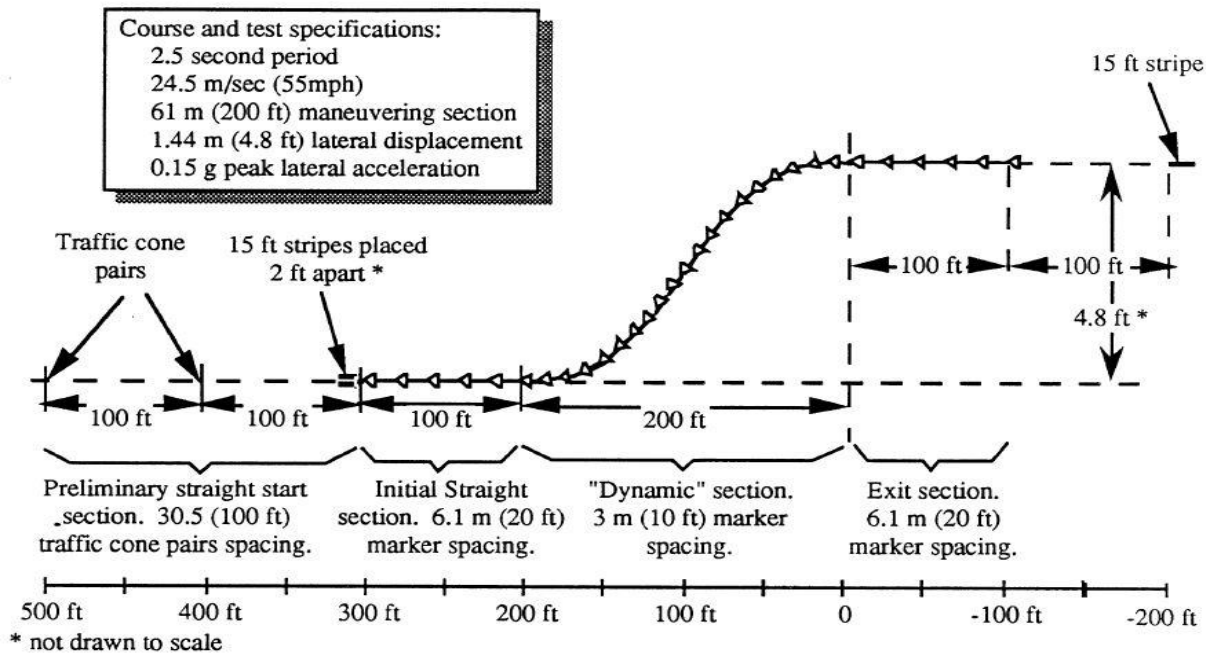

Figure 2-8. SLC test maneuver for acquiring RA of MTAHVs [58].

In 1992, Fancher and Winkler investigated a closed-loop SLC test maneuver for quantifying the RA measures [59]. In 1993, the Society of Automotive Engineers (SAE) issued the SLC test method, SAE-J2179, to determine the RA measures [33]. This test procedure involves a test course especially designed to excite the RA tendencies of MTAHVs. The test driver follows the prescribed trajectory under the testing maneuver. Built upon the test procedure specified by SAE-J2179, the International Organization for Standardization (ISO) released the standard test procedures ISO-14791 in 2000 for evaluating the lateral stability of heavy commercial vehicle combinations and articulated buses [57]. ISO-14791 recommends two SLC test maneuvers: 1) an open-loop test procedure based on a single sine-wave steering input; and 2) a closed-loop test maneuver based on a single sine-wave lateral acceleration input.

Despite the fact that the RA is frequency-dependent, Thomas and El-Gindy showed that the steering input frequency of most heavy vehicles can be chosen as 0.4 Hz for two main reasons [60]. First, simulation and road test results showed that most heavy commercial vehicles would elicit the peak RA around 0.4 Hz. Second, simplicity could be achieved using an input with a single frequency for simulations and road tests.

In 2007, Woodrooffe and Milliken reported the dynamic performance of MTAHVs with the configurations of B-Train Double and Triple [61]. Based on the test maneuver specified by SAE-J2179, the RA measures of these MTAHVs were determined. Simulation results show that the RA measure in terms of lateral acceleration is around 0.85 for DTAHVs. As mentioned above, the MTO launched the LCV program in 2011 to allow LCVs traveling on designated Ontario highways [14]. In this program, dimension and weight limit of LCVs with the B-Train Double configuration are prescribed.

2.6 DHIL Real-Time Simulation Platform

Islam et al. in 2012 published one paper in which driver and model based numerical simulation is conducted to evaluate the ATS system designed for AHVs [62]. Ref. [63] listed several driver models applied to automobile dynamics. However, it could be far too complex to model one real driver and assure its fidelity in mathematics due to many unpredictable factors. To solve this problem, Ref. [26] presented one Driver-Software-In-the-Loop (DSIL) real-time simulation for the evaluation of the ATS controller system of DTAHVs. Simulation results show the effectiveness in applying DSIL real-time simulation to evaluate DTAHV's directional performance. Fig. 2-9 shows the DSIL platform introduced in Ref. [26].

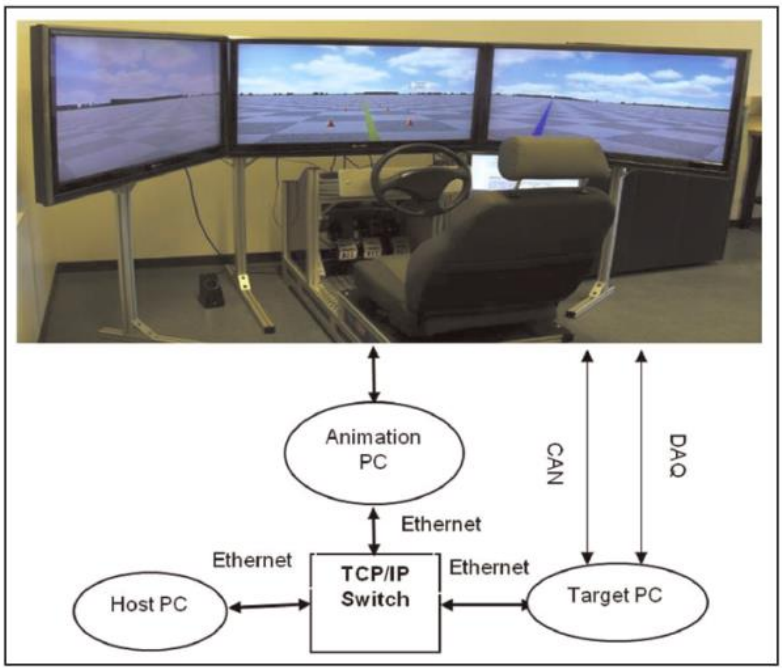

Figure 2-9. Structure of the DSIL real-time simulator located in MVSD laboratory at UOIT.

Later on, DHIL real-time simulation is proposed to evaluate the performance of control system [51]. DHIL real-time simulation platform is developed from UOIT vehicle simulator as shown in Fig. 2-9 and a test rig which is the axle prototype from Ingersoll Axle. The UOIT vehicle simulator is a tool to investigate driver-vehicle-road interactions for various passenger cars and commercial vehicles. It consists of the following components: 1) a visual database that enables the real-time animation; 2) multibody vehicle modelling software, including CarSim and TruckSim, which can generate high-fidelity vehicle models, various road conditions, and provides vehicle responses to various driving conditions; 3) a driver-hardware interface including a steering wheel, throttle/brake/clutch pedals, and gear shifters; 3) networked data transmission that connects the visual database, vehicle model, and driver-hardware interface to form a virtual environment for real-time

simulations. The UOIT vehicle simulator will be combined with the test rig for integrated control systems of DTAHVs to perform DHIL real-time simulations.

As mentioned in the first chapter, field test is indispensable to validate the ASSs of DTAHVs. However, this process can be time-consuming, dangerous and costly to accomplish. As computer performance improves, DHIL real-time simulations are being used to assess the performance and impact of new devices such as ATS system in this thesis. The application of DHIL real-time simulations to the design of ASSs for DTAHVs can reduce expensive field tests, facilitate the examination of the interactions between control systems and driver-vehicle-road, and resolve the potential problems prior to in-vehicle testing.

3 DHIL Real-Time Simulation

3.1 Introduction

This chapter introduces DHIL real-time simulation platform developed in the MVSD laboratory at UOIT, the models of a DTAHVs for evaluating the low-speed maneuverability and the high-speed stability, and the LQR technique used to design the ATS controller for DTAHV. As mentioned before, field and road tests of real physical prototypes are indispensable in order to validate and improve the controller designed for ATS systems. However, field and road tests are costly for such large vehicle combinations as DTAHVs, dangerous for the test driver, and time-consuming. Therefore, DHIL real-time simulation is proposed and accepted by most researchers and it turns out that DHIL real-time simulation is an effective method for evaluating control system performance prior to in-vehicle road tests. Built upon the existing driving simulator, DHIL real-time simulation platform is developed in the MVSD laboratory at UOIT.

3.2 DHIL Real-Time Simulation Platform

3.2.1 UOIT Vehicle Simulator

The UOIT vehicle simulator consists of a host computer, an animator computer, a LabVIEW-RT computer, i.e. target PC, and three 46 inch monitors, and these units are connected by a Controller Area Network (CAN) and an Ethernet network. The host computer is installed with TruckSim/CarSim and LabVIEW software packages to define and compile the real-time DTAHV model and the controller for the ATS system, which are

transmitted to the LabVIEW-RT computer. The host computer also stores all the data of defined DTAHV models and ATS controllers. During real-time simulations, the real-time computer runs the DTAHV model and sends the vehicle motion data to the animator computer, which provides video feeds to three monitors. Through two Peripheral Component Interconnect (PCI) buses leading away from the LabVIEW-RT computer, one Data Acquisition (DAQ) unit will collect the data generated by the driver from the pedals and shifters except that from steering wheel system and then send to LabVIEW-RT computer, while the other one will be in charge of collecting and transmitting data from LabVIEW-RT computer and two active steering axles which will be introduced later on. Steering wheel and LabVIEW-RT computer are connected directly using a CAN bus. During the real-time simulation, the driver literally controls the vehicle by handling throttle/brake/clutch pedals (it should be noted that whether or not using the clutch pedal is dependent on the virtual transmission set-up), gear shifter, and steering wheel. After simulation is completed, data stored in LabVIEW-RT computer will be transferred into host computer through File Transfer Protocol (FTP) for data post-processing.

3.2.2 LabVIEW-RT Model

To be fully functional for this DHIL real-time simulation platform, there are at least three timed loops inside this LabVIEW-RT model block diagram. One timed loop is for receiving analog/digital input signals from throttle/brake/clutch pedals and gear shifters. The other one is for communication between steering wheel and LabVIEW-RT computer, and sending/receiving output/input values between the TruckSim model and the LabVIEW-RT model. The last one is for designing the controller, as is to ATS controller in this thesis. The communication between each timed loop is established by creating shared variables.

In order to coordinate the two DAQ units for this DHIL real-time simulation platform to work simultaneously, the priority for each timed loop should be well defined. Fig. 3-1 shows the front panel of the designed LabVIEW-RT model. Fig. 3-2 shows the ATS controller inside the block diagram, which is a partial graph of the last timed loop mentioned above. Fig. 3-3 shows the principle, what the functionality of each timed loop is and how those three timed loops communicate with each other, of this LabVIEW-RT model.

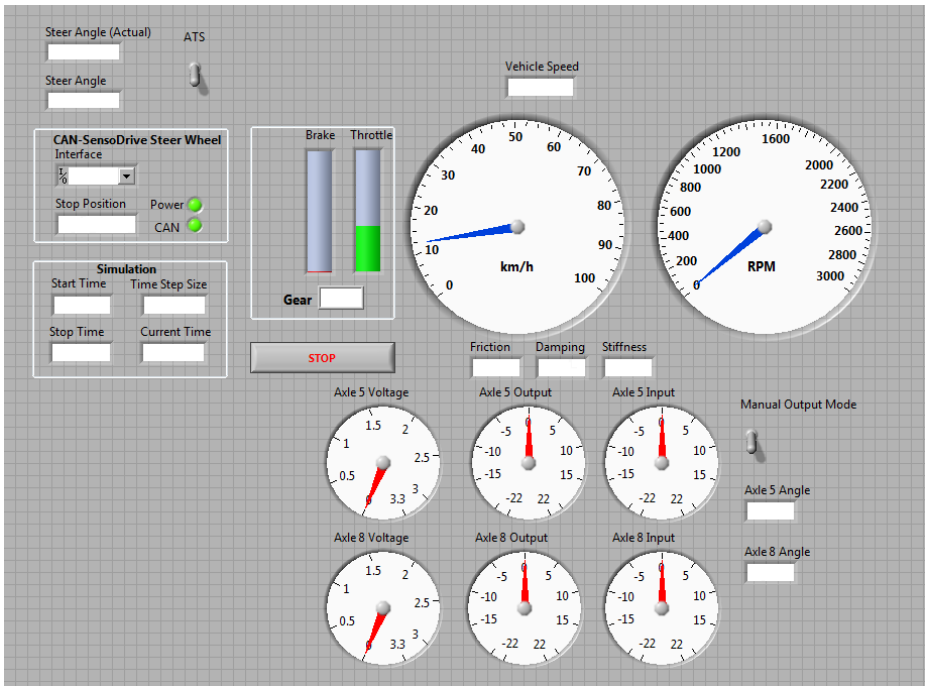

Figure 3-1. The front panel of LabVIEW-RT model.

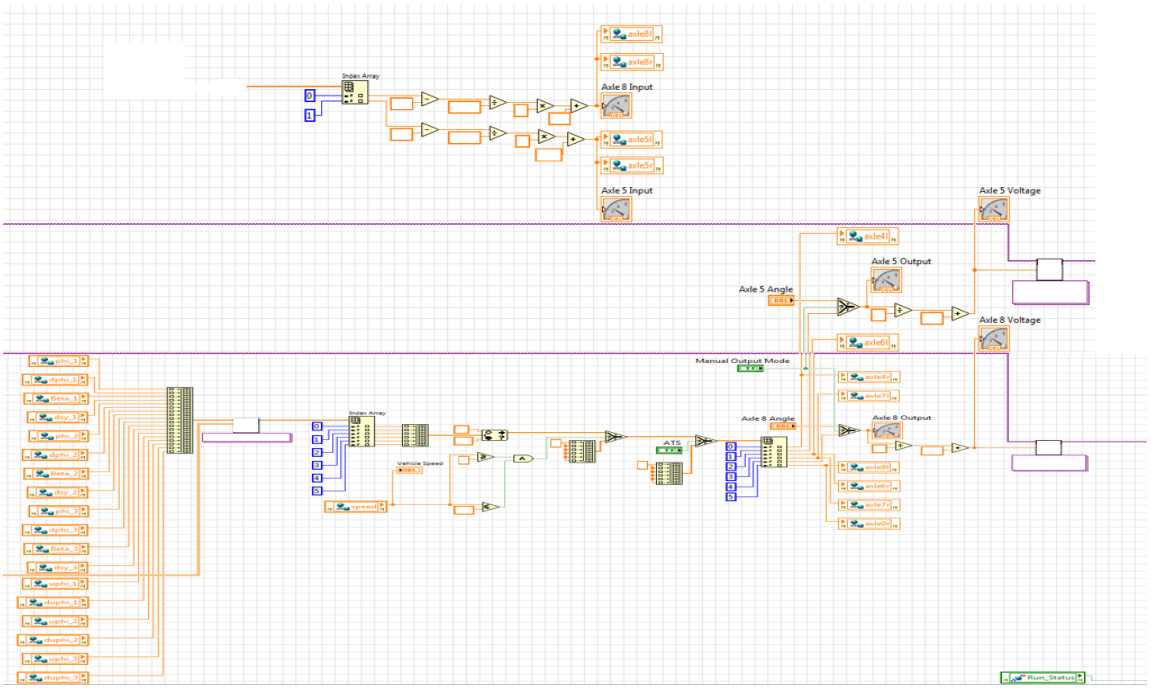

Figure 3-2. The ATS controller within the last timed loop of LabVIEW-RT block diagram.

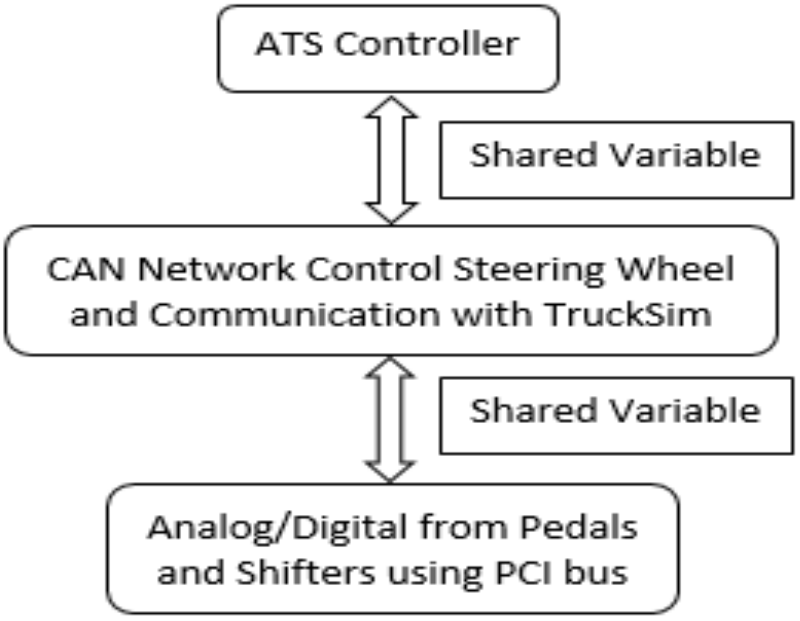

Figure 3-3. Principle for LabVIEW-RT model inside block diagram.

3.2.3 Physical Prototype of ATS Axles

Based on two self-steering axles produced by Ingersoll Axles, Ontario [19], two active steering axles with different control and actuator systems are developed in the MVSD laboratory. Fig. 3-4(a) shows an ATS axle with an electric steering actuator. For this ATS axle, the wheels on the axle are actuated by a double acting single rod electric linear actuator. Fig. 3-4(b) illustrates an ATS axle with a hydraulic steering actuator. In this case, the wheels on the axle are steered by a double acting single rod hydraulic actuator. Compared to the original version of this test rig reported in Ref. [51], the performance, as is to stability and precision of the hydraulic actuated axle, is improved recently by replacing the directional valve with a directional & proportional valve combo. Same as the original test rig [51], each axle is controlled by Arduino Mega with the input values from the output ports of DAQ units. Even so, the controllers written into the Arduino Mega boards this time are coded with a PID controller to make sure each axle can respond to the input timely and accurately. The sensor on each axle, which is a potentiometer, is installed on the kingpin of each axle. The axle steering angle is calculated based on variable resistance of this potentiometer.

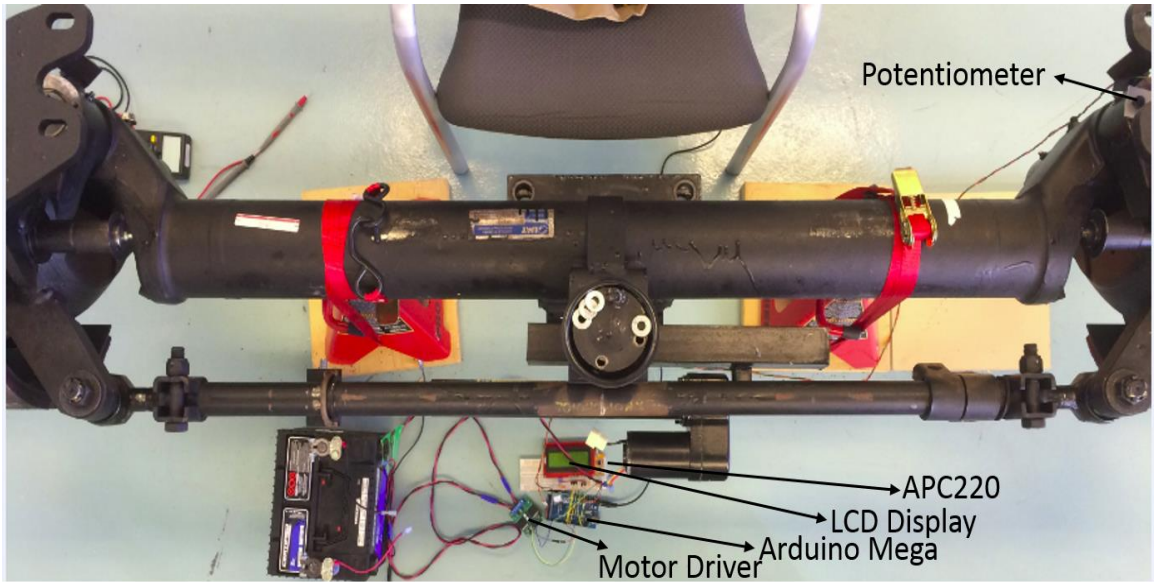

(a)

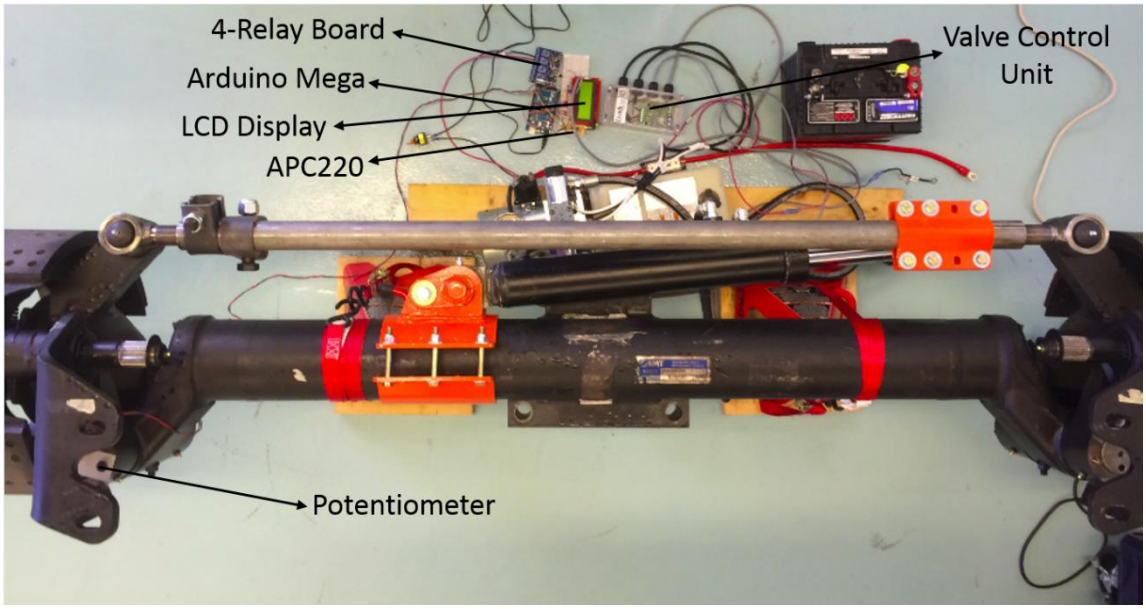

(b)

Figure 3-4. The physical prototype of two ATS axles: (a) the axle with an electrical steering actuator; and (b) the axle with a hydraulic steering actuator.

3.2.4 Communication between LabVIEW-RT Computer and ATS Axle Prototype

To talk with the LabVIEW-RT computer, some indispensable components are used, i.e. PCI bus, DAQ unit, Arduino microcontroller and radio communication module. PCI bus is for data transmission between the DAQ and the LabVIEW-RT computer. The DAQ is hardwired to Arduino Due microcontroller. The radio communication module for each Arduino board is configured so that these three Arduino boards can wirelessly communicate with each other. Serial communication is utilized between each Arduino microcontroller and its corresponding radio module. Fig. 3-5(a) shows the Arduino Mega microcontroller; Fig. 3-5(b) shows the Arduino Due microcontroller. Figs. 3-6 and 3-7 show the radio module used and its configuration interface.

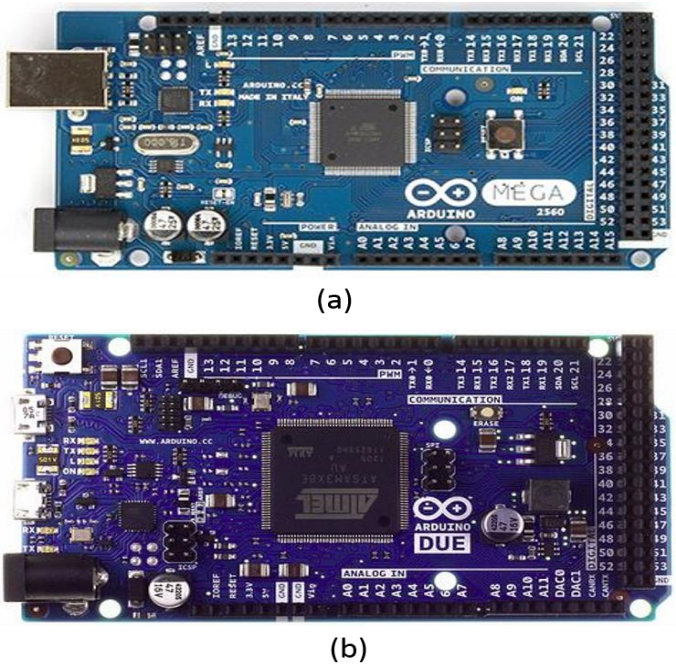

Figure 3-5. (a) Arduino Mega board; (b) Arduino Due board.

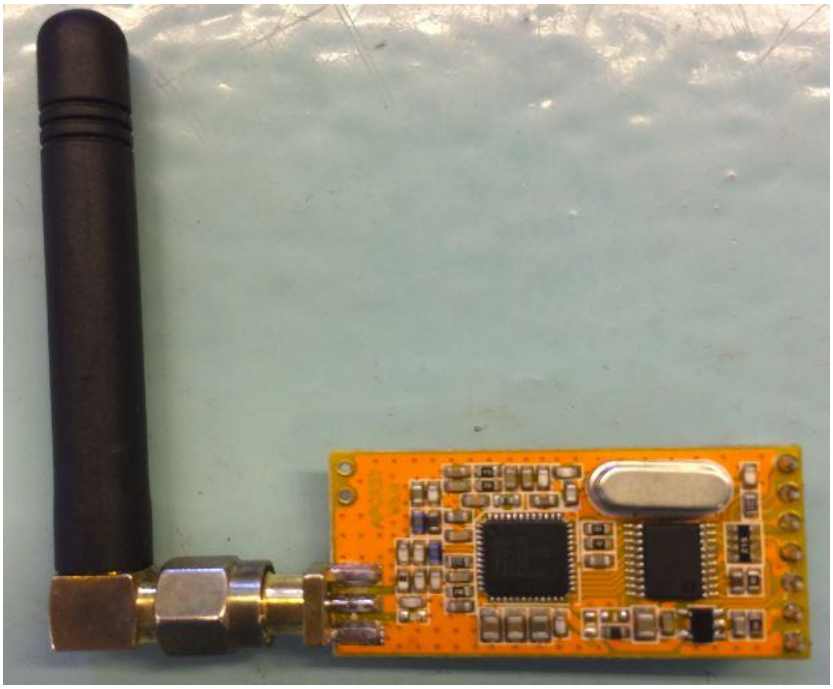

Figure 3-6. APC220 radio module.

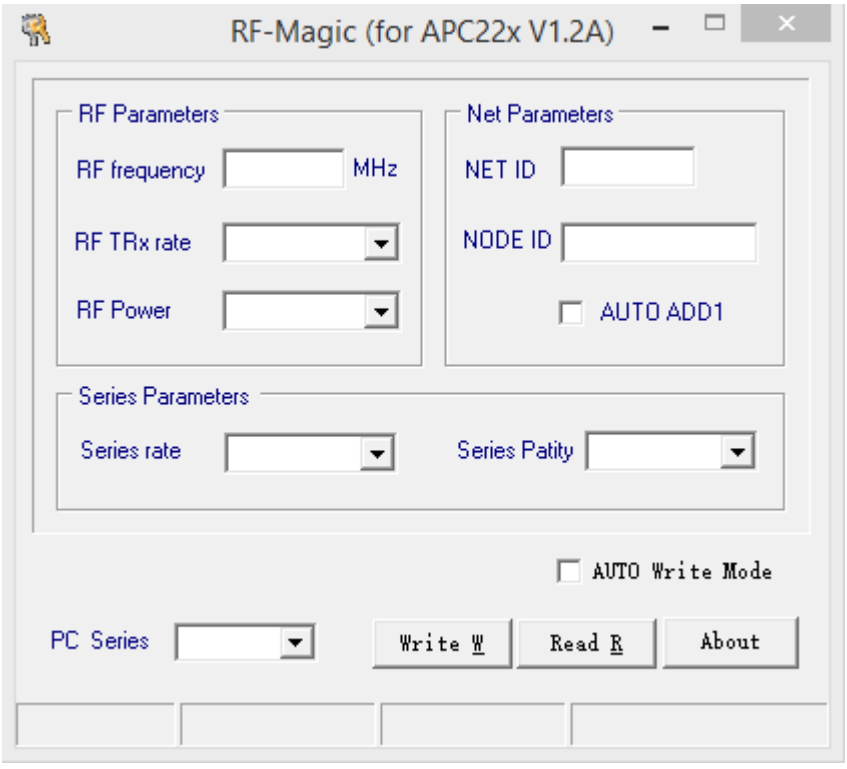

Figure 3-7. Configuration interface of APC220.

3.2.5 Integration of DTAHV Model, ATS Controller, Two ATS Axles, and Human Driver

During DHIL real-time simulation, the ATS axle with hydraulic steering actuator will represent the middle axle of the first semitrailer of the DTAHV TruckSim model, and the ATS axle with electrical steering actuator will behave as the middle axle of the second semitrailer of the DTAHV TruckSim model. When the DTAHV TruckSim model is running, the wheel steering angle on the middle axle of each semitrailer calculated by the ATS controller on the LabVIEW-RT computer is transmitted to the corresponding ATS axle prototype as desired steering angle through the PCI bus, DAQ unit, Arduino Due board and wireless communication as shown in Fig. 3-8. The Arduino Mega board on each axle will read the data from the corresponding potentiometer to get the actual steering angle of the wheels on each ATS axle. By comparing the difference between the desired and current steering angles, the Arduino Mega board will instruct the steering actuator to turn the wheels on the axle. At the same time, the current wheel steering angle of wheels on each axle is sent back to the LabVIEW-RT computer. The returned wheel steering angles will be used as the feedback for the ATS controller.

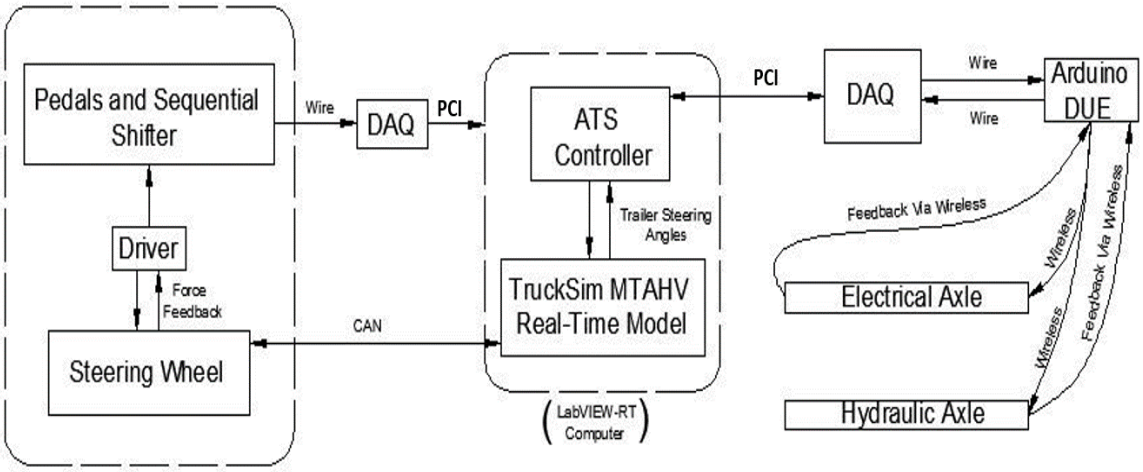

Figure 3-8. Schematic representation of the connection of the ATS axles with the UOIT vehicle simulator.

In order to perform real-time simulations, the DTAHV TruckSim model, ATS controller, the ATS axles, and the human driver need to be integrated as a DHIL closed-loop dynamic system. Using LabVIEW library functions, the DTAHV TruckSim model is compiled with three operations, i.e., initializing, updating, and terminating. The three operations will be used in the DHIL real-time simulation to initialize the vehicle states, to calculate the simulation data, to save the related data to memory, to send the current states of DTAHV TruckSim model to the live animator and to return the updated results back to the host computer.

DHIL real-time simulations are conducted on the LabVIEW-RT computer as shown in Fig. 3-8. The LabVIEW-RT computer provides a real-time environment for the integrated DTAHV TruckSim model, the ATS controller, the ATS axles, and the human driver. The real-time computer deploys fixed-time computing, high-speed communication, and a real-time interface to enable the DHIL operation at certain time instants. In the real-time

environment, the DAQ unit and signal-processing operations are synchronized together. The solution to the ATS controller design and the resulting performance measures are deployed in an embedded real-time system, which expands the graphical LabVIEW program environment and implements the DAQ unit and data-processing tasks under a real-time operation system. Thus, the time constraint is assured in the DHIL real-time simulation. The LabVIEW-RT platform involves a target PC, a National Instruments real-time operation system, a communication link, and input-output boards. These components allow a connection between the simulation program and the external physical devices, including the ATS axles, the steering wheel for the driver steering commands, the throttle or brake pedal for the driver accelerating or decelerating commends, and the sequential shifter for the driver gear ratio changing comments. Based on the vehicle dynamics information from the DTAHV TruckSim model, the LabVIEW-RT platform enables the ATS controller in LabVIEW code to generate the trailers' steering angles and to feed back to the virtual vehicle to form a closed loop. Fig. 3-8 shows the interactions among the DTAHV model, ATS controller, ATS axles, and the driver in the LabVIEW-RT environment.

The above integration provides a tool to research the driver-vehicle-controller-road interactions in a virtual environment. Fig. 3-9 shows the resulting DHIL real-time simulation platform built upon the UOIT vehicle simulator. With this tool, the directional performance of the DTAHV can be examined using the real-time closed-loop dynamic simulation considering the complex interactions of driver-vehicle-controller-road.

Figure 3-9. The DHIL real-time simulation platform built upon the UOIT vehicle simulator.

3.3 Vehicle System Modelling

3.3.1 Linear Model for Low-Speed Case

An optimization method is proposed to design ATS controller for DTAHV considering driver-vehicle-road interactions [4]. In the design optimization, a 7 DOF linear yaw-roll vehicle model, as shown in Fig. 3-10, is generated to represent the DTAHV; a driver model based on PID controller is introduced to emulate the driving efforts of a human driver; the ATS controller is constructed using the LQR technique; and a low-speed 90-degree intersection turn test maneuver is simulated to assess the PFOT performance measurements of the DTAHV.

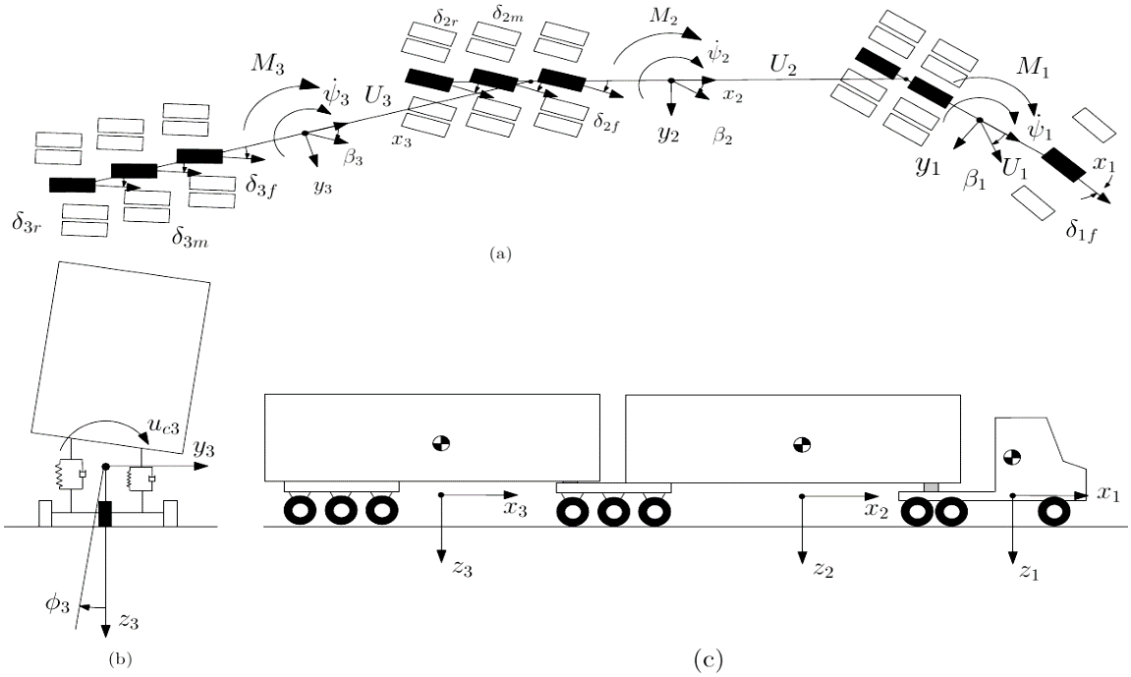

Figure 3-10. Schematic representation of the DTAHV model: (a) top view, (b) rear view, (c) side view.

The design optimization is based on closed-loop simulations, in which the virtual driver 'drives' the virtual DTAHV following the specified testing maneuver emulated, the vehicle system design variable dependent PFOT performance measurements can be achieved. In the design optimization of the DTAHV with ATS system, the interactions of driver-vehicle-road are coordinated by means of finding optimal design variables of the driver model, the DTAHV model, and the ATS controller. Numerical simulation results show that the derived optimal design is superior to the baseline design in the directional performance. The proposed method may be used for identifying desired design variables and predicting performance envelops in the early design stages of AHVs with ATS systems.

3.3.2 Linear Model for High-Speed Case

High-speed test is to research the lateral stability of DTAHV with ATS system under the SLC recommended by SAE-J2179 and ISO-14791. The peak lateral acceleration for the leading unit in completing SLC test maneuver is around 0.15g. According to Ref. [55], the RA is around 0.85 for DTAHV which is a fairly crucial dynamic feature for this research. This leads to the condition that the lateral acceleration of last unit at the center of gravity (CG) is within 0.15g. The simulation results provided in Ref. [22] show that the system response of linear model of DTAHV can fairly well comply with that of highly nonlinear TruckSim model when the lateral acceleration is lower than $0.3g$. Therefore, the linear model of DTAHV is highly sufficient to represent the real vehicle in performing SLC test maneuver and design the controller for ATS system afterwards.

The yaw-roll model has 10 DOF, i.e., tractor's lateral translation, three units' yaw motion and roll motion of sprung/un-sprung mass of each unit [35]. Each axle is represented as a single tire, which is so called bicycle model. The governing equations of each unit are given from Eq. (3.1) to Eq. (3.3), while the geometric relations which could be seen as the constraints are provided from Eq. (3.4) to Eq. (3.6). To derive and solve these governing equations, the following assumptions are made. (1) The leading unit's forward speed is given as the constant; (2) Front wheel steering angle is acquired from steering wheel angle which is treated as the disturbance generated by driver; (3) The tire model is linear in lateral force to tire side-slip angle; (4) Articulation angles are sufficiently small; (5) Roll stiffness and damping coefficients are constant; (6) The forward speed of first semitrailer and second semitrailer are the same as that of tractor; (7) The braking and aerodynamic forces are ignored.

Governing equations of motion for tractor:

$$m_1 U_1\left(\dot{\beta}_1 + \dot{\psi}_1\right) + m_{s1}(h_{s1} - h_{r1})\ddot{\phi}_1 = Y_{\beta_1}\beta_1 + Y_{\dot{\psi}_1}\dot{\psi}_1 + Y_{\delta_{1f}}\delta_{1f} + F_{y1} \tag{3.1.a}$$

$$-I_{xz1}\ddot{\phi}_1 + I_{zz1}\ddot{\psi}_1 = N_{\beta_1}\beta_1 + N_{\dot{\psi}_1}\dot{\psi}_1 + N_{\delta_{1f}}\delta_{1f} - F_{y1}l_{c1} \tag{3.1.b}$$

$$[I_{xx1} + m_{s1}(h_{s1} - h_{r1})^2]\ddot{\phi}_1 - I_{xz1}\ddot{\psi}_1 + m_{s1}U_1(h_{s1} - h_{r1})\left(\dot{\beta}_1 + \dot{\psi}_1\right) = m_{s1}g(h_{s1} - h_{r1})\phi_1 - \left(K_{f1} + K_{r1}\right)(\phi_1 - \phi_{t1}) - \left(L_{f1} + L_{r1}\right)\left(\dot{\phi}_1 - \dot{\phi}_{t1}\right) - K_{12}(\phi_1 - \phi_2) + F_{y1}h_{cr1} \tag{3.1.c}$$

$$[I_{xxt1} + m_{u1}(h_{u1} - h_{r1})^2]\ddot{\phi}_{t1} - I_{xzt1}\ddot{\psi}_1 + m_{u1}U_1(h_{u1} - h_{r1})\left(\dot{\beta}_1 + \dot{\psi}_1\right) = -h_{r1}\left(Y_{\beta_1}\beta_1 + Y_{\dot{\psi}_1}\dot{\psi}_1 + Y_{\delta_{1f}}\delta_{1f}\right) + m_{u1}g(h_{u1} - h_{r1})\phi_{t1} - \left(K_{f1} + K_{r1}\right)(\phi_{t1} - \phi_1) - \left(L_{f1} + L_{r1}\right)(\dot{\phi}_{t1} - \dot{\phi}_1) - \left(K_{tf1} + K_{tr1}\right)\phi_{t1} \tag{3.1.d}$$

Governing equations of motion for first semitrailer:

$$m_2 U_2\left(\dot{\beta}_2 + \dot{\psi}_2\right) + m_{s2}(h_{s2} - h_{r2})\ddot{\phi}_2 = Y_{\beta_2}\beta_2 + Y_{\dot{\psi}_2}\dot{\psi}_2 + Y_{\delta_{2f}}\delta_{2f} + Y_{\delta_{2m}}\delta_{2m} + Y_{\delta_{2r}}\delta_{2r} - F_{y1} + F_{y2} \tag{3.2.a}$$

$$-I_{xz2}\ddot{\phi}_2 + I_{zz2}\ddot{\psi}_2 = N_{\beta_2}\beta_2 + N_{\dot{\psi}_2}\dot{\psi}_2 + N_{\delta_{2f}}\delta_{2f} + N_{\delta_{2m}}\delta_{2m} + N_{\delta_{2r}}\delta_{2r} - F_{y1}l_{c21} - F_{y2}l_{c22} \tag{3.2.b}$$

$$[I_{xx2} + m_{s2}(h_{s2} - h_{r2})^2]\ddot{\phi}_2 - I_{xz2}\ddot{\psi}_2 + m_{s2}U_2(h_{s2} - h_{r2})\left(\dot{\beta}_2 + \dot{\psi}_2\right) = m_{s2}g(h_{s2} - h_{r2})\phi_2 + -K_{r2}(\phi_2 - \phi_{t2}) - L_{r2}\left(\dot{\phi}_2 - \dot{\phi}_{t2}\right) - K_{12}(\phi_2 - \phi_1) - K_{23}(\phi_2 - \phi_3) - F_{y1}h_{cr2} + F_{y2}h_{cr3} \tag{3.2.c}$$

$$[I_{xxt2} + m_{u2}(h_{u2} - h_{r2})^2]\ddot{\phi}_{t2} - I_{xzt2}\ddot{\psi}_2 + m_{u2}U_2(h_{u2} - h_{r2})\left(\dot{\beta}_2 + \dot{\psi}_2\right) =$$

$$-h_{r2}\left(Y_{\beta_2}\beta_2 + Y_{\dot{\psi}_2}\dot{\psi}_2 + Y_{\delta_{2f}}\delta_{2f} + Y_{\delta_{2m}}\delta_{2m} + Y_{\delta_{2r}}\delta_{2r}\right) + m_{u2}g(h_{u2} - h_{r2})\phi_{t2} -$$

$$K_{r2}(\phi_{t2} - \phi_2) - L_{r2}(\dot{\phi}_{t2} - \dot{\phi}_2) - K_{tr2}\phi_{t2} \quad (3.2.d)$$

Governing equations of motion for second semitrailer:

$$m_3U_3\left(\dot{\beta}_3 + \dot{\psi}_3\right) + m_{s3}(h_{s3} - h_{r3})\ddot{\phi}_3 = Y_{\beta_3}\beta_3 + Y_{\dot{\psi}_3}\dot{\psi}_3 + Y_{\delta_{3f}}\delta_{3f} + Y_{\delta_{3m}}\delta_{3m} +$$

$$Y_{\delta_{3r}}\delta_{3r} - F_{y2} \quad (3.3.a)$$

$$-I_{xz3}\ddot{\phi}_3 + I_{zz3}\ddot{\psi}_3 = N_{\beta_3}\beta_3 + N_{\dot{\psi}_3}\dot{\psi}_3 + N_{\delta_{3f}}\delta_{3f} + N_{\delta_{3m}}\delta_{3m} + N_{\delta_{3r}}\delta_{3r} - F_{y2}l_{c3}$$

(3.3.b)

$$[I_{xx3} + m_{s3}(h_{s3} - h_{r3})^2]\ddot{\phi}_3 - I_{xz3}\ddot{\psi}_3 + m_{s3}U_3(h_{s3} - h_{r3})\left(\dot{\beta}_3 + \dot{\psi}_3\right) =$$

$$m_{s3}g(h_{s3} - h_{r3})\phi_3 - K_{r3}(\phi_3 - \phi_{t3}) - L_{r3}\left(\dot{\phi}_3 - \dot{\phi}_{t3}\right) - K_{23}(\phi_3 - \phi_2) - F_{y2}h_{cr3}$$

(3.3.c)

$$[I_{xxt3} + m_{u3}(h_{u3} - h_{r3})^2]\ddot{\phi}_{t3} - I_{xzt3}\ddot{\psi}_3 + m_{u3}U_3(h_{u3} - h_{r3})\left(\dot{\beta}_3 + \dot{\psi}_3\right) =$$

$$-h_{r3}\left(Y_{\beta_3}\beta_3 + Y_{\dot{\psi}_3}\dot{\psi}_3 + Y_{\delta_{3f}}\delta_{3f} + Y_{\delta_{3m}}\delta_{3m} + Y_{\delta_{3r}}\delta_{3r}\right) + m_{u3}g(h_{u3} - h_{r3})\phi_{t3} -$$

$$K_{r3}(\phi_{t3} - \phi_3) - L_{r3}(\dot{\phi}_{t3} - \dot{\phi}_3) - K_{tr3}\phi_{t3} \quad (3.3.d)$$

The kinematic constraint between the tractor and the first semitrailer as well as that between the first semitrailer and the second semitrailer are given as:

$$\beta_1 - \beta_2 + \frac{h_{cr1}}{U}\dot{\phi}_1 - \frac{h_{cr2}}{U}\dot{\phi}_2 - \frac{l_{c1}}{U}\dot{\psi}_1 - \frac{l_{c21}}{U}\dot{\psi}_2 + \psi_1 - \psi_2 = 0 \quad (3.4)$$

$$\beta_2 - \beta_3 + \frac{h_{cr2}}{U}\dot{\phi}_2 - \frac{h_{cr3}}{U}\dot{\phi}_3 - \frac{l_{c22}}{U}\dot{\psi}_2 - \frac{l_{c3}}{U}\dot{\psi}_3 + \psi_2 - \psi_3 = 0 \quad (3.5)$$

$$F_{y1} = m_1U_1\left(\dot{\beta}_1 + \dot{\psi}_1\right) + m_{s1}(h_{s1} - h_{r1})\ddot{\phi}_1 - Y_{\beta_1}\beta_1 - Y_{\dot{\psi}_1}\dot{\psi}_1 - Y_{\delta_{1f}}\delta_{1f} \quad (3.6)$$

$$F_{y2} = -m_3 U_3\left(\dot{\beta}_3 + \dot{\psi}_3\right) - m_{s3}(h_{s3} - h_{r3})\ddot{\phi}_3 + Y_{\beta_3}\beta_3 + Y_{\dot{\psi}_3}\dot{\psi}_3 + Y_{\delta_{3f}}\delta_{3f} + Y_{\delta_{3m}}\delta_{3m} + Y_{\delta_{3r}}\delta_{3r} \quad (3.7)$$

Eliminating the coupling forces between the governing equations of motion and rearranging them in state-space form lead to the following state differential equation:

$$\dot{\boldsymbol{x}} = \boldsymbol{A}\boldsymbol{x} + \boldsymbol{B}\boldsymbol{u} + \boldsymbol{C}\boldsymbol{\delta_{1f}} \quad (3.8)$$

Where, $\boldsymbol{A}$ is the system matrix; $\boldsymbol{B}$ is the input matrix; $\boldsymbol{C}$ is the disturbance matrix; $\boldsymbol{x}$ is the state vector; $\boldsymbol{u}$ is the input vector; δ_{1f} is the disturbance. $\mathbf{A} = -\mathbf{M^{-1}N}$, $\mathbf{B} = -\mathbf{M^{-1}T}$, $\mathbf{C} = -\mathbf{M^{-1}Q}$, $\boldsymbol{x} = [\boldsymbol{x_1}\ \boldsymbol{x_2}\ \boldsymbol{x_3}\ \boldsymbol{x_t}]^T$, $\boldsymbol{x_1} = [\Phi_1\ \dot{\Phi}_1\ \beta_1\ \dot{\psi}_1]$, $\boldsymbol{x_2} = [\Phi_2\ \dot{\Phi}_2\ \beta_2\ \dot{\psi}_2]$, $\boldsymbol{x_3} = [\Phi_3\ \dot{\Phi}_3\ \beta_3\ \dot{\psi}_3]$, $\boldsymbol{x_t} = [\Phi_{1t}\ \dot{\Phi}_{1t}\ \Phi_{2t}\ \dot{\Phi}_{2t}\ \Phi_{3t}\ \dot{\Phi}_{3t}]$, $\boldsymbol{u} = \left[\delta_{2f}\ \delta_{2m}\ \delta_{2r}\ \delta_{3f}\ \delta_{3m}\ \delta_{3r}\right]^T$. The notation is paraphrased in Appendix 1. The matrix is provided in Appendix 2.

3.3.3 Nonlinear TruckSim Model

Based on the dimension and weight limits of DTAHV provided in the Ontario's LCV program launched by MTO [14], one nonlinear DTAHV model is built under TruckSim program environment. In the TruckSim model, the motions considered are as follows. Each of the sprung masses is considered as a rigid body with five DOF, namely the lateral, the vertical, the pitch, the roll and the yaw DOF. The forward speed of the tractor is assumed to remain as constant, thus the longitudinal DOF is not included. The fifth wheel is modelled as a ball-joint, about which the roll, yaw and pitch motions are allowed. Each axle is treated as a beam axle that can roll and bounce with respect to the sprung mass to which it is attached. To present more severe situation, the payload on each trailer is increased as much as possible to get close to the weight limits on axles listed within

Ontario's LCV program. Fig. 1-1 shows the structure of this DTAHV in TruckSim. The input to this TruckSim model would be the steering angles of all trailer axles, while the output is set up based on its corresponding linear model.

3.4 ATS Controller Design

The LQR algorithm is used to obtain optimal feedback control gain k. The solution of optimization is the feedback controller in the following form:

$$u = -k \cdot x \tag{3.9}$$

With optimal gain matrix k:

$$k = R^{-1}B^{T}P \tag{3.10}$$

Where *P* is a symmetric, positive semi-definite symmetric matrix which satisfies the Riccati equation:

$$A^{T}P + PA - PBR^{-1}BP + Q = 0 \tag{3.11}$$

The selection of the appropriate weighting factors Q and R is critical to achieve an acceptable and steady state solution of above Riccati equation. The values of weighting factors are carefully tuned with acceptable performance measure under a range of vehicle maneuvers by trial and error methods. After the desktop numerical simulation, the ATS controller needs to be reconstructed in LabVIEW-RT model to implement DHIL real-time simulation.

4 Simulation Results and Analysis on Directional Performance of DTAHV

4.1 Introduction

This chapter presents the simulation results and analysis on the directional performance of DTAHV with ATS controller. First, the simulation results derived from the emulated low-speed path-following maneuver are presented and discussed. Then, the simulation results derived from the emulated high-speed SLC test maneuvers are provided and analyzed. The low-speed real-time simulation is to validate the design optimization of DTAHV with ATS controller reported in Ref. [4]. The high-speed simulation is to examine whether both of SLC test maneuvers specified in ISO-14791 are applicable for RA measurements of AHVs with ATS controller.

4.2 Low-Speed Simulation Results and Analysis

In order to validate the optimized DTAHV with PFOT-oriented ATS controller reported in Ref. [4], the real-time simulations are performed for the following three cases: 1) baseline design, investigating the maneuverability of the design using the UOIT vehicle simulator; 2) optimal design, examining the maneuverability of the design based on DSIL real-time simulations; and 3) optimal design with ATS axles, assessing the maneuverability of the design using the DHIL real-time simulations. The PFOT-oriented ATS controller is designed to reduce the PFOT for improving the maneuverability of AHVs at low speeds

[11, 62]. In order to evaluate the maneuverability of the three designs, the low-speed 90-degree intersection turn maneuver to acquire PFOT is simulated. Note that the design variables for this DTAHV, the ATS controller, and the driver model are available in Refs. [4, 5].

In the low-speed 90-degree intersection turn, the center of the tractor's front axle is required to follow a path consisting of a straight entry segment that is tangent to a 90-degree circular arc, followed by a straight exit segment. The vehicle forward speed for this maneuver is 10 km/h. During the real-time simulations, the driver controls the vehicle heading direction and forward speed by manipulating the steering wheel, the throttle or brake pedal, and the sequential shifter in order to follow the predefined path.

Figs. 4-1, 4-2 and 4-3 show the simulation results for the case of baseline design, DSIL, and DHIL, respectively. For the baseline design case shown in Fig. 4-1, the PFOT between the first trailer and tractor is 3.71m, while the PFOT between the second trailer and tractor is 6.77m; for the DSIL case illustrated in Fig.4-2, the corresponding PFOT values are 1.60m and 2.16m, respectively; for the DHIL case indicated in Fig. 4-3, the respective PFOT values are 2.17m and 2.50m. Compared to the baseline case, 68.1% and 63.1% reduction of the PFOT between the second trailer and tractor can be achieved by the DSIL and DHIL case, respectively. The better measure of the DSIL and DHIL cases is attributed to the ATS controller. The comparison of the DSIL and DHIL indicates that the introduction of the ATS axles will degrade the PFOT measure. This phenomenon may be explained by the fact that the time delay, the actuation and control errors of the ATS axles will have negative impact on the performance measure.

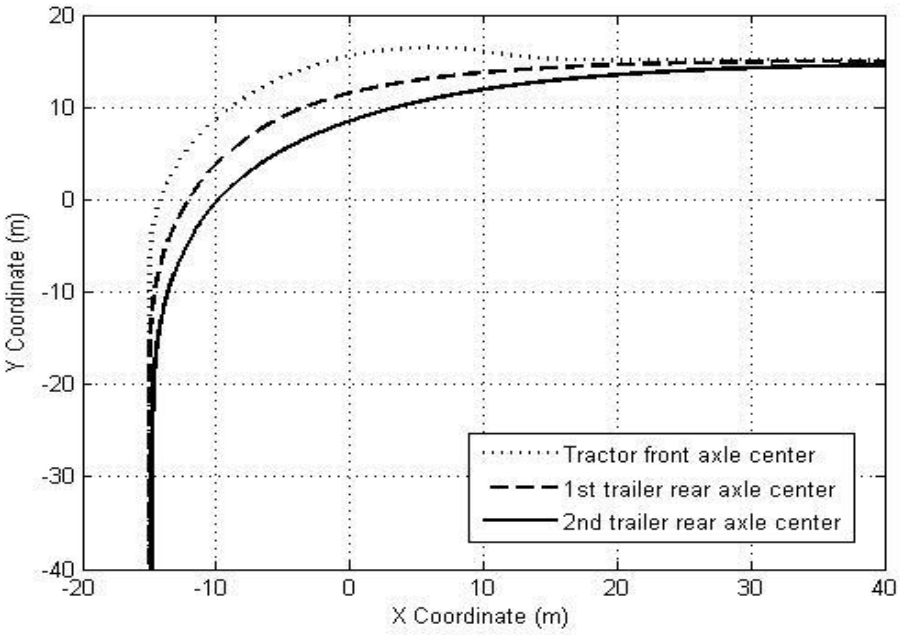

Figure 4-1. Trajectories of the axle centers of the DTAHV in the 90-degree turn (the baseline design case).

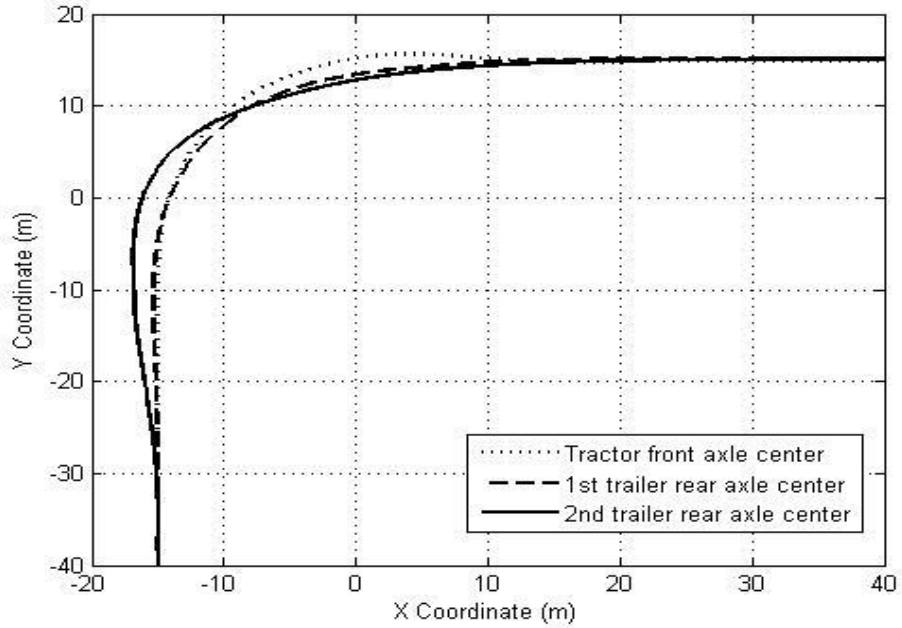

Figure 4-2. Trajectories of the axle centers of the DTAHV in the 90-degree turn (the optimal design, i.e., DSIL case).

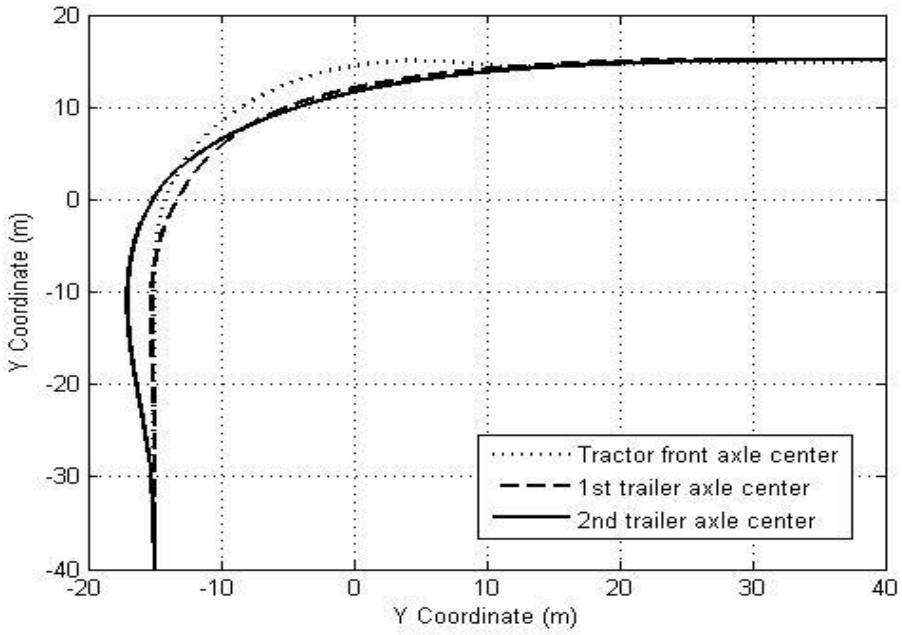

Figure 4-3. Trajectories of the axle centers of the DTAHV in the 90-degree turn (the optimal design with ATS axles, i.e., DHIL case).

Fig. 4-4 shows the maximum absolute values of the side-slip angles of the tires on the rear axle of the first and second trailer during the emulated low-speed 90-degree intersection turn. A close observation of the results shown in Fig. 4-4 discloses the fact that to complete the intersection turn maneuver, the baseline design case requires the largest tire side-slip angles, the DSIL case needs the minimal tire side-slip angles, and the DHIL case requests the medium tire side-slip angles. Larger tire side-slip angle means heavier tire wear. Conjoining the results shown in Fig. 4-4 and those illustrated in Figs. 4-1, 4-2 and 4-3, we can conclude that better path-following performance is helpful to reduce trailer tire wear.

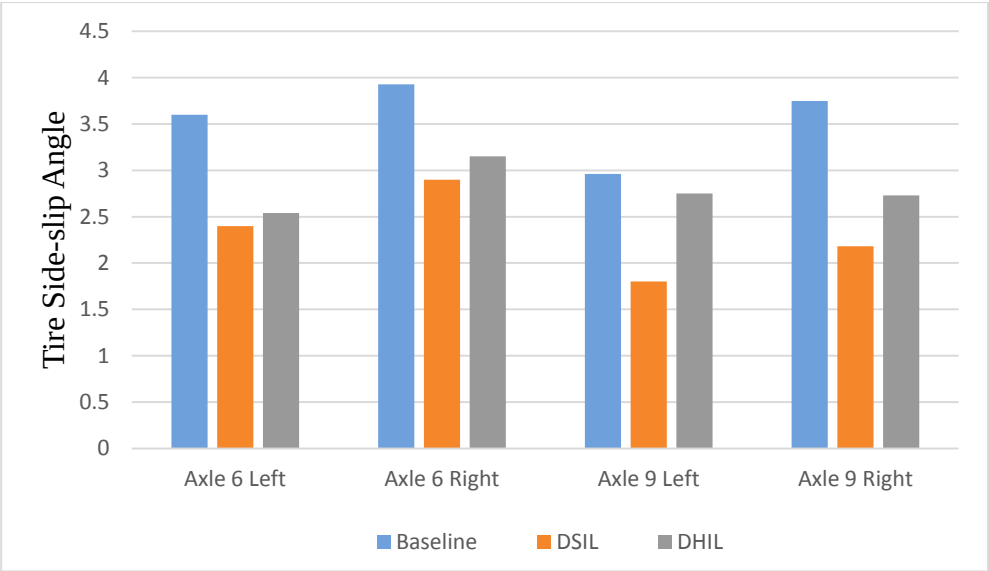

Figure 4-4. Maximum absolute values of the side-slip angles of the tires on the rear axle of the first and second trailer during the emulated 90-degree intersection turn.

Fig. 4-5 offers the time-history of the human driver steering wheel angle for the three cases over the emulated low-speed 90-degree intersection turn maneuver. Note that the angular ratio of the DTAHV's tractor steering system is 25.0. In Fig. 4-5, if the horizontal line corresponding to the 0-degree of the steering wheel angle is treated as the base line, we may quantitatively calculate the total absolute value of the area enclosed by the base line and the steering wheel angle curve for each individual case.

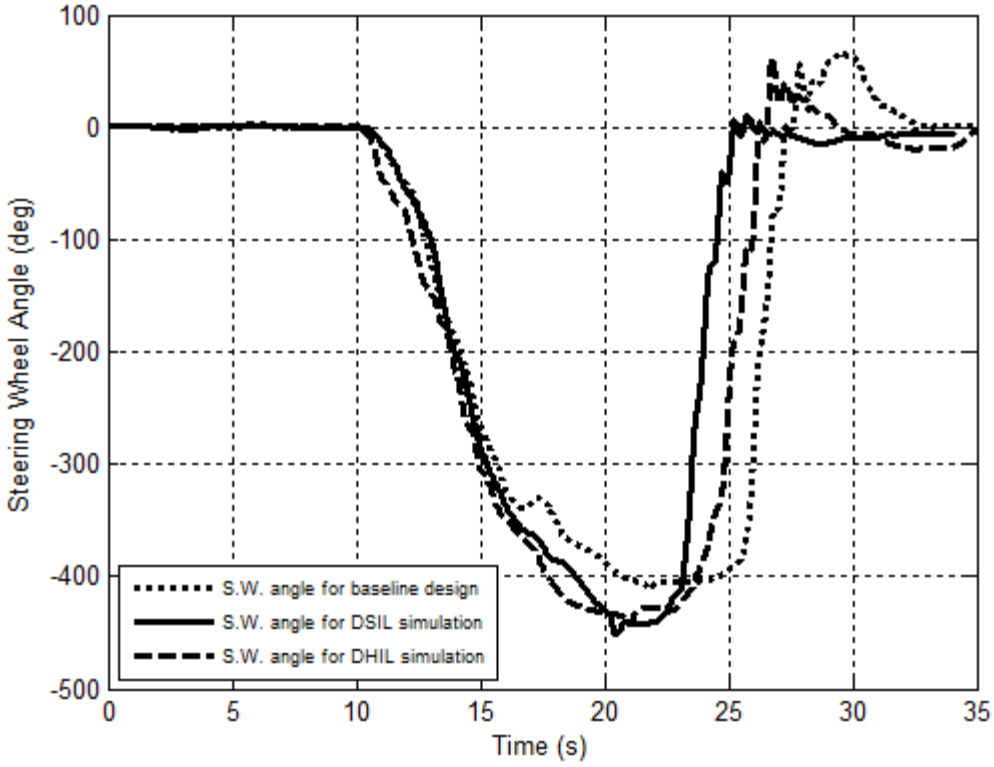

Figure 4-5.The time-history of the human driver steering wheel angle over the emulated low-speed 90-degree intersection turn maneuver.

As shown in Fig. 4-5, the value of the area for the baseline design, DSIL, and DHIL case is the largest, smallest, and median, respectively. During a curved path negotiation, the magnitude and time duration of a steering wheel angle can be used as an indicator for the human driver's steering effort [54]. Thus, the value of the area for individual curve shown in Fig. 4-5 can be utilized to represent the extent of the human driver's steering effort. For the current case study, in order to complete the low-speed 90-degree intersection turn, the baseline design, DSIL, and DHIL case requires the largest, smallest and median driver steering effort, respectively. The benchmark of the three cases leads to the conclusion that to negotiate the designed intersection turn, the ATS system can mitigate the human driver's steering effort, while a larger driver steering effort is needed to compensate the negative effect of the time delay, the actuation and control errors of the ATS axles.

4.3 High-Speed Simulation Results and Analysis

This section presents and discusses the simulation results based on the following three cases: 1) numerical simulation on desktop computers to simulate the lateral dynamics of the DTAHV under the open-loop SLC test maneuver with the predefined tractor steering-wheel angle input; 2) numerical simulation on desktop computers to simulate the lateral dynamics of the DTAHV under the closed-loop SLC test maneuver introduced; and 3) real-time simulation on the DHIL platform to simulate the lateral dynamics of the DTAHV under the closed-loop SLC test maneuver.

4.3.1 Numerical Simulation Results Derived under Open-Loop Test Maneuver

For the DTAHV without ATS under the open-loop maneuver, Figs. 4-6(a), 4-7(a), and 4-8(a) show the lateral acceleration of each vehicle unit, the yaw rate of each vehicle unit, and the trajectory of the center of axles 1, 6, and 9, respectively. The maximum peak lateral acceleration and yaw rate of the tractor is 0.155 g and 4.708 deg/s. For the DTAHV with ATS under the maneuver, Figs. 4-6(b), 4-7(b), and 4-8(b) illustrate the lateral acceleration of each vehicle unit, the yaw rate of each vehicle unit, and the trajectory of the center of axles 1, 6, and 9, respectively. The peak lateral acceleration and yaw rate of tractor are 0.141 g and 4.137 deg/s. The HSTO and RA measures are listed in Table 4-1.

Table 4-1. HSTO measures and RA measures of the lateral acceleration and yaw rate under the open-loop maneuver.

	Semitrailer 1	Semitrailer 2
RA_Acc_0	0.974	0.923
RA_Yaw_0	0.844	0.797
HSTO_0(m)	0.094	0.117
RA_Acc_1	1.043	0.801
RA_Yaw_1	0.666	0.705
HSTO_1(m)	0.041	0.024

RA_Acc_0: the RA of the lateral acceleration between the first or second semitrailer and the tractor without ATS; RA_Yaw_0: the RA of the yaw rate between the first or second semitrailer and the tractor without ATS; RA_Acc_1: the RA of the lateral acceleration between the first or second semitrailer and the tractor with ATS; and RA_Yaw_1: the RA of the yaw rate between the first or second semitrailer and the tractor with ATS; HSTO_0: high-speed transient off-tracking of the center of the rear axle of the first semitrailer or the second semitrailer with respect to the center of the front axle of the tractor in the case of the DTAHV without ATS; HSTO_1: high-speed transient off-tracking of the center of the rear axle of the first semitrailer or the second semitrailer with respect to the center of the front axle of the tractor in the case of the DTAHV with ATS.

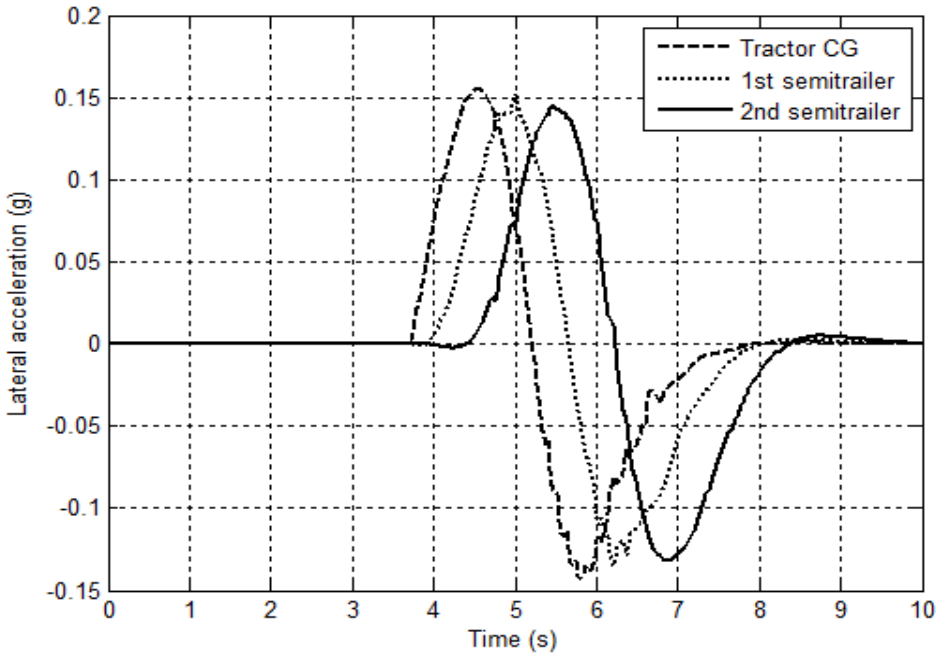

(a)

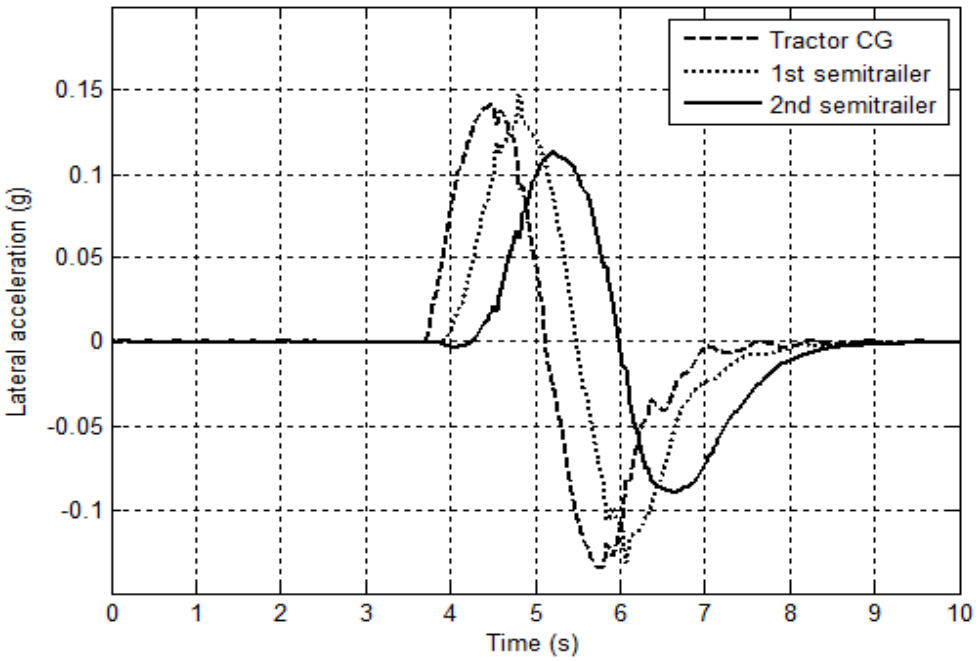

(b)

Figure 4-6. Time history of the lateral acceleration at the CG of each vehicle unit under the open-loop maneuver for: (a) the case without ATS; and (b) the case with ATS.

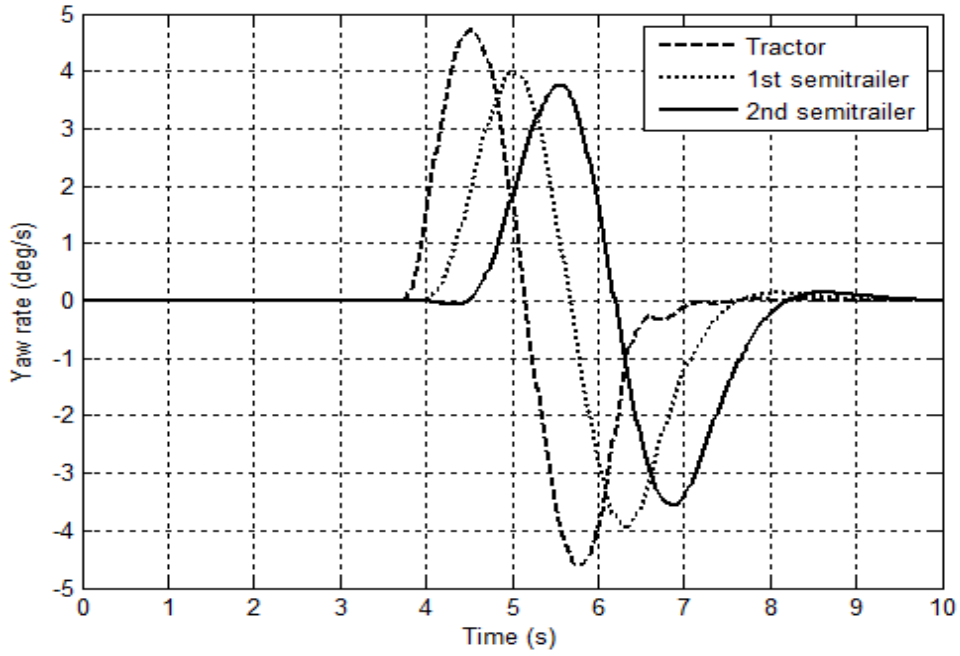

(a)

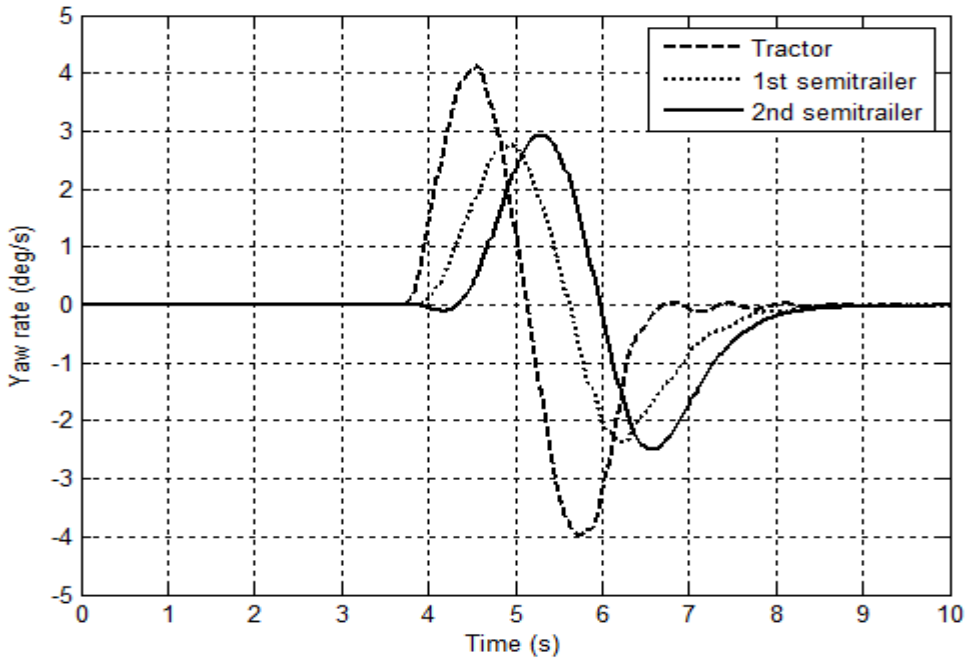

(b)

Figure 4-7. Time history of the yaw rate of each vehicle unit under the open-loop maneuver for: (a) the case without ATS; and (b) the case with ATS.

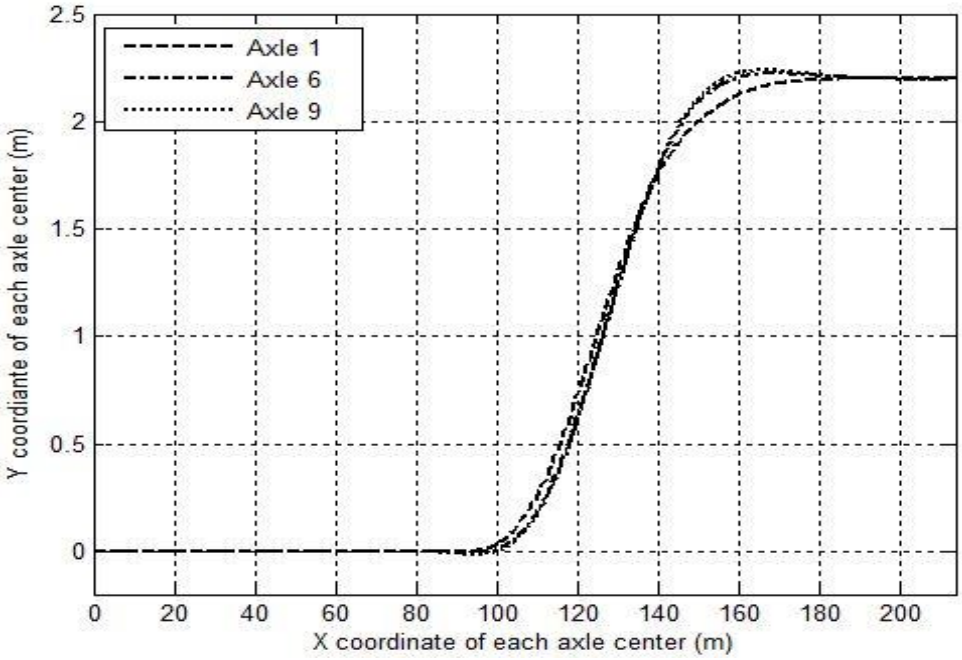

(a)

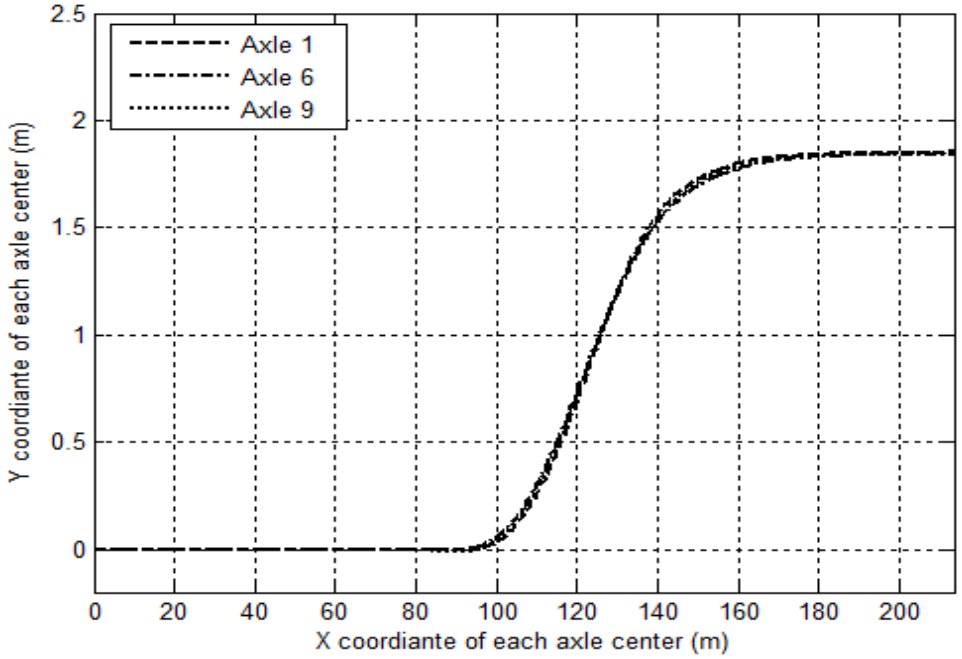

(b)

Figure 4-8. Trajectory of the center of axles 1, 6, and 9 under the open-loop maneuver for: (a) the case without ATS; and (b) the case with ATS.

4.3.2 Numerical Simulation Results Derived under Closed-Loop Test Maneuver

In the case of the DTAHV without ATS under the closed-loop test maneuver, Figs. 4-9(a), 4-10(a), and 4-11(a) show the lateral acceleration of each vehicle unit, the yaw rate of each unit, and the trajectory of the center of axles 1, 6, and 9, respectively. The peak lateral acceleration and the yaw rate of the tractor are $0.165g$ and 5.307 deg/s. Note that axles 1, 6, and 9 are the front axle of the tractor, the rear axle of the first trailer, and the rear axle of the second trailer respectively. In the case of the DTAHV with ATS under the closed-loop test maneuver, Figs. 4-9(b), 4-10(b), and 4-11(b) show the lateral acceleration of each vehicle unit, the yaw rate of each vehicle unit, and the trajectory of the center of axles 1, 6, and 9, respectively. The peak lateral acceleration and the yaw rate of the tractor are $0.158g$ and 4.681 deg/s. The RA measures of lateral acceleration and yaw rate with and without ATS under the closed-loop maneuvers are listed in Table 4-2. Moreover, under the closed-loop maneuver, the measures of HSTO of the DTAHV with and without ATS are also offered in Table 4-2. As shown in Table 4-2, the ATS controller reduces the HSTO of the first trailer from 0.101 m to 0.045 m, decreased by 55.4%, and reduces the HSTO of the second trailer from 0.120 m to 0.027 m, decreased by 77.5%. Thus, the ATS controller greatly reduce the high-speed transient off-tracking of the DTAHV under the closed-loop maneuver.

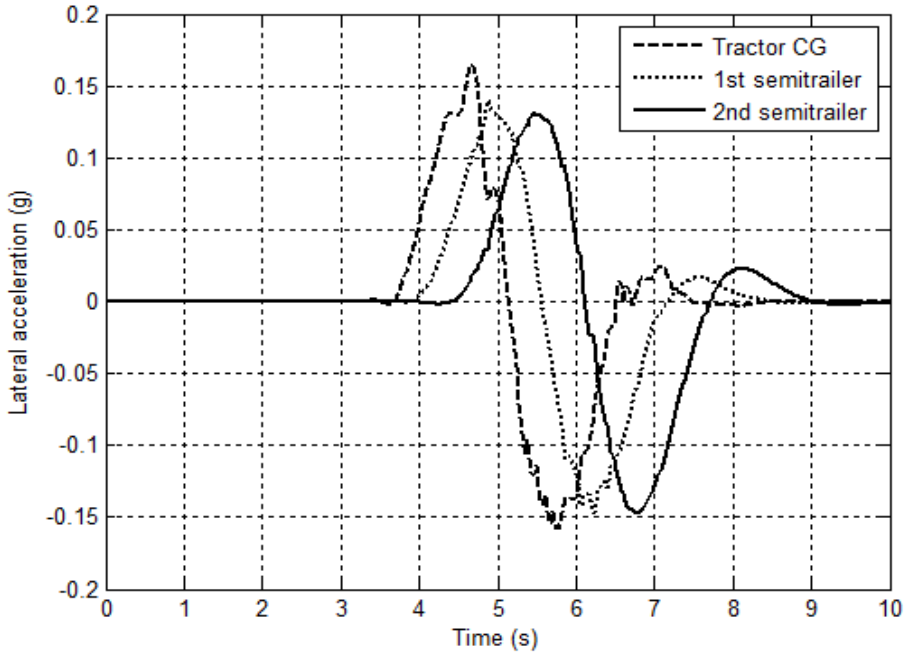

(a)

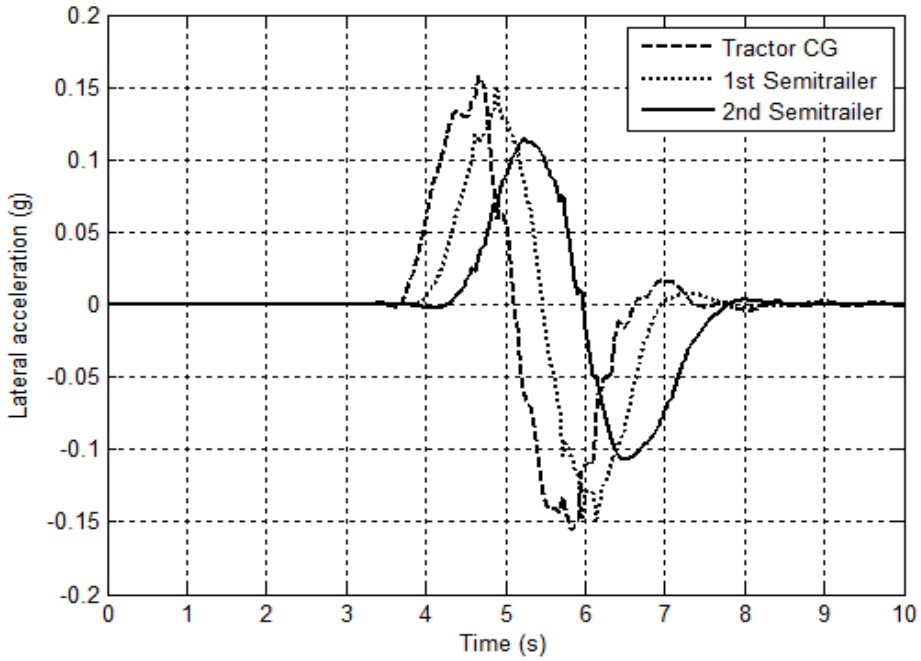

(b)

Figure 4-9. Time history of the lateral acceleration at the CG of each vehicle unit under the closed-loop maneuver for: (a) the case without ATS; and (b) the case with ATS.

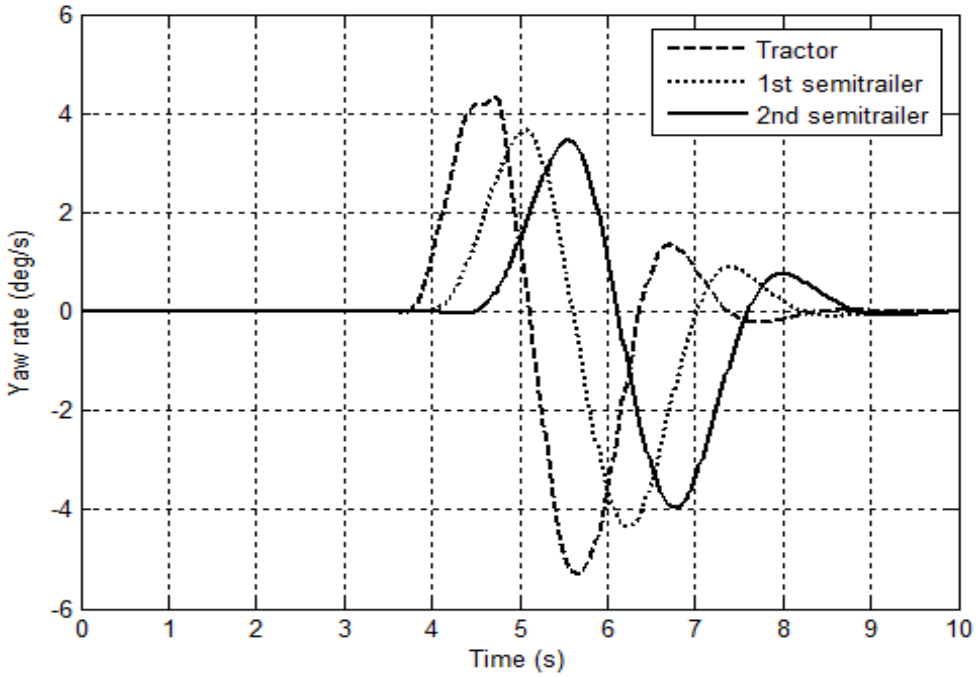

(a)

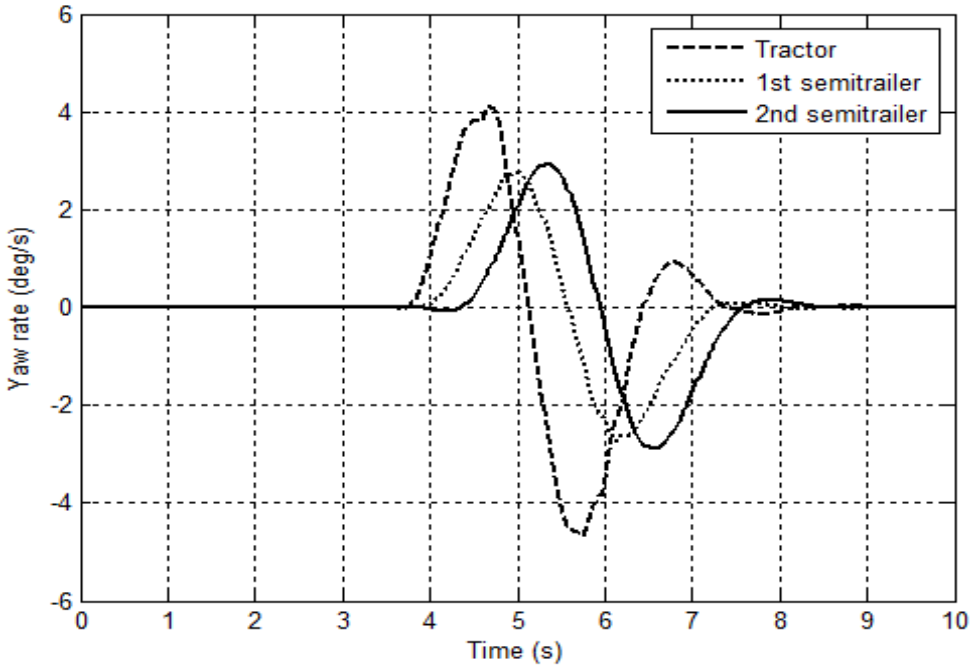

(b)

Figure 4-10. Time history of the yaw rate of each vehicle unit under the closed-loop maneuver for: (a) the case without ATS; and (b) the case with ATS.

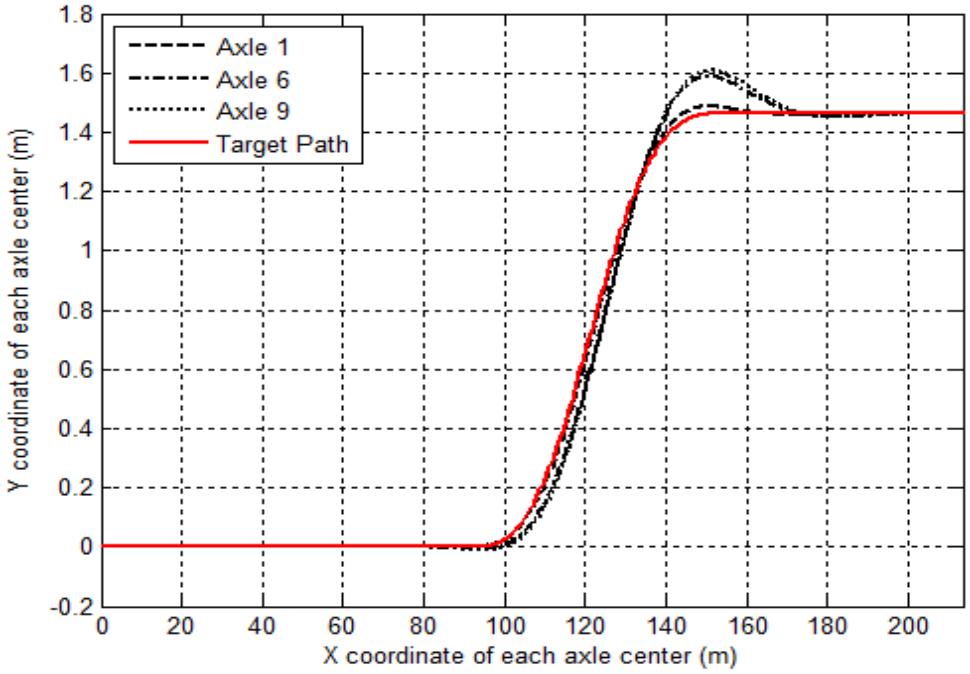

(a)

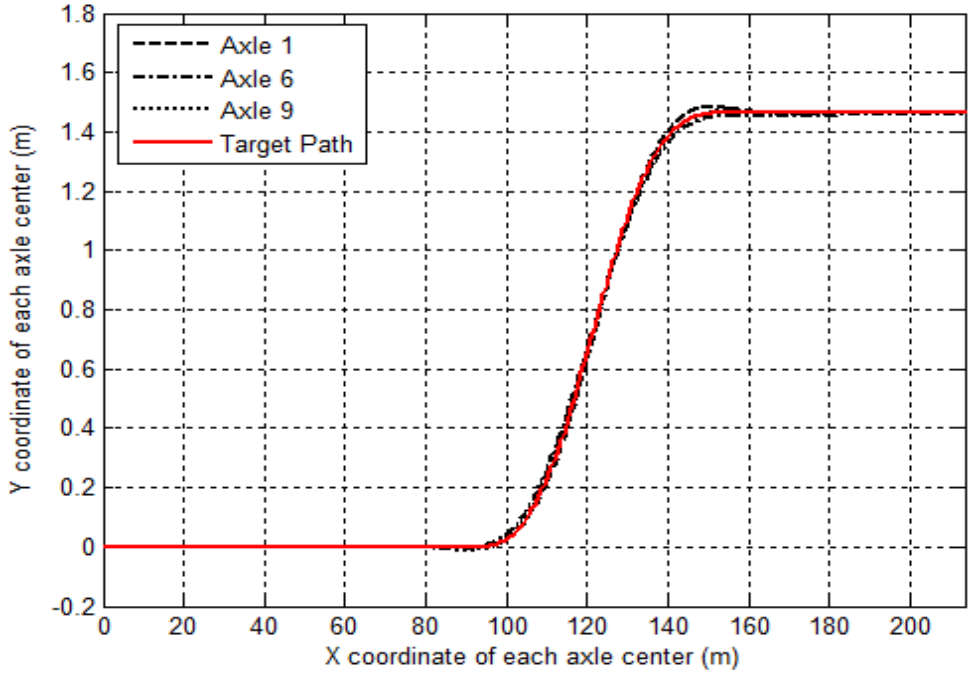

(b)

Figure 4-11. Trajectory of the center of axles 1, 6, and 9 under the closed-loop maneuver for: (a) the case without ATS; and (b) the case with ATS.

Table 4-2. HSTO measures and RA measures of the lateral acceleration and the yaw rate derived under the closed-loop maneuver.

	Semitrailer 1	Semitrailer 2
RA_Acc_0	0.891	0.891
RA_Yaw_0	0.820	0.745
HSTO_0 (m)	0.101	0.120
RA_Acc_1	0.942	0.718
RA_Yaw_1	0.587	0.626
HSTO_1 (m)	0.045	0.027

4.3.3 Real-time Simulation Results Derived under Closed-Loop Test Maneuver

In order to further investigate the directional performance of the DTAHV with and without ATS, real-time simulation is conducted on the DHIL platform under the emulated closed-loop SLC maneuver. In the case of the DTAHV without ATS, Figs. 4-12(a), 4-13(a), and 4-14(a) show the lateral acceleration of each vehicle unit, the yaw rate of each vehicle unit, and the trajectory of the center of axles 1, 6, and 9, respectively. As shown in Figs. 4-12(a) and 4-13(a), the peak lateral acceleration and the peak yaw rate of the tractor are 0.1409 g and 4.392 deg/s. In the case of the DTAHV with ATS, Figs. 4-12(b), 4-13(b), and 4-14(b) illustrate the lateral acceleration of each vehicle unit, the yaw rate of each vehicle unit, and the trajectory of the center of axles 1, 6, and 9, respectively. As shown in Figs. 4-12(b) and 4-13(b), the peak lateral acceleration and the peak yaw rate of the tractor are 0.1336 g and 3.874 deg/s. For the closed-loop real-time simulation, the RA measures of lateral

acceleration and yaw rate with and without ATS are listed in Table 4-3. Moreover, the corresponding measures of HSTO are also offered in Table 4-3.

Table 4-3. HSTO measures and RA measures of the lateral acceleration and the yaw rate derived from the closed-loop real-time simulation on the DHIL real-time simulation platform.

	Semitrailer 1	Semitrailer 2
RA_Acc_0	0.890	0.862
RA_Yaw_0	0.832	0.747
HSTO_0 (m)	0.085	0.112
RA_Acc_1	1.016	0.877
RA_Yaw_1	0.729	0.779
HSTO_1 (m)	0.009	0.017

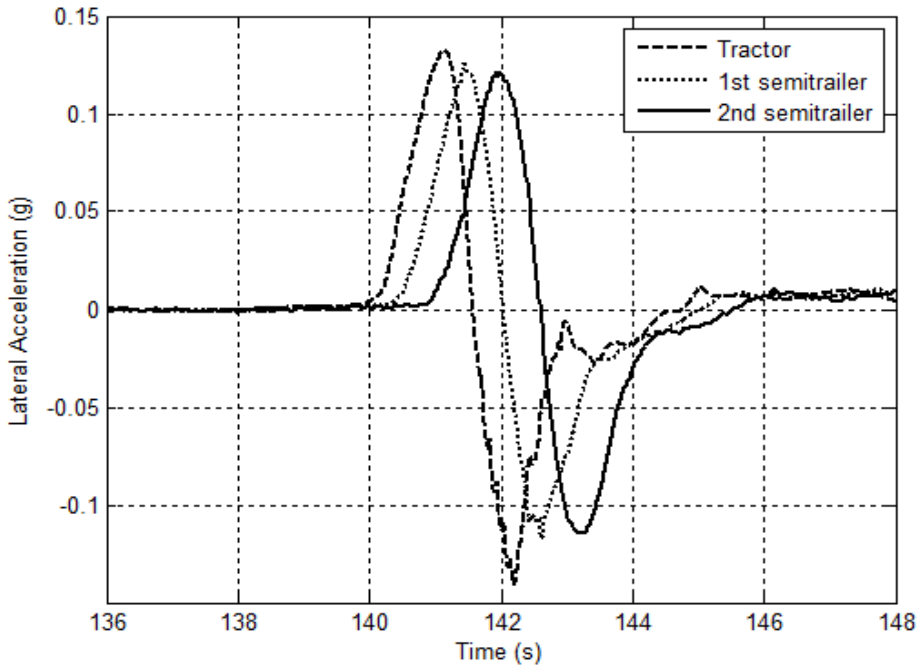

(a)

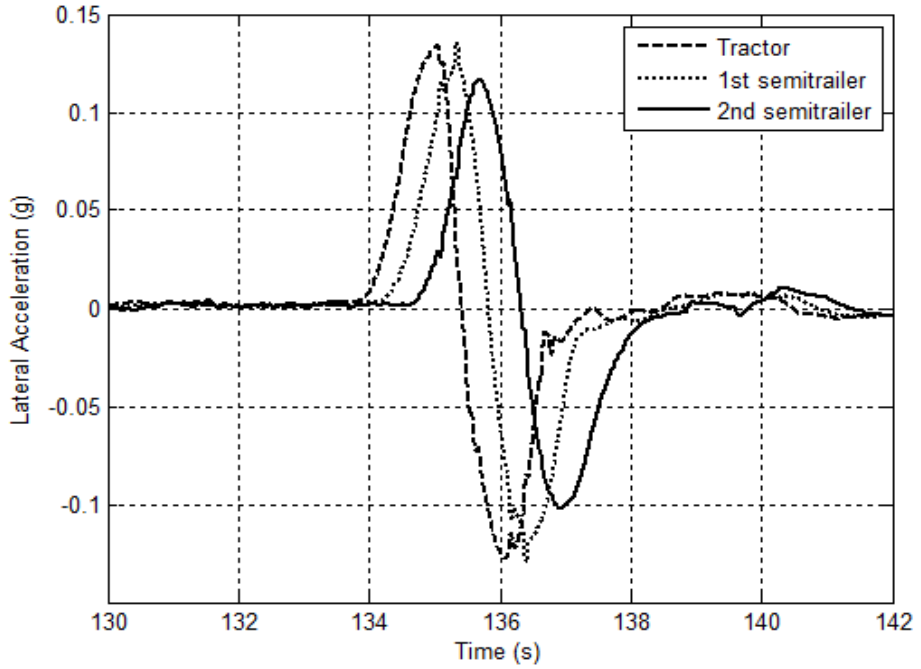

(b)

Figure 4-12. Time history of the lateral acceleration at the CG of each vehicle derived from the real-time simulation for: (a) the case without ATS; and (b) the case with ATS.

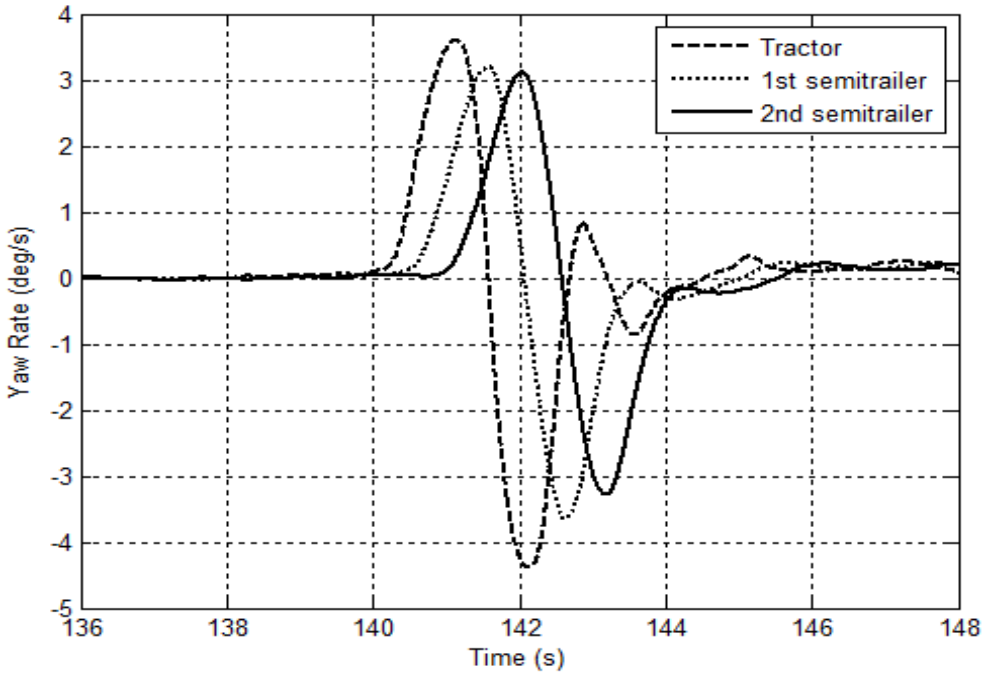

(a)

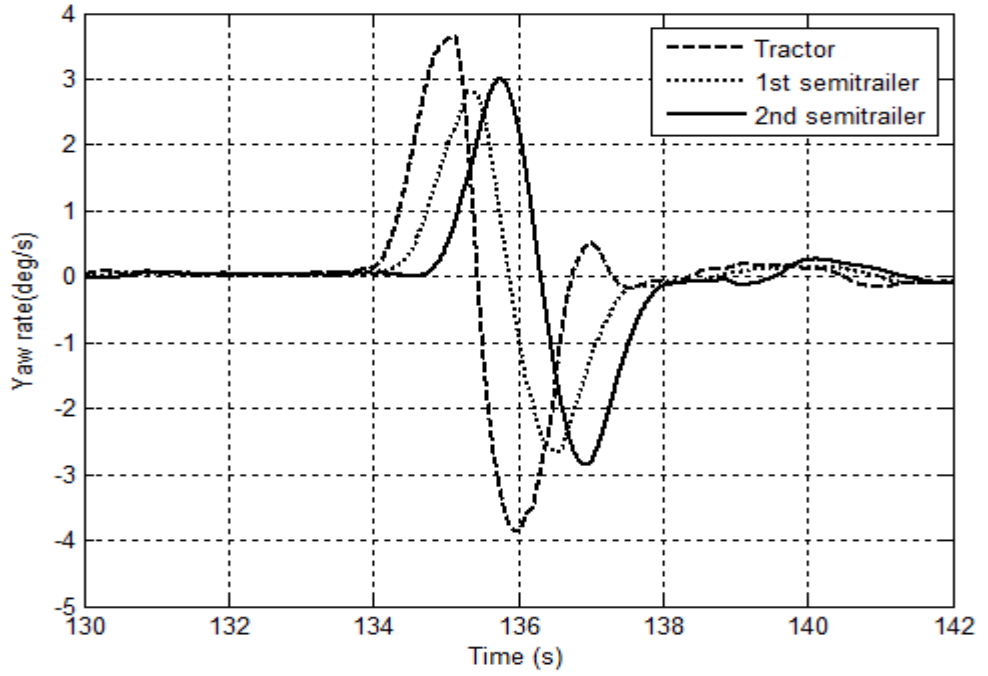

(b)

Figure 4-13. Time history of the yaw rate of each vehicle unit derived from the real-time simulation for: (a) the case without ATS; and (b) the case with ATS.

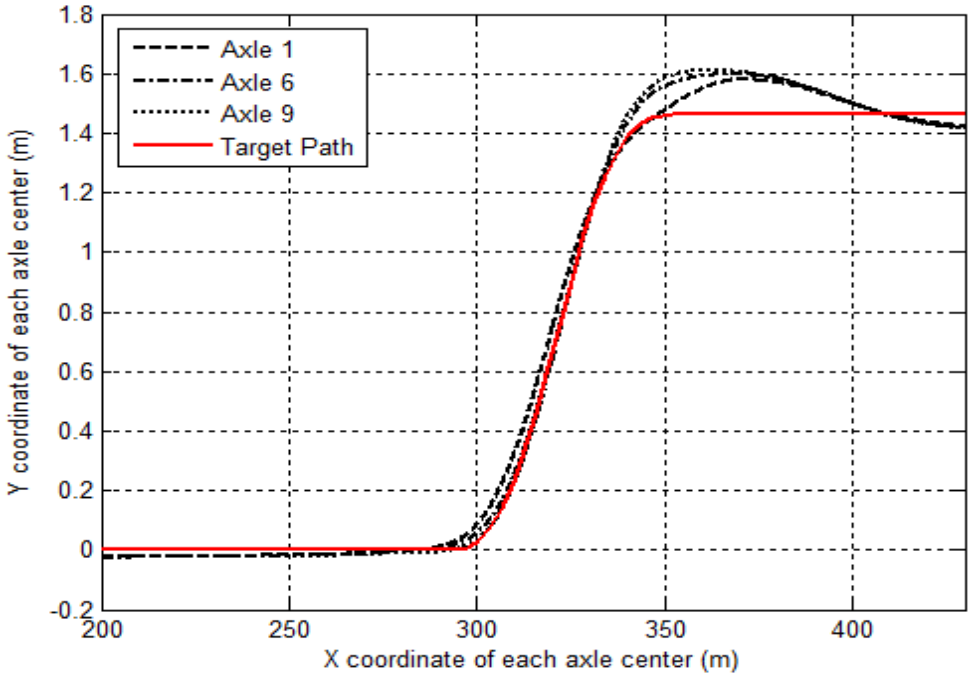

(a)

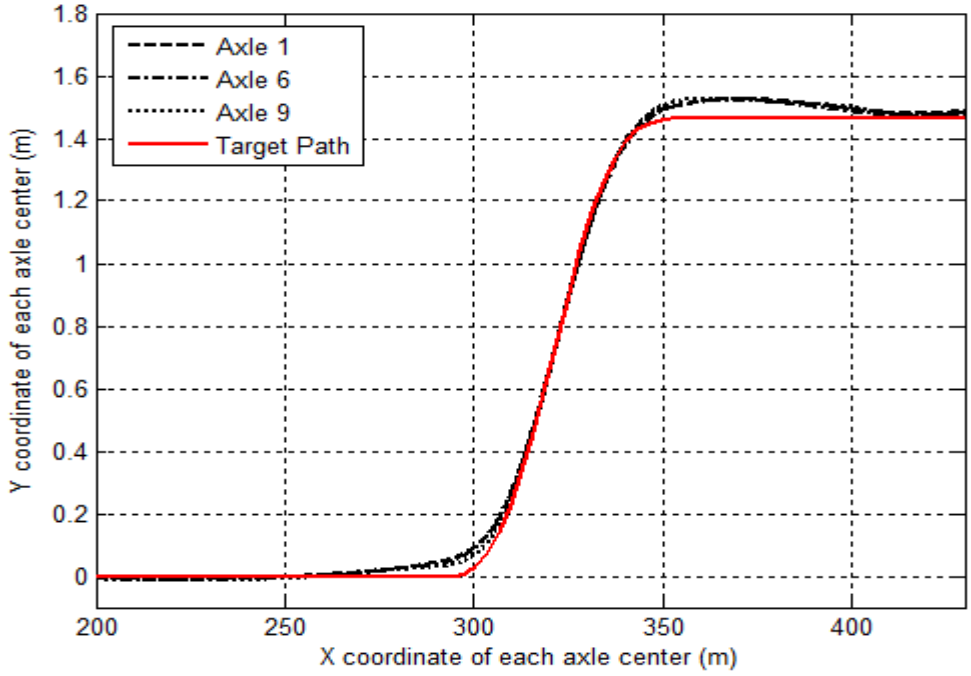

(b)

Figure 4-14. Trajectory of the center of axles 1, 6, and 9 derived from the real-time simulation for: (a) the case without ATS; and (b) the case with ATS.

4.3.4 Simulation Results Analysis and Discussion

In this sub-section, the results derived from the above numerical and real-time simulations are compared, analyzed and discussed. For the first and second trailers, Figs. 4-15(a) and 4-15(b) show the measures of the RA and the HSTO achieved from the numerical and real-time simulations, respectively. A close observation of Figs. 4-15(a) and 4-15(b) reveals the following insightful findings: 1) in the case of DTAHV without ATS, the results derived from the numerical and real-time simulations under the closed-loop SLC test maneuver are in good agreement; 2) in the case of the DTAHV with ATS, the measures of the RA based on the real-time simulation are larger than those derived from the numerical simulation under the closed-loop maneuver; and 3) in the case of numerical simulation on desktop computers, the difference between the RA measures without ATS under the open-loop and the closed-loop maneuvers is smaller than that with ATS under the two maneuvers. In order to further elaborate the above findings, detailed numerical result analysis is conducted.

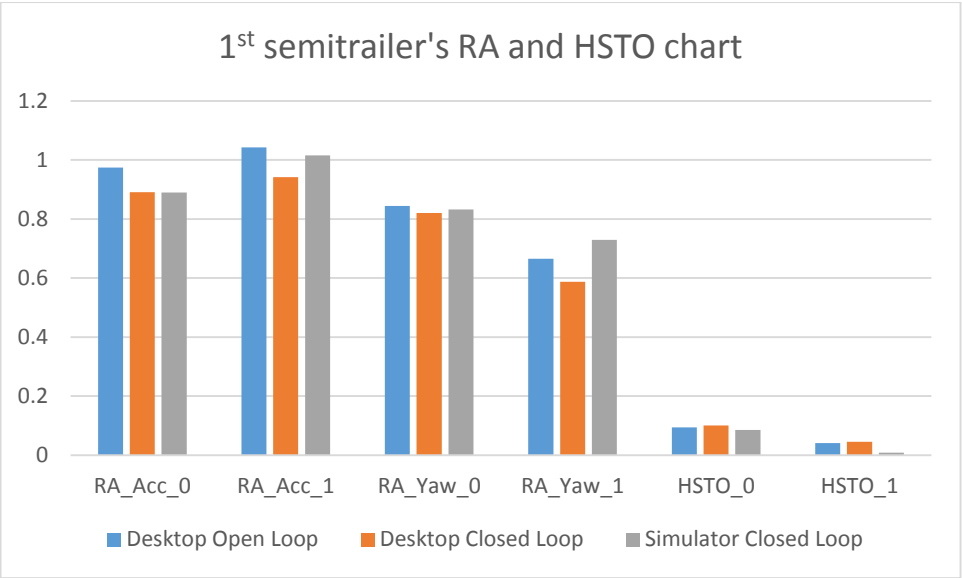

(a)

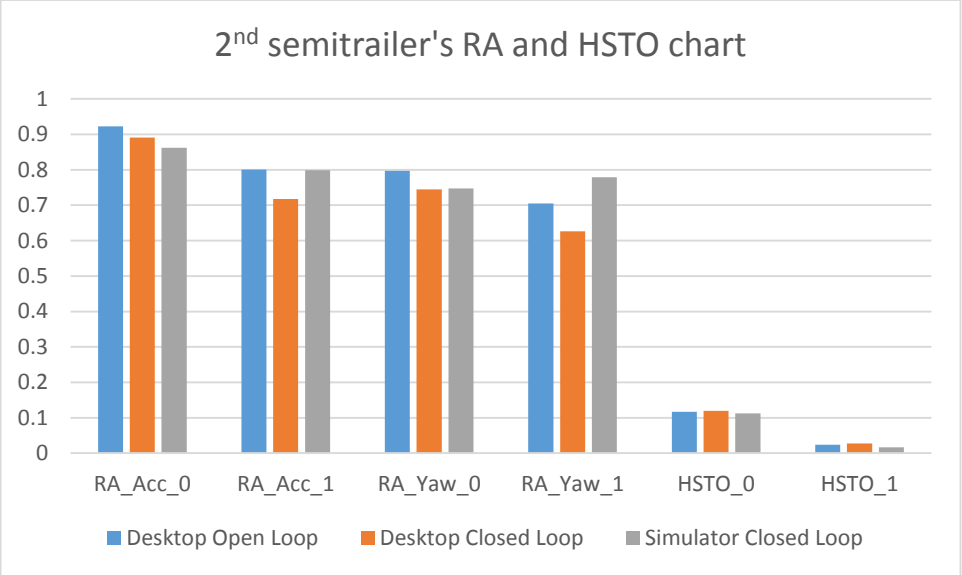

(b)

Figure 4-15. Measures of the RA and HSTO of: (a) semitrailer 1; and (b): semitrailer 2.

Table 4-4 offers the measures of HSTO and RA of the first trailer without ATS derived from the numerical and real-time simulations under the closed-loop maneuver. As shown in the table, the relative errors of $RA\_Acc\_0_1$, $RA\_Yaw\_0_1$, and $HSTO\_0_1$ of the first trailer

are -0.11%, 1.46%, and -15.8%, and the corresponding relative errors of the second trailer are -3.25%, 0.27%, and -6.67%. The relative errors of the results between the real-time and numerical simulations further confirm the fact that in the case of the DTAHV without ATS, the results derived from the real-time and numerical simulations under the closed-loop maneuver are in good agreement. The real-time simulation results validate the results based on the numerical simulation under the closed-loop maneuver.

In contrast with the results shown in Table 4-4, simulation results listed in Table 4-5 disclose the fact that in the case of the DTAHV with ATS, the performance measures predicted by the real-time simulation deviate from those estimated by the numerical simulation under the closed-loop maneuver. As shown in Table 4-5, compared with the results based on the numerical simulation, the performance measures predicted by the real-time simulation on the DHIL platform are larger, and the highest relative error could be -80.0%. The performance degradation of the DTAHV with ATS based on the real-time simulation may be attributed to the following reasons: 1) the wireless communication for data exchange between the UOIT vehicle simulator and the physical prototype of the ATS axle; and 2) zero payload on the ATS axles. It is indicated that the time delay due to the wireless communication can result in the performance degradation of ATS systems [55]. It should be noted that under a low-speed (10 km/h) path following maneuver, the real-time simulation results based on the DHIL platform and the performance measures based on numerical simulation achieved excellent agreement [43]. This implies that under a high-speed maneuver, the ATS controller has higher requirement on the time delay of the wireless communication. The zero payload on the ATS axles may lead to large errors of active steering angles of the relevant trailer axle wheels. Due to the performance

degradation of the DTAHV with ATS based on the DHIL real-time simulation, the following analysis and discussion is focused on the results derived from the numerical simulation on desktop computers.

Table 4-6 provides the RA measures of the first and second semitrailers without ATS under the open-loop and closed-loop test maneuvers. A close observation of the results shown in Table 6 discloses that in the case of the DTAHV without ATS, compared with the results derived from the open-loop simulation, the RA measures based on the closed-loop simulation are smaller. As shown in Table 4-6, among the four RA measures, the minimum relative error (absolute value) is 2.84%, the maximum relative error (absolute value) is 8.52%, and the average relative error of the four measures (absolute value) is 5.34%. Table 4-7 offers the RA measures of the first and second semitrailers with ATS under the open-loop and closed-loop test maneuvers. As in the case of the DTAHV without ATS shown in Table 4-6, in the case of the DTAHV with ATS shown in Table 4-7, the RA measures based on the closed-loop maneuver are smaller than those derived from the open-loop maneuver. However, the relative error of each RA measure (absolute value) listed in Table 4-7 is much larger than its counterpart shown in Table 4-6. As shown in Table 4-7, among the four RA measures, the minimum relative error (absolute value) is 9.68%, the maximum relative error (absolute value) is 11.9%, and the average relative error of the four measures (absolute value) is 10.8%. The numerical results shown in Tables 4-6 and 4-7 quantitatively confirm the previous finding that the difference between the RA measures without ATS under the open-loop and closed-loop maneuvers is smaller than that with ATS under the two SLC test maneuvers. In other words, in the case of the DTAHV without ATS, the RA measures based on the open-loop and closed-loop test maneuvers are in very good agreement.

However, in the case of the DTAHV with ATS, the RA measures derived under the closed-loop test maneuver deviate from those achieved under the open-loop maneuver.

Table 4-4. HSTO measures and RA measures of the lateral acceleration and the yaw rate of the semitrailers without ATS derived under the closed-loop maneuver.

	RA_Acc_0_1[a]	RA_Yaw_0_1	HSTO_0_1 (m)	RA_Acc_0_2[b]	RA_Yaw_0_2	HSTO_0_2 (m)
Numerical simulation	0.891	0.820	0.101	0.891	0.745	0.120
Real-time simulation	0.890	0.832	0.085	0.862	0.747	0.112
Relative error [c]	-0.11 %	1.46 %	-15.8 %	-3.25 %	0.27 %	-6.67 %

[a] the subscript 1 means the first semitrailer; [b] the subscript 2 means the second semitrailer; [c] The relative error is defined as the ratio of the difference between the results based on the real-time simulation and the numerical simulation to that based on the numerical simulation.

Table 4-5. HSTO measures and RA measures of the lateral acceleration and the yaw rate of the semitrailers with ATS derived under the closed-loop maneuver.

	RA_Acc_1_1[a]	RA_Yaw_1_1	HSTO_1_1 (m)	RA_Acc_1_2[b]	RA_Yaw_1_2	HSTO_1_2 (m)
Numerical simulation	0.942	0.587	0.045	0.718	0.626	0.010
Real-time simulation	1.016	0.729	0.009	0.877	0.779	0.068
Relative error [c]	7.86 %	24.2%	-80.0 %	22.2 %	24.4%	-37.0 %

[a] the subscript 1 means the first semitrailer; [b] the subscript 2 means the second semitrailer; [c] The relative error is defined as the ratio of the difference between the results based on the real-time simulation and the numerical simulation to that based on the numerical simulation.

Table 4-6. RA measures of the lateral acceleration and the yaw rate of each semitrailer without ATS derived under the open- and closed-loop maneuvers.

	RA_Acc_0_1[a]	RA_Yaw_0_1	RA_Acc_0_2[b]	RA_Yaw_0_2
Open-loop	0.974	0.844	0.923	0.797
Closed-loop	0.891	0.820	0.891	0.745
Relative error [c]	-8.52 %	-2.84 %	-3.47 %	-6.52 %

[a] The subscript 1 means the first semitrailer; [b] The subscript 2 means the second semitrailer; [c] The relative error is defined as the ratio of the difference between the results based on the closed-loop simulation and the open-loop simulation to that based on the open-loop simulation.

Table 4-7. RA measures of the lateral acceleration and the yaw rate of each semitrailer with ATS derived under the open- and closed-loop maneuvers.

	$RA\_Acc\_1_1$[a]	$RA\_Yaw\_1_1$	$RA\_Acc\_1_2$[b]	$RA\_Yaw\_1_2$
Open-loop	1.043	0.666	0.801	0.705
Closed-loop	0.942	0.587	0.718	0.626
Relative error [c]	-9.68 %	-11.9 %	9.76 %	-11.2 %

[a] The subscript 1 means the first semitrailer; [b] The subscript 2 means the second semitrailer; [c] The relative error is defined as the ratio of the difference between the results based on the closed-loop simulation and the open-loop simulation to that based on the open-loop simulation.

The aforementioned finding implies that in the case of the DTAHV without ATS, both the open-loop and closed-loop test maneuvers are valid for determining the RA measures. In the case of the DTAHV with ATS, however, the closed-loop maneuver may be more applicable than the open-loop maneuver for acquiring the RA measures [10, 11]. In order to justify the applicability of the closed-loop maneuver for acquiring the RA measures for the DTAHV with ATS, we focus our analysis on the peak lateral acceleration of the tractor under the open-loop and the closed-loop test maneuvers. As shown in Figs. 4-6(a) and 4-6(b), under the open-loop test maneuver, the peak lateral acceleration of the tractor for the case without ATS is 0.155 g, while the peak lateral acceleration of the tractor for the case with ATS is 0.141g. The relative error of the latter with respect to the former is -9.03%. As illustrated in Figs. 4-8(a) and 4-8(b), under the closed-loop test maneuver, the peak lateral acceleration of the tractor for the case without ATS is 0.165 g, while the peak lateral acceleration of the tractor for the case with ATS is 0.158 g. The relative error of the latter with respect to the former is only -4.24 %.

The above relative errors disclose the following findings: 1) under both the open-loop and closed-loop test maneuvers, the peak lateral acceleration of the tractor for the case with ATS is smaller than that for the case without ATS; and 2) the relative error of the peak lateral acceleration under the open-loop test maneuver is much larger than that under the closed-loop maneuver. The first finding may be explained with the fact that the ATS system leads to the suppression of the rearward amplification of the DTAHV, and the increased yaw damping due to the ATS control results in the decrease of the peak lateral acceleration of the tractor.

The second finding could be interpreted with the distinguished features of the two SLC test maneuvers. Under the closed-loop test maneuver, even though the RA suppression effect due to the ATS system may cause the decrease of the peak lateral acceleration of the tractor, the virtual driver continuously adjusts the steering wheel angle in order to make the tractor follow the predefined trajectory, and the resulting drop of the peak lateral acceleration of the tractor can be controlled within the acceptable range. Under this maneuver, the desired single sine-wave lateral acceleration input of the tractor may be guaranteed if the tractor could precisely follow the predefined trajectory. Thus, the RA of the DTAHV could be effectively excited, and acquiring RA measures may be precisely and reasonably represent the dynamic behavior of the DTAHV, no matter whether the vehicle is equipped with the ATS system or not. Under the open-loop test maneuver with the given steering wheel angle, the time history of the lateral acceleration of the tractor is dependent on whether the DTAHV is equipped with the ATS system or not. This case dependent feature of the open-loop test maneuver may well explain the phenomenon reported in [10]: with a given tractor front wheel steering angle input, an articulated heavy vehicle without ATS can conduct a

SLC test maneuver with a specific lateral displacement; with the same tractor front wheel steering angle input, the articulated heavy vehicle with an ATS system, however, can only complete a SLC with less lateral displacement due to the RA suppression effect of the ATS system. Thus, the open-loop maneuver may not be applicable for acquiring the RA measures of the DTAHV with ATS, at least this maneuver is not suitable for comparing the RA measures of the DTAHV equipped with and without an ATS system.

5 MRAC for ATS System Design of STAHV

5.1 Introduction

LQR technique has been widely adopted to design ATS controller of AHVs. Such ATS system is designed under the assumption that vehicle forward speed and semitrailer's payload are given and remain as constants. In reality, vehicle forward speed, semitrailer's payload, and other external disturbances are inevitably changing. Therefore, LQR technique has difficulties ensuring robust lateral stability of AHVs in designing ATS controller over a wide range of vehicle system parameter uncertainties and various operating conditions. In contrast, MRAC technique offers flexibility in guaranteeing the robustness of lateral stability of AHVs with ATS controller. Simulation results derived from MATLAB/SIMULINK & TruckSim co-simulation demonstrate that MRAC technique can achieve robust lateral stability of STAHVs despite of varied semitrailer payload and vehicle forward speed.

5.2 STAHV Modelling

5.2.1 Linear Yaw-Plane Model

It is reported that vehicle active steering techniques are effective under maneuvers at low lateral accelerations [64]. Moreover, it is indicated that ATS systems for AHVs are mainly used in maneuvers when lateral acceleration is lower than 0.35g, below which linear AHV

models are justified [62]. Thus, in the present research, a linear yaw-plane STAHV model is generated to derive the reference model.

As shown in Fig. 5-1, the STAHV consists of a tractor with two axles and a semitrailer with three axles, which are represented by an equivalent trailer axle. The vehicle system is telescoped laterally and each axle set is represented by one wheel. Based on the body-fixed coordinate systems $x_1 - y_1$ and $x_2 - y_2$ for the tractor and semitrailer, respectively, the governing equations of the model can be derived.

The motions considered are tractor side-slip angle β_1, tractor yaw rate $\dot{\psi}_1$, and articulation angle $\Delta\psi$, between the tractor and semitrailer. In this model, the aerodynamic forces, the rolling and pitching motions, and the longitudinal forces between tire and road are ignored. To derive the vehicle model, the following assumptions have been made: (1) the tractor forward speed U_1 is constant; (2) the trailer forward speed is the same as that of the tractor; (3) tractor front wheel steer angle δ_{1f} is small; (4) the articulation angle $\Delta\psi$ is small; (5) all products of variables are ignored; and (6) tire side-slip angles are small, and the lateral tire force is a linear function of the tire side-slip angle.

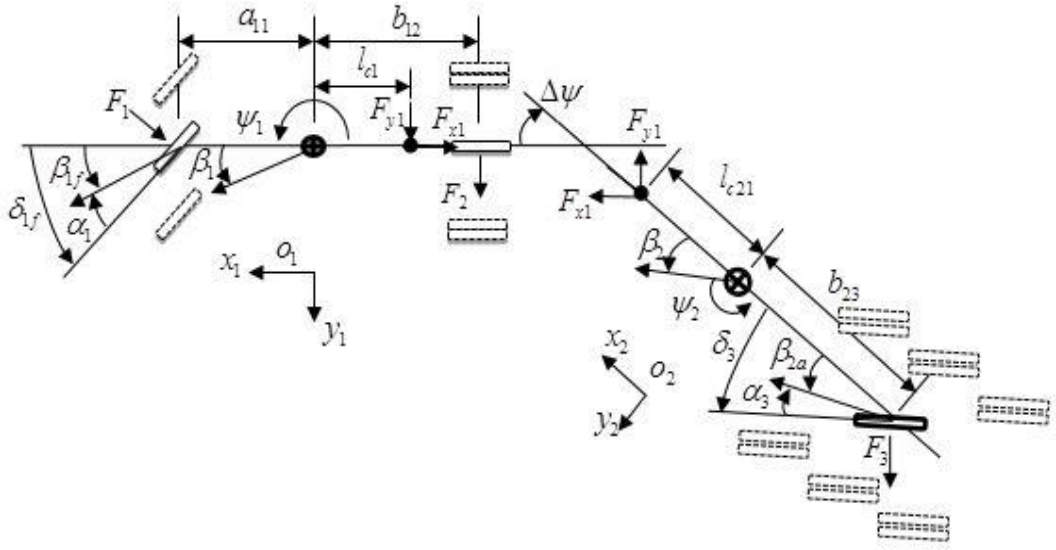

Figure 5-1. Schematic representation of linear yaw-plane model for STAHV.

Based on Newton's law of dynamics, the equations of motion of the tractor are derived as

$$m_1 U_1\left(\dot{\psi}_1 + \dot{\beta}_1\right) = F_1 + F_2 + F_{y1} \tag{5.1.a}$$

$$I_{zz1}\ddot{\psi}_1 = F_1 a_{11} - F_2 b_{12} - F_{y1} l_{c1} \tag{5.1.b}$$

and the equations of motion of the semitrailer are given as

$$m_2 U_2\left(\dot{\psi}_2 + \dot{\beta}_2\right) = F_3 - F_{y1} \tag{5.2.a}$$

$$I_{zz2}\ddot{\psi}_2 = -F_3 b_{23} - F_{y1} l_{c21} \tag{5.2.b}$$

As shown in Figure 1, the following geometric relationships are held:

$$\alpha_1 = \beta_1 + \left(\frac{a_{11}}{U_1}\right)\dot{\psi}_1 - \delta_{1f} \tag{5.3.a}$$

$$\alpha_2 = \beta_1 - \left(\frac{b_{12}}{U_1}\right)\dot{\psi}_1 \tag{5.3.b}$$

$$\Delta\psi = \psi_2 - \psi_1 \tag{5.3.c}$$

$$\alpha_3 = \beta_1 - \Delta\psi - \frac{l_{c21}+b_{23}+l_{c1}}{U_1}\dot{\psi}_1 - \frac{l_{c21}+b_{23}}{U_2}\Delta\dot{\psi} - \delta_3 \tag{5.3.d}$$

$$\beta_2 = \beta_1 - \Delta\psi - \frac{l_{c1}+l_{c21}}{U_1}\dot{\psi}_1 - \frac{l_{c21}}{U_2}\Delta\dot{\psi} \tag{5.3.e}$$

The lateral tire force is determined by its linear relationship with the corresponding tire side-slip angle:

$$F_1 = -C_{f1}\alpha_1 \tag{5.4.a}$$

$$F_2 = -C_{r12}\alpha_2 \tag{5.4.b}$$

$$F_3 = -C_{r23}\alpha_3 \tag{5.4.c}$$

Eliminate the coupling force F_{y1}in Eq. (5.1) and Eq. (5.2), then back-substitute Eq. (5.3) and Eq. (5.4) into Eq. (5.1) and Eq. (5.2) to generate the following state-space form:

$$\mathbf{M}\dot{\boldsymbol{x_p}} = \mathbf{P}\boldsymbol{x_p} + \mathbf{H_1}u + \mathbf{H_2}\delta_{1f} \tag{5.5}$$

where matrices $\mathbf{M}$, $\mathbf{P}$, $\mathbf{H_1}$, and $\mathbf{H_2}$ are given in Appendix 4, the state variable vector is defined as $\boldsymbol{x_p} = [\dot{\psi}_1,\ \Delta\dot{\psi},\ \beta_1,\ \Delta\psi]$, and the control variable vector is specified as $u = [\delta_3]$. The state-space form of the yaw plane model can be further inferred from Eq. (5.5), resulting in:

$$\dot{\boldsymbol{x}}_{\boldsymbol{p}} = \mathbf{A}\boldsymbol{x_p} + \mathbf{B_1}u + \mathbf{B_2}\delta_{1f} \tag{5.6}$$

where $\mathbf{A} = \mathbf{M^{-1}P}$, $\mathbf{B_1} = \mathbf{M^{-1}H_1}$, $\mathbf{B_2} = \mathbf{M^{-1}H_2}$. The output of this system is chosen as the semitrailer's lateral acceleration. With the state space equation generated above, the output equation is derived as:

$$y_p = \mathbf{C}\boldsymbol{x_p} + \mathbf{D_1}u + \mathbf{D_2}\delta_{1f} \tag{5.7}$$

where the notations and values are listed in Appendix 3. The matrices $\mathbf{C}$, $\mathbf{D_1}$, and $\mathbf{D_2}$ are given in the Appendix 4.

5.2.2 Nonlinear Yaw-Roll Model

In order to conduct co-simulation for evaluating the performance of proposed MRAC, a nonlinear yaw-roll STAHV model is developed using TruckSim software package. Both yaw-plane model and nonlinear yaw-roll model share the same configuration and vehicle system parameters. The values of key parameters for both linear and nonlinear models are listed in Appendix 3. Fig. 1-2 shows the nonlinear TruckSim model.

5.3 Design of MRAC

5.3.1 Controller Structure

The MRAC controller is designed following the MRAC framework reported in Ref. [65]. The controller structure shown in Fig. 5-2 includes a controller gain $k(t)$, a feedforward control loop with the parameter $\theta_1(t)$, and a feedback control loop with the parameters $\theta_0(t)$ and $\theta_2(t)$. The control input $u(t)$ is composed of the controllers mentioned above and the tuner that $\omega_1(t)$ and $\omega_2(t)$. The controller is completely described by the following differential equations:

$$\dot{\omega_1}(t) = \Lambda\omega_1(t) + \iota u(t) \tag{5.8.a}$$

$$\dot{\omega_2}(t) = \Lambda\omega_2(t) + \iota y_p(t) \tag{5.8.b}$$

$$\theta(t) = \left[k(t), {\theta_1}^T(t), \theta_0(t), {\theta_2}^T(t)\right]^T \tag{5.8.c}$$

$$\omega(t) = \left[r(t), {\omega_1}^T(t), y_p(t), {\omega_2}^T(t)\right]^T \tag{5.8.d}$$

$$u(t) = \theta^T(t)\omega(t) \tag{5.8.e}$$

where $k(t)$, θ_0, θ_1, and θ_2 are adaptive, which will be expressed in the following section, and Λ is an asymptotically stable matrix. The values for Λ and ι are achieved through online tuning.

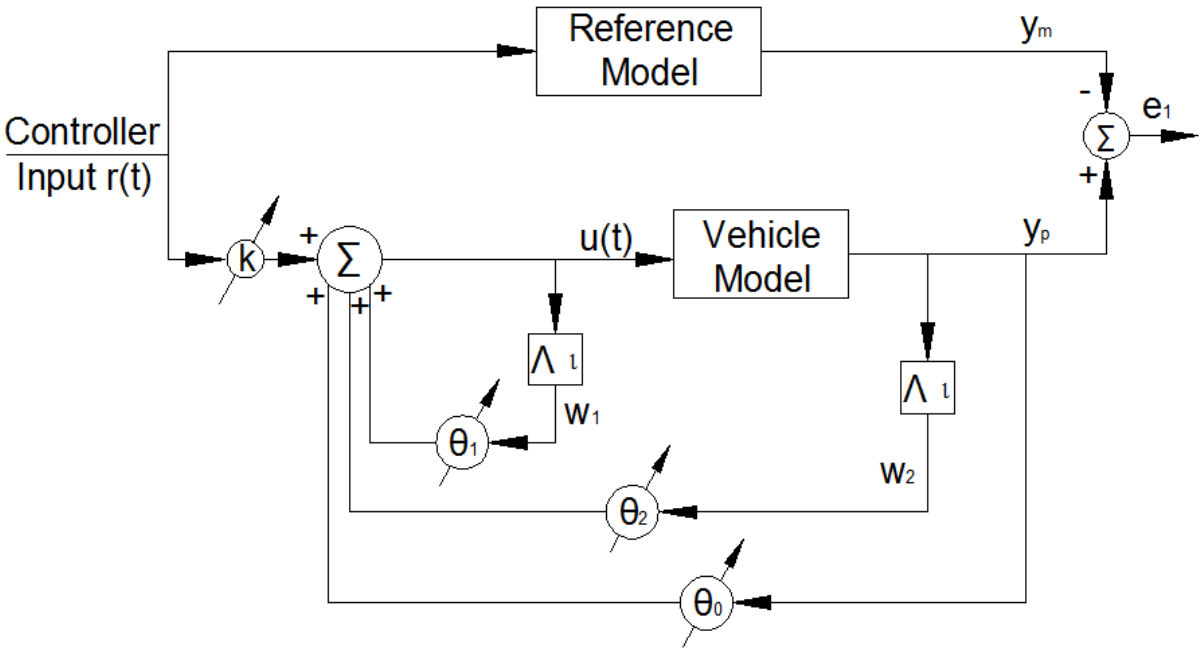

Figure 5-2. Structure of the proposed MRAC controller.

5.3.2 Adaptive Law

Define the following parameter errors, in which the variables denoted with an asterisk '*' mean the 'true' adaptation parameter values that:

$$\tilde{k}(t) = k(t) - k^* \tag{5.9.a}$$

$$\widetilde{\theta_0}(t) = \theta_0(t) - \theta_0{}^* \tag{5.9.b}$$

$$\widetilde{\theta_1}(t) = \theta_1(t) - \theta_1{}^* \tag{5.9.c}$$

$$\widetilde{\theta_2}(t) = \theta_2(t) - \theta_2{}^* \tag{5.9.d}$$

$$\boldsymbol{\Phi}(\boldsymbol{t}) = \left[\tilde{k}(t), \widetilde{\theta_1}^T(t), \widetilde{\theta_0}(t), \widetilde{\theta_2}^T(t)\right]^T \tag{5.9.e}$$

where the values of 'true' adaptation parameters are also obtained through online tuning.

Substituting Eq. (5.8) and Eq. (5.9) into output equation, which is Eq. (5.7), yields the augmented output vector for the linear yaw-plane STAHV model

$$\mathrm{y} = \mathbf{C_{mn}}\boldsymbol{x} + \mathbf{D_{mn1}}[\boldsymbol{\Phi}^T\omega + k^*r] + \mathbf{D_{mn2}}\delta_{1f} \tag{5.10}$$

where $\mathbf{C_{mn}}$, $\mathbf{D_{mn1}}$, and $\mathbf{D_{mn2}}$ are shown in Appendix 2, and $\boldsymbol{x} = \left[\boldsymbol{x_p}, \omega_1, \omega_2\right]^T$.

Substituting Eq. (5.8), Eq. (5.9), and Eq. (5.10) into Eq. (5.6), Eq. (5.8.a), and Eq. (5.8.b) yields the augmented state vector for the linear yaw-plane STAHV model

$$\dot{\boldsymbol{x}} = \mathbf{A_{mn}}\boldsymbol{x} + \mathbf{B_{mn1}}[\boldsymbol{\Phi}^T\omega + k^*r] + \mathbf{B_{mn2}}\delta_{1f} \tag{5.11}$$

where $\mathbf{A_{mn}}$, $\mathbf{B_{mn1}}$, and $\mathbf{B_{mn2}}$ are shown in Appendix 4.

Therefore, the reference model can be described in the following two differential equations:

$$\dot{\boldsymbol{x}}_{\boldsymbol{m}} = \mathbf{A_{mn}}\boldsymbol{x_m} + \mathbf{B_{mn1}}k^*r + \boldsymbol{B_{mn2}}\delta_{1f} \tag{5.12}$$

$$\mathrm{y}_m = \mathbf{C_{mn}}\boldsymbol{x_m} + \mathbf{D_{mn1}}k^*r + \mathbf{D_{mn2}}\delta_{1f} \tag{5.13}$$

where $\boldsymbol{x_m} = \left[\boldsymbol{x_p^*}, \omega_1^*, \omega_2^*\right]$. The error equation for the augmented vehicle model could be written as:

$$\dot{\boldsymbol{e}} = \mathbf{A_{mn}}\boldsymbol{e} + \mathbf{B_{mn1}}\boldsymbol{\Phi}^T\omega \tag{5.14.a}$$

$$e_1 = \mathbf{C_{mn}}\boldsymbol{e} + \mathbf{D_{mn1}}\boldsymbol{\Phi^T}\omega \tag{5.14.b}$$

According to Lemma 5.1 in Ref. [65], the adaptive laws can be adjusted as:

$$\dot{k} = -sgn(k_p)e_1r \tag{5.15.a}$$

$$\dot{\theta_0} = -sgn(k_p)e_1 y_p \tag{5.15.b}$$

$$\dot{\theta_1} = -sgn(k_p)e_1 \omega_1 \tag{5.15.c}$$

$$\dot{\theta_2} = -sgn(k_p)e_1 \omega_2 \tag{5.15.d}$$

Thus, Eq. (5.14) will be uniformly stable.

5.3.3 Control Input to Reference Model

The control input, which is the steering angle of the wheels on the semitrailer axles of reference model, is generated using the LQR technique. The performance index for LQR controller is specified as

$$J = \int_0^\infty \left(y_m^T q y_m + u'^T r u'\right) dt \tag{5.16}$$

where q and r are weighting matrices. Substituting the augmented output vector expressed in Eq. (5.13) into Eq. (5.16) leads to the performance index in terms of the augmented state vector

$$J = \int_0^\infty \left(\boldsymbol{x_m^T} Q \boldsymbol{x_m} + u'^T R u' + x_m^T N u'\right) dt \tag{5.17}$$

where $\mathbf{Q} = \mathbf{C^T} q \mathbf{C}$, $\mathbf{R} = \mathbf{D_1^T} r \mathbf{D_1}$, $\mathbf{N} = \mathbf{C^T} n \mathbf{D_1}$. The parameters that q, r, n are obtained by on-line tuning. Minimize Eq. (5.17) to determine controller gain K, and then the optimal controller input to reference model can be determined by the following equation:

$$u' = -Kx \tag{5.18}$$

Note that u' in Eq. (5.18) has the different meaning from the u in Eq. (5.8). u' is the controller input to reference model; while u is the controller input to the TruckSim nonlinear model.

5.4 Simulation Results and Discussion

To test the performance of MRAC controller designed using linear yaw-plane vehicle model, the controller developed in MATLAB/SIMULINK is interfaced with TruckSim software package. Under an emulated SLC closed loop test maneuver, MATLAB/SIMULINK & TruckSim co-simulations have been conducted using the corresponding TruckSim model with or without the MRAC. The test course is shown in Fig. 2-7.

The objective is to examine the lateral acceleration at the semitrailer CG and then compare it to that of reference model. To accomplish this, the MATLAB/SIMULINK & TruckSim simulations under SLC test maneuver are conducted in four scenarios: 1) nominal semitrailer payload at vehicle forward speed of 88km/h; 2) varied semitrailer payload at vehicle forward speed of 88km/h; 3) nominal semitrailer payload at varied vehicle forward speed; 4) varied semitrailer payload at varied vehicle forward speed.

5.4.1 Simulation Results

Fig. 5-3 shows the simulation results acquired in first scenario. This figure illustrates the lateral acceleration at the CG of tractor and semitrailer in four cases: i) reference model, ii) TruckSim model with MRAC, iii) TruckSim model with LQR, iv) TruckSim model without control. The peak values of lateral acceleration for each case, the absolute relative errors between the reference signal and the TruckSim model with MRAC, and the RA measurements of lateral acceleration for TruckSim models are provided in Table 5-1.

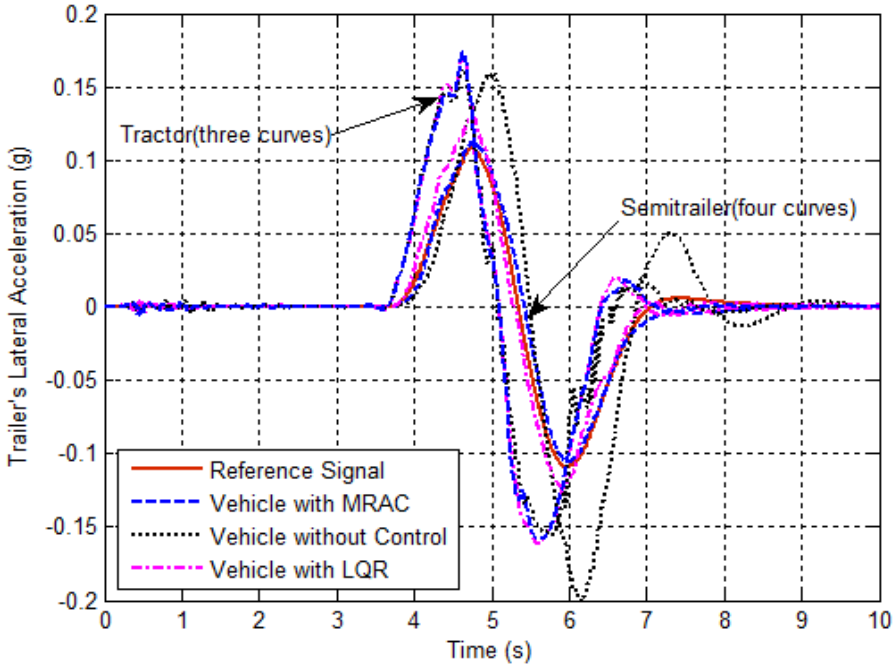

Figure 5-3. Simulation results achieved in first scenario for four cases: i) reference model, ii) TruckSim model with MRAC, iii) TruckSim model with LQR, iv) TruckSim model without control.

Table 5-1. . Peak values of lateral acceleration of each model, the absolute relative errors of peak values between the reference signal and the MRAC-loaded TruckSim model, and the RA measurements of lateral acceleration for TruckSim models in the first scenario.

	First Peak	Second Peak	RA
Reference Signal	0.108g	-0.109g	--
Vehicle with MRAC	0.112g	-0.106g	0.647
Absolute Relative Error	3.70%	2.75%	--
Vehicle with LQR	0.130g	-0.122g	0.756
Vehicle without MRAC	0.159g	-0.198g	1.21

To examine the robustness of MRAC to varied semitrailer payloads, a lower payload (10,000kg less than the nominal semitrailer payload) and a higher payload (10,000kg more than nominal semitrailer payload) are loaded on semitrailer separately. Note that all other vehicle system parameters and testing conditions in the second scenario remain the same as that in the first scenario except the variation of semitrailer's payload. Figs. 5-4 and 5-5 show the simulation results achieved in the second scenario with a lower and a higher semitrailer payload, respectively. The figures illustrate the lateral acceleration at the CG of tractor and semitrailer in following four cases: i) reference model, ii) TruckSim model with MRAC, iii) TruckSim model with LQR, iv) TruckSim model without control. Table 5-2 lists the peak values of lateral acceleration at semitrailer CG for each case, absolute relative errors between the reference model and TruckSim model with MRAC, and RA measurements of lateral acceleration for TruckSim models in this scenario.

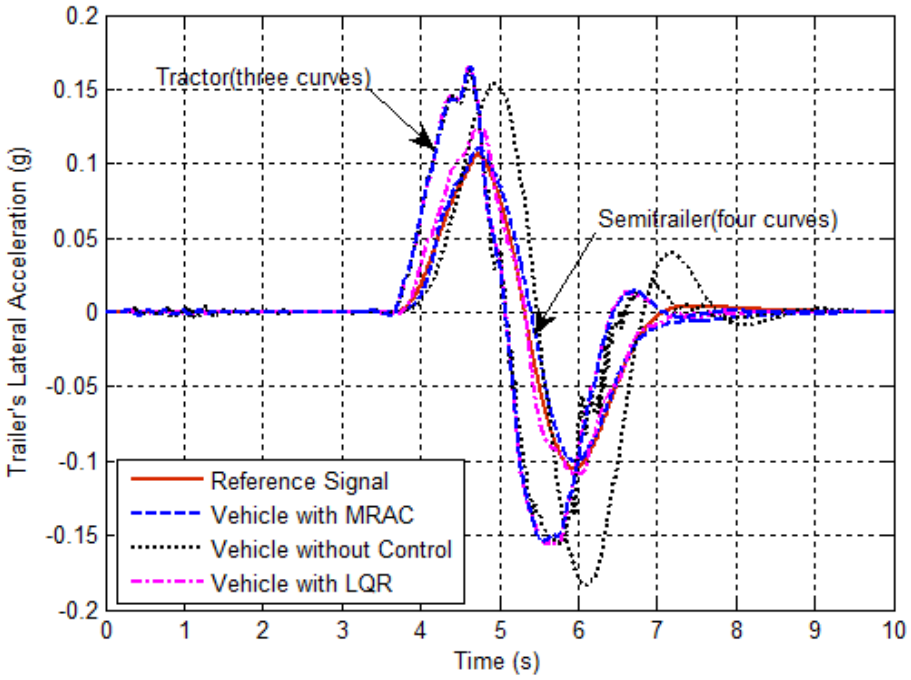

Figure 5-4. Simulation results achieved in the second scenario with a lower semitrailer payload for four cases: i) reference model, ii) TruckSim model with MRAC, iii) TruckSim model with LQR, iv) TruckSim model without control.

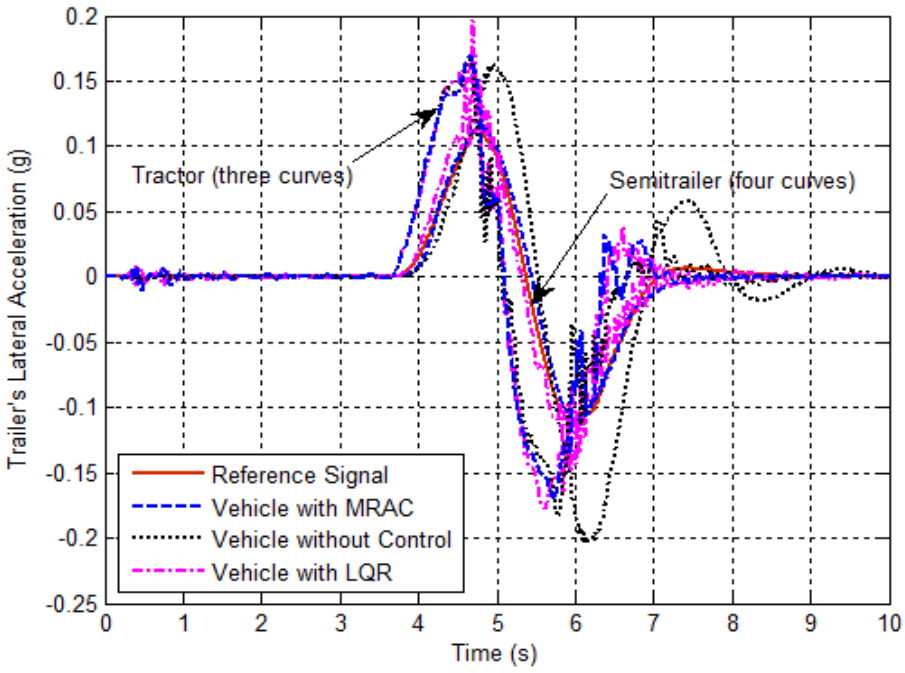

Figure 5-5. . Simulation results achieved in the second scenario with a higher semitrailer payload for four cases: i) reference model, ii) TruckSim model without MRAC, iii) TruckSim model with LQR, iv) TruckSim model without control.

Table 5-2. Peak values of lateral acceleration of each case, absolute relative errors of peak values between the reference signal and the MRAC-loaded TruckSim model, and the RA measurements of lateral acceleration for TruckSim models in the second scenario.

	First Peak (less payload)	Second Peak (less payload)	RA	First Peak (more payload)	Second Peak (more payload)	RA
Reference Signal	0.106g	-0.105g	--	0.112g	-0.113g	--
Vehicle with MRAC	0.110g	-0.100g	0.663	0.118g	-0.116g	0.694
Absolute Relative Error	3.78%	4.76%	--	5.36%	2.65%	--
Vehicle with LQR	0.125g	-0.109g	0.753	0.156g	-0.165g	0.825
Vehicle without Control	0.154g	-0.184g	1.13	0.163g	-0.204g	1.11

Figs. 5-6 and 5-7 show the simulation results achieved in the third scenario with a lower vehicle forward speed (76 km/h) and a higher vehicle forward speed (100 km/h), respectively. Note that all other vehicle system parameters and testing conditions in the third scenario remain the same as that in the first scenario except the variation of vehicle forward speed. The figures illustrate the lateral acceleration at the CG of tractor and semitrailer in the following four cases: i) reference model, ii) TruckSim model with MRAC, iii) TruckSim model with LQR, iv) TruckSim model without control. Table 5-3 lists the peak values of lateral acceleration at semitrailer CG for the above four cases, absolute relative errors between the reference model and the TruckSim model with MRAC, and the RA measurements of lateral acceleration for TruckSim models in this scenario.

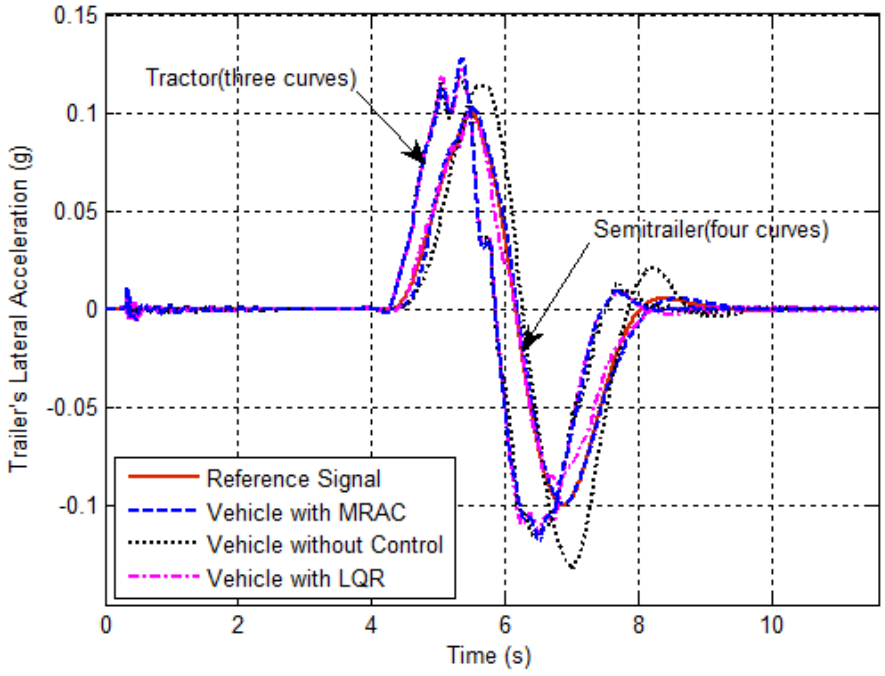

Figure 5-6. Simulation results achieved in the third scenario at vehicle forward speed of 76 km/h for four cases: i) reference model, ii) TruckSim model with MRAC, iii) TruckSim model with LQR, iv) TruckSim model without control.

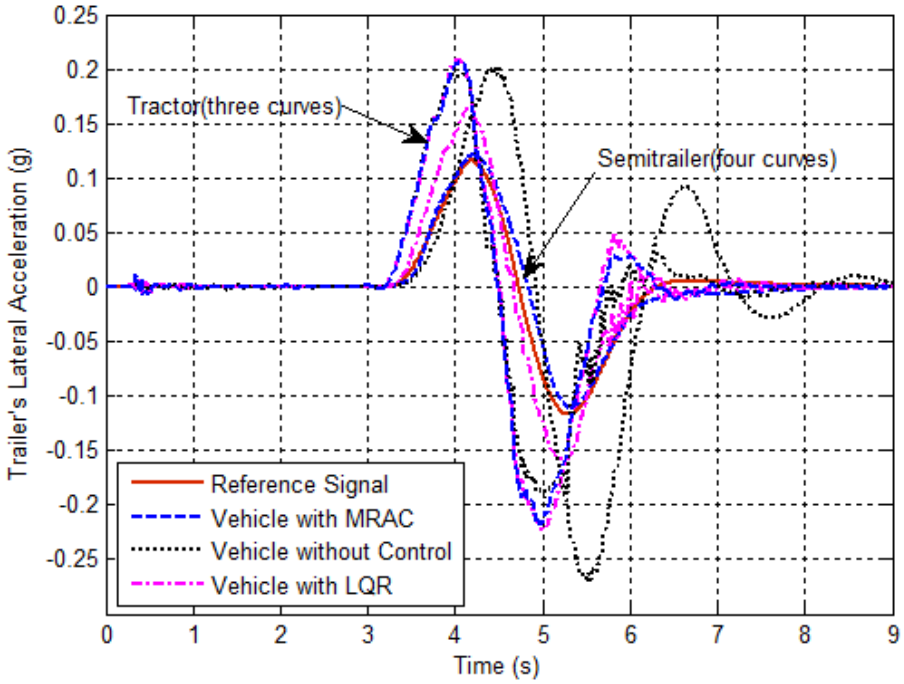

Figure 5-7. Simulation results achieved in the third scenario at vehicle forward speed of 100 km/h for four cases: i) reference model, ii) TruckSim model with MRAC, iii) TruckSim model with LQR, iv) TruckSim model without control.

Table 5-3. Peak values of lateral acceleration of each model, absolute relative errors of peak values between the reference signal and the MRAC-loaded TruckSim model, and the RA measurements of lateral acceleration for TruckSim models in the third scenario.

	First Peak (less speed)	Second Peak (less speed)	RA	First Peak (more speed)	Second Peak (more speed)	RA
Reference Signal	0.100g	-0.100g	--	0.116g	-0.117g	--
Vehicle with MRAC	0.102g	-0.099g	0.803	0.121g	-0.111g	0.558
Absolute Relative Error	2.00%	1.00%	--	4.31%	5.13%	--
Vehicle with LQR	0.100g	-0.088g	0.813	0.164g	-0.158g	0.735
Vehicle without Control	0.113g	-0.131g	1.11	0.202g	-0.270g	1.38

Fig. 5-8 shows the simulation results achieved in the fourth scenario with a lower semitrailer payload (10,000 kg less than the nominal trailer payload) and a smaller vehicle forward speed (76 km/h). This figure illustrates the lateral acceleration at CG of tractor and semitrailer in the following four cases: i) reference model, ii) TruckSim model with MRAC, iii) TruckSim model with LQR, iv) TruckSim model without control. Fig. 5-9 shows the simulation results achieved in the fourth scenario with a higher semitrailer payload (10,000 kg more than the nominal trailer payload) and a larger vehicle forward speed (100 km/h). This figure illustrates the lateral acceleration at CG of tractor and semitrailer in four cases: i) reference model, ii) TruckSim model with MRAC, iii) TruckSim model with LQR, iv) TruckSim model without control. Table 5-4 provides the corresponding peak values of lateral acceleration of each case, absolute relative errors between the reference signal and the MRAC-loaded TruckSim model, and the RA measurements of lateral acceleration for TruckSim models in this scenario.

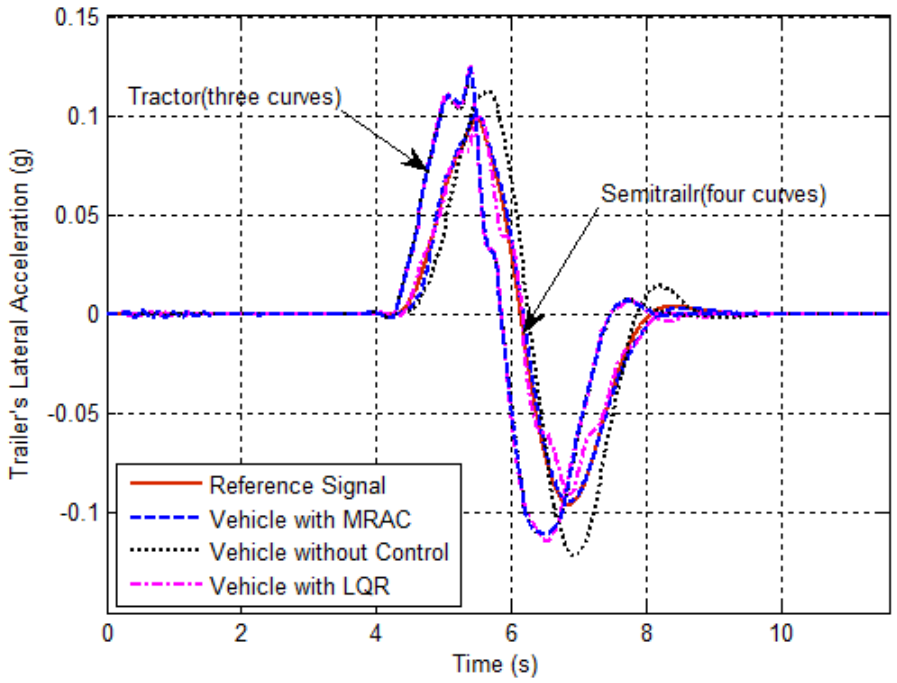

Figure 5-8. Simulation results achieved in the fourth scenario with a lower semitrailer payload and a smaller vehicle forward speed for four cases: i) reference model, ii) TruckSim model with LQR, iii) TruckSim model with MRAC, iv) TruckSim model without control.

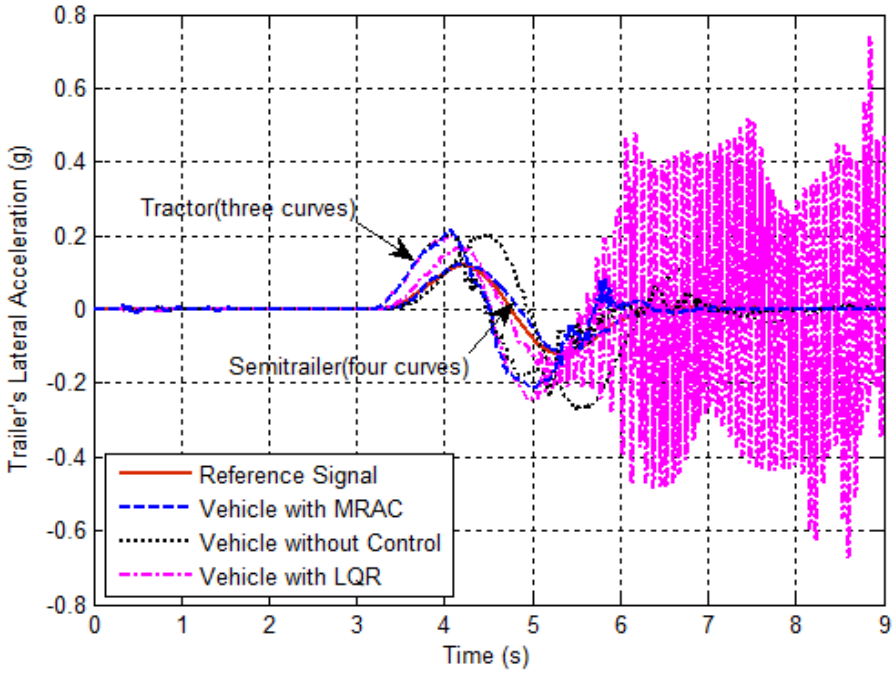

Figure 5-9. Simulation results achieved in the fourth scenario with a higher semitrailer payload and a larger vehicle forward speed for three cases: i) reference model, ii) TruckSim model with MRAC, iii) TruckSim model with LQR, iv) TruckSim model without control.

Table 5-4. Peak values of lateral acceleration of each model, absolute relative errors of peak values between the reference signal and the MRAC-loaded TruckSim model, RA measurements of lateral acceleration for TruckSim models in the fourth scenario.

	First Peak (less speed & payload)	Second Peak (less speed & payload)	RA	First Peak (more speed & payload)	Second Peak (more speed & payload)	RA
Reference Signal	0.099g	-0.096g	--	0.119g	-0.121g	--
Vehicle with MRAC	0.101g	-0.095g	0.815	0.126g	-0.122g	0.530
Absolute Relative Error	2.02%	1.04%	--	5.88%	0.83%	--
Vehicle with LQR	0.100g	-0.091g	0.800	0.169g	NaN	NaN
Vehicle without control	0.112g	-0.122g	0.992	0.203g	-0.272g	1.14

5.4.2 Simulation Results Analysis

A close observation of results shown in Fig. 5-3 to Fig. 5-9 discloses the phenomena that the semitrailer's lateral acceleration is lowered. From the lateral stability point of view, the lower lateral acceleration of semitrailer results in a lower RA of the AHV, which will reduce semitrailer's tendency to rollover. In Fig. 5-9, it is noticed that the semitrailer's lateral acceleration for vehicle with LQR has a drastic oscillation, which clearly shows the problem in using LQR technique to realize ATS system of STAHV. However, MRAC can deal with the variation of semitrailer's payload and vehicle forward speed fairly well to maintain semitrailer's stable lateral acceleration.

Comparing the two curves with the legends of 'Reference Signal' and 'Vehicle with MRAC' shown from Fig. 5-3 to Fig. 5-9, we find the two curves achieve an excellent agreement. Results listed in Tables 5-1 and 5-4 indicate that the maximum relative error between the two curves is below 6%. Considering the wide variation range of semitrailer's payload and vehicle forward speed, we can conclude that MRAC can ensure the robust lateral stability of AHV.

Focusing on the curve with the legend of 'Vehicle without Control' illustrated in Fig. 5-3 to Fig. 5-9, we can observe that the vehicle forward speed variation imposes more influence on trailer's lateral acceleration than the varied semitrailer's payload, and using LQR technique cannot resolve this problem. However, using MRAC can close the gap between the influence imposed by vehicle forward speed and semitrailer payload. This can be more intuitively demonstrated with the data shown in Tables 5-5, 5-6, and 5-7. Table 5-5 shows the absolute relative errors of the semitrailer's peak values between scenario 1 and scenarios 2, 3, and 4 respectively, in the case of the TruckSim model without control. Table 5-6 shows the absolute relative errors of the semitrailer's peak values between scenario 1 and scenarios 2, 3, and 4 respectively, in the case of the TruckSim model equipped with LQR. Table 5-7 shows the absolute relative errors of the semitrailer's peak values between scenario 1 and scenarios 2, 3, and 4, respectively, in the case of the TruckSim model equipped with MRAC.

Table 5-5. Absolute relative errors of the peak values between scenario 1 and scenarios 2, 3, and 4, respectively, in the case of the TruckSim model without control.

	Less Payload	More Payload	Less Speed	More Speed	Less Payload & Speed	More Payload & Speed
First Peak	3.14%	2.50%	28.9%	27.0%	29.6%	27.7%
Second Peak	7.07%	3.03%	33.8%	36.4%	38.4%	37.4%

Table 5-6. Absolute relative errors of the peak values between scenario 1 and scenarios 2, 3, and 4, respectively, in the case of the TruckSim model with LQR.

	Less Payload	More Payload	Less Speed	More Speed	Less Payload & Speed	More Payload & Speed
First Peak	3.84%	20.0%	23.1%	26.2%	23.1%	30%
Second Peak	10.7%	35.2%	27.9%	29.5%	25.4%	NaN

Table 5-7. Absolute relative errors of the peak values between scenario 1 and scenarios 2, 3, and 4, respectively, in the case of the TruckSim model with MRAC.

	Less Payload	More Payload	Less Speed	More Speed	Less Payload & Speed	More Payload & Speed
First Peak	1.79%	5.36%	8.93%	8.04%	9.82%	12.5%
Second Peak	5.66%	9.43%	6.60%	4.72%	10.4%	15.1%

From Table 5-1 to Table 5-4, it is noticed that the RA of vehicle with MRAC is more subject to variation of semitrailer payload and vehicle forward speed than that with LQR.

This is due to the fact that the reference model is fixed and should be fixed through the whole scenarios during the simulation. The only difference for the reference model relies on the front wheel steering angle, which is extracted directly from TruckSim model during the simulation. Since the simulation is conducted to complete closed-loop SLC test maneuver, the steering wheel angle is almost the same for all scenarios. Therefore, the reference signal (semitrailer's lateral acceleration) is also nearly the same through the whole scenarios, which leads to the nearly invariable semitrailer's lateral acceleration of TruckSim model. However, the tractor's lateral acceleration will clearly change due to the variation of vehicle's forward speed in completing SLC test maneuver. This is why the RA of vehicle with ATS system is subject to changing when MRAC technique is adopted.

6 Conclusions and Recommendations

6.1 Conclusions

This thesis outlines the state-of-the-art of investigations in ATS for AHVs, introduces the motivations of the current research, and describes the methodology employed in the research. The conclusions drawn from the research are summarized as follows.

To push lab research of ATS system of DTAHVs towards real-world application, the DHIL real-time simulation platform based on our exiting driving simulator is developed. Two active steering axles are developed to represent the middle or rear axle of each semitrailer. The connections between those two active steering axles and the existing driving simulator are established using wireless communication.

With respect to the low-speed maneuverability of DTAHVs, the following insightful findings are disclosed in the research: 1) the involvement of the real physical ATS axles may introduce time delay, actuation and control errors of the axles, which will degrade the maneuverability of DTAVHs; 2) the ATS controller can reinforce the low-speed maneuverability of DTAHVs and at the same time reduce tire wear; 3) in curved path negotiations, the ATS controller can mitigate the driver's steering effort; and 4) to negotiate a curved path, certain amount of steering effort from the driver is required to compensate the negative effect of the time delay, the actuation and control errors of ATS axles.

With respect to the high-speed lateral stability, this research examines the applicability of the two SLC test maneuvers specified in ISO-14791 for determining the RA for DTAHVs

with ATS systems. Simulation results conducted in the research reveal the following insightful findings: 1) the RA measures of DTAHVs with an ATS system acquired under the closed-loop SLC test maneuver are smaller than that determined under the open-loop test procedure; 2) for conventional DTAHVs without an ATS system, RA measures calculated under the two SLC test maneuver are in good agreement; 3) compared to the open-loop SLC test maneuver, the closed-loop SLC test procedure is more applicable for determining the RA measures of DTAHVs with an ATS system. The derived results and proposed simulation methods may be used as valuable guideline for the determination of RA of DTAHVs with ATS systems.

To date, the LQR technique has been commonly used to the design of controller for ATS systems. However, we found some problems in using the LQR technique in real-world application, e.g. parametric variation of trailer payload and vehicle forward speed. To explore robustness of ATS controllers, the MRAC technique is introduced for the design of controllers for ATS systems. The MRAC is examined using numerical simulation of a STAHV. Simulation results indicate that the proposed MRAC controller: 1) enables the trailer's lateral acceleration of virtual vehicle to track that of the reference model, and 2) is robust to varied trailer payload and vehicle forward speed.

6.2 Recommendations

6.2.1 DHIL Real-Time Simulation Platform

For the DHIL real-time simulation platform used in the research, further improvements should be made in the following issues: 1) selecting and designing effective wireless

communication networks, and 2) considering the effect of trailer payload of the real physical ATS axles in the DHIL real-time simulation platform.

6.2.2 SLC Test Maneuvers Specified in ISO-14791

This research only selects a DTAHV as an example to examine the applicability of the two SLC test maneuvers specified in ISO-14791 for acquiring RA measures of AHVs with ATS systems. The examination will be more persuasive if other AHV combinations, e.g. A-train double, are tested in the near future.

6.2.3 Application of the MRAC Controller for ATS Systems

The MRAC controller is only tested in this research for Single Input Single Output (SISO) applications. For Multiple Input Multiple Output (MIMO) applications, the MRAC controller is of more interest considering its application to multiple units of DTAHVs.

Reference

[1] M. El-Gindy, N. Mrad, and X. Tong, "Sensitivity of Rearward Amplification Control of A Tractor/Full Trailer to Tyre Cornering Stiffness Variable", Proc. IMechE, Part D: Journal of Automotive Engineering, 2001, Vol. 215, pp. 579-588.

[2] J. Woodrooffe and L. Ash, "Economic Efficiency of Long Combination Transport Vehicle in Alberta", Woodrooffe and Associates, 2001, pp. 1-30.

[3] A.T. McCartt, V.S. Northrup, and R.A. Retting, "Types and Characteristics of Ramp-Related Motor Vehicle Crashes on Urban Interstate Roadways in North Virginia", Journal of Safety Research, 2004, Vol. 35, pp. 107 – 114.

[4] M.M. Islam, Y. He, and T. Hu, "Design Optimization of Multi-Trailer Articulated Heavy Vehicles with Active Safety Systems". In: 23rd symposium on dynamics of vehicles on roads and tracks. IA VSD 13–38. 1-ID358 (the paper number), Qingdao, People's Republic of China, 19-23 August 2013, 10 pages(digital conference proceedings on USB).

[5] M.M. Islam, "Parallel Design Optimization of Multi-Trailer Articulated Heavy Vehicle with Active Safety Systems" PhD Thesis, University of Ontario Institute of Technology, Oshawa, Ontario, Canada, 2013.

[6] S. Kharrazi, M. Lidberg, R. Roebuck, and J. Fredriksson, "A Generic Controller for Improving Lateral Performance of Heavy Vehicle Combinations", Proc IMechE Part D: J Automobile Engineering, 2012; 227(5): 619-642.

[7] K. Rangavajhula and H.S.J. Tsao, “Active Trailer Steering Control of An Articulated System with A Tractor and Three Full Trailers for Tractor-Track Following”, Int. J Heavy Veh. Systems, 2007; 14(3): 271-293.

[8] K. Friedman and J. Hutchinson, “Review of Existing Repeatable Vehicle Rollover Dynamic Physical Testing Methods”, ASME International Mechanical Engineering Congress and Exposition, 2009, Vol. 16, pp. 51-59.

[9] M. Short and M.J. Pont, “Assessment of High-Integrity Embedded Automotive Control System Using Hardware in the Loop Simulation”, Journal of Systems & Software, 2008, Vol. 81(7), pp. 1163-1183.

[10] Y. He, M.M. Islam, and T.D. Webster, “An Integrated Design Method for Articulated Heavy Vehicles with Active Trailer Steering Systems”, 2012, Vol. 119-6, pp. 158-174.

[11] Y. He and M. Islam, “An Automated Design Method for Active Trailer Steering Systems of Articulated Heavy Vehicles”, ASME Journal of Mechanical Design, 2012, Vol.134/041002, pp. 1-15.

[12] Statistics Canada, Transportation, http://www.statcan.gc.ca/pub/11-402-x/2012000/chap/trans/trans01-eng.htm

[13] P. S. Fancher and C.B. Winkler, “Directional Performance Issues in Evaluation and Design of Articulated Heavy Vehicles”, Vehicle System Dynamics, 2007, 45(7-8), pp. 607-647.

[14] Ontario Ministry of Transportation, “Ontario’s Long Combination Vehicle Program”, [online]: http://ontruck.org/ota-classroom-training/ontarios-long-combination-vehicle-program/ (May 7, 2015).

[15] New Brunswick Department of Transportation, 2011, "Guidelines for Long Combination Vehicles (LCVs) in the Province of New Brunswick", Version 5.

[16] Nova Scotia Department of Transportation and Infrastructure Renewal, 2012, "Long Combination Vehicle Program: Program Guidelines".

[17] California Truck Accident Statistics, http://www.esteybomberger.com/california-truck-accident/statistics/

[18] A.T. McCartt, V.S. Northrup, and R.A. Retting, "Types and Characteristics of Ramp-Related Motor Vehicle Crashes on Urban Interstate roadways in North Virginia", Journal of Safety Research, 2004, Vol. 35, pp. 107-114.

[19] Ingersoll Axles, an IMT Company, http://ingersollaxles.com/

[20] Trackaxle Pty Ltd, https://en-gb.facebook.com/trackaxlesolutions

[21] Vehicle System Engineering, "Electronic Trailer Steering", https://www.v-s-e.com/uploads/files/ets_trailer_eng_2009.pdf

[22] M.M. Islam, Y. He, S. Zhu, and Q. Wang, "A Comprehensive Study of Multi-Trailer Articulated Heavy Vehicle Models", Proc. IMechE Part D: J. Automobile Engineering, DOI: 10.1177/0954407014557053, pp. 1-29.

[23] Y. He and J. McPhee, "A Review of Automated Design Synthesis Approaches for Virtual Development of Ground Vehicle Suspensions", SAE paper 2007-01-0856, 2007.

[24] W. Kortum. "Review of Multibody Computer, Codes for Vehicle System Dynamics", Vehicle System Dynamics, 1993, 22(Suppl 1): 3-31.

[25] M.W. Sayers and D. Han, "A Generic Multibody Vehicle Model for Simulating Handling and Braking", Vehicle System Dynamics, 1996, 25 (Suppl. 1): 599-613.

[26] X. Ding, S. Mikaric, and Y. He, “Design of An Active Trailer Steering System for Multi-Trailer Articulated Heavy Vehicles Using Real-Time Simulations”, Journal of Automobile Engineering, 2013, Vol, 227(5), pp. 643-655.

[27] R.J. Anderson and E.F. Kurtz, “Handling-Characteristics Simulations of Car-Trailer Systems”, SAE paper 800545, 1980.

[28] T. Sun, Y. He, and J. Ren, “A Comparative Study of Car-Trailer Dynamics Models”, SAE paper 2013-01-0802, 2013.

[29] T. Sun, Y. He, and J. Ren, “Dynamics Analysis of Car-Trailer Systems with Active Trailer Differential Braking Strategies”, SAE paper 2014-01-0143, 2014.

[30] R. Allen, T. Rosenthal, and H. Szostak, “Steady State and Transient Analysis of Ground Vehicle Handling”, SAE paper 870495, 1987.

[31] D.E. Smith and J.M. Starkey, “Effects of Model Complexity on the Performance of Automated Vehicle Steering Controllers: Controller Development and Evaluation”, Vehicle System Dynamics, 1994, 23(1): 627-645.

[32] D.E. Smith and J.M. Starkey, “Effects of Model Complexity on the Performance of Automated Vehicle Steering Controllers: Model Development, Validation and Comparison”, Vehicle System Dynamics, 1995, 24(2): 163-181.

[33] Society of Automotive Engineers, “A Test for Evaluating the Rearward Amplification of Multi-Articulated Vehicles”, SAE Recommended Practice J2179, Warrendale, USA, 1994.

[34] International Standardization Organization, “Road Vehicles – Heavy Commercial Vehicle Combinations and Articulated Buses – Lateral Stability Test Methods”, ISO-14791: 2000(E), Geneva: International Organization for Standardization; 2000.

[35] Y. He, M. M. Islam, S. Zhu, and T. Hu, "Directional Performance Optimization of Multi-Trailer Articulated Heavy Vehicles with Trailer Lateral Dynamic Control Systems", Under Review, Proceedings of the Institution of Mechanical Engieers, Part D: Journal of Automobile Engineering.

[36] Mechanical Simulation Corporation. TruckSim options, https://www.carsim.com/products/trucksim/package.php

[37] M. W. Sayers, "Vehicle Models for RTS Applications", Vehicle System Dynamics, 1999, 32(4-5): 421-438.

[38] H. Prem, E. Ramsay, J.D. Pont, et al. "Comparison of Modelling System for Performance-Based Assessments of Heavy Vehicles (Performance Based Standards – NRTC/AUSTROADS Project A3 and A4)", Working Paper, National Road Transport Commission, Melbourne, Victoria, Australia, 2001.

[39] MSC Software Corporation. Adams, the multibody dynamics simulation solution, http://www.mscsoftware.com/product/adams (April 6, 2014).

[40] T.D. Gillespie and C.C. MacAdam, "Constant Velocity Yaw/Roll Program – User's Manual", Report UMTRI-82-39, The University of Michigan Transportation Research Institute, Ann Arbor, Michigan, USA, 1982.

[41] P.F. Sweatman and S. McFarlane, "Investigation into the Specification of Heavy Trucks and Consequent Effects on Truck Dynamics and Driver: Final Report", Report Prepared for Federal Office of Road Safety by Roaduser International Pty Ltd, FORS, Canberra, Australia, 2000.

[42] D.J. Latto, "Road Trial for Model Validation. Report to Transit New Zealand by Transport Engineering Research New Zealand Ltd", Auckland, New Zealand, 1999.

[43] M. El-Gindy and J.Y. Wong, “A Comparison of Various Computer Simulation Models for Predicting the Directional Responses of Articulated Vehicles”, Vehicle System Dynamics, 1987, 16: 249-268.

[44] Q. Wang, S. Zhu, and Y. He, “Model Reference Adaptive Control for Active Trailer Steering of Articulated Heavy Vehicles”, SAE Technical Paper 2015-01-1495, 2015, doi: 10.4271/2015-01-1495.

[45] A.M.C. Odhams, R. L. Roebuck, D. Cebon, and C.B. Winkler, “Dynamics Safety of Active Trailer Steering Systems”, J. Multi-body Dynamics, 2008, Vol. 222, pp. 367-380.

[46] C. Cheng and D. Cebon, “Improving Roll Stability of Articulated Heavy Vehicles Using Active Semi-Trailer Steering”, Vehicle System Dynamics, 2008, Vol. 46, pp. 373-388.

[47] P. Sweatman and B. Coleman, “Productivity Opportunities with Steerable Axles”, 7th International Symposium on Heavy Vehicle Weights & Dimensions Delft, the Netherlands, June 16-20, 2002.

[48] L. Palkovics and M. EI-Gindy, “Examination of Different Control Strategies of Heavy Vehicle Performance”, Journal of Dynamics Systems, Measurement, and Control, 1996 Vol. 118, pp. 489-498.

[49] K. Rangavajhla and H-S. J. Tsao, “Active Trailer Steering Control of An Articulated System with A Tractor and Three Full Trailers for Tractor-Tracking Following”, International Journal of Heavy Vehicle Systems, 2007, Vol, 14, pp. 271-293.

[50] L. Song, S. Mikaric, Q. Wang, and Y. He, “Driver-Software-in-the-Loop Real-Time Simulations for the Design of SUV Differential Braking Controllers”, Proceedings

of the Canadian Society for Mechanical Engineering International Congress, June 1-4, 2014, Toronto, Ontario, Canada.

[51] Y. He and Q. Wang, "Driver-Hardware/Software-in-the-Loop Real-Time Simulations for the Design of Active Trailer Steering Systems of Multi-Trailer Articulated Heavy Vehicles", Proceedings of the 12th International Symposium on Advanced Vehicle Control, September 22-26, 2014, Tokyo University of Agriculture and Technology, Tokyo, Japan.

[52] R. H. Byrne and C. T. Abdallah, "Design of A Model Reference Adaptive Controller for Vehicle Road Following", Journal of Mathematical Computer Modelling, 1995, Vol. 22(4-7), pp. 343-354.

[53] L.K. Chen and Y.A. Shieh, "Jackknife Prevention for Articulated Vehicles Using Model Reference Adaptive Control", Journal of Automobile Engineering, 2010, Vol. 25, pp. 28-42.

[54] J. Aurell and C.B. Winkler, "Standard Test Procedures for the Lateral Stability of Heavy Vehicle Combinations", Road Transport Technology. Vol. 4, University of Michigan Transportation Research Institution, Ann Arbor, 1995, pp. 463-471.

[55] J. Woodrooffe and P. Milliken, "Safety Analysis of A Double & Triple B-Train Carrying Loaded Containers", Report for Saskatchewan Highways and Transportation, Woodrooffe & Associates Incorporated; 2007.

[56] J. Edgar, "Development of Performance Standards for Australian Heavy Vehicles", Eighth International Symposium on Heavy Vehicle Weights and Dimensions, 14-18th March 2004, South Africa.

[57] International Standardization Organization, "Road Vehicles – Heavy Commercial Vehicle Combinations and Articulated Buses – Lateral Stability Test Methods", ISO-14791: 2000(E), Geneva: International Organization for Standardization; 2000.

[58] C.B. Winkler, P.S. Fancher, Z. Bareket, S. Bogard, etc. "Heavy Vehicle Size and Weight Test Procedures for Minimum Safety Performance", Final Technical Report to The National Highway Traffic Safety Administration Contract No. DTNH22-87-D-17174, April, 1992.

[59] P.S. Fancher and C.B. Winkler, "A Methodology for Measuring Rearward Amplification", Proceedings of the 3rd International Symposium on Heavy Vehicle Weights and Dimensions, Queens College, Cambridge, United Kingdom, 1992.

[60] J.P. Thomas and M. El-Gindy, "Path Compliance in Lane-Change Tests Designed to Evaluate Rearward Amplification", Road Transport Technology, University of Michigan Transportation Research Institution, Ann Arbor, 1995, Vol. 4, pp. 473-482.

[61] J. Woodrooffe and P. Milliken, "Safety Analysis of A Double & Triple B-Train Carrying Loaded Containers", Report for Saskatchewan Highways and Transportation, Woodrooffe & Associates Incorporated; 2007.

[62] M.M. Islam, X. Ding, and Y. He, "A Closed-Loop Dynamic Simulation Based Design Method for Articulated Heavy Vehicles with Active Trailer Steering Systems", Vehicle System Dynamics, 2012, Vol. 50, No. 5, pp. 675-697.

[63] M. Plochl and J. Edelmann, "Driver Models in Automobile Dynamics Application", Vehicle System Dynamics, 2007, 45(7-8): 699-741.

[64] K. Koibuchi, M. Yamamoto, Y. Fukada, and S. Inagaki, "Vehicle Stability Control in Limit Cornering by Active Brake", SAE Technical Paper, 960487, 1996.

[65] K. S. Narendra and A. M. Annaswamy, “Stable Adaptive Systems”, Prentice Hall, Englewood Cliffs, New Jersey, 1989.

Appendix

Appendix 1: Nomenclature and Parameter Values of DTAHV

Symbol	Paraphrase	Value
m_1	Tractor's total mass	$8258\ kg$
m_2	1st semitrailer's total mass	$22997\ kg$
m_3	2nd semitrailer's total mass	$22997\ kg$
m_{s1}	Tractor's sprung mass	$6308\ kg$
m_{s2}	1st semitrailer's sprung mass	$20927\ kg$
m_{s3}	2nd semitrailer's sprung mass	$20927\ kg$
U_1	Tractor's forward speed	m/s
U_2	1st semitrailer's forward speed	m/s
U_3	2nd semitrailer's forward speed	m/s
β_1	Tractor's side-slip angle	rad
β_2	1st semitrailer's side-slip angle	rad
β_3	2nd semitrailer's side-slip angle	rad
$\dot{\psi}_1$	Tractor's yaw rate	rad/s
$\dot{\psi}_2$	1st semitrailer's yaw rate	rad/s
$\dot{\psi}_3$	2nd semitrailer's yaw rate	rad/s
ϕ_1	Roll angle of tractor's sprung mass	rad

ϕ_2	Roll angle of 1st semitrailer's sprung mass	rad
ϕ_3	Roll angle of 2nd semitrailer's sprung mass	rad
δ_{1f}	Tractor front wheel steering angle	rad
h_{s1}	Height of CG of tractor sprung mass, measured upwards from ground	$1.019\ m$
h_{s2}	Height of CG of 1st semitrailer sprung mass, measured upwards from ground	$1.220\ m$
h_{s3}	Height of CG of 2nd semitrailer sprung mass, measured upwards from ground	$1.220\ m$
h_{r1}	Height of roll center of tractor sprung mass, measured upwards from ground	$0.475\ m$
h_{r2}	Height of roll center of 1st semitrailer sprung mass, measured upwards from ground	$0.705\ m$
h_{r3}	Height of roll center of 2nd semitrailer sprung mass, measured upwards from ground	$0.705\ m$
$Y_{\beta1}$	Partial derivative of tractor's net tire lateral force with respect to its side-slip angle	N/rad
$Y_{\beta2}$	Partial derivative of 1st semitrailer's net tire lateral force with respect to its side-slip angle	N/rad
$Y_{\beta3}$	Partial derivative of 2nd semitrailer's net tire lateral force with respect to its side-slip angle	N/rad

$Y_{\dot{\psi}_1}$	Partial derivative of tractor's net tire lateral force with respect to its yaw rate	Ns/rad
$Y_{\dot{\psi}_2}$	Partial derivative of 1st semitrailer's net tire lateral force with respect to its yaw rate	Ns/rad
$Y_{\dot{\psi}_3}$	Partial derivative of 2nd semitrailer's net tire lateral force with respect to its yaw rate	Ns/rad
$Y_{\delta 1f}$	Partial derivative of tractor's net tire lateral force with respect to its front wheel steering angle	N/rad
F_{y1}	Tractor's lateral tire force	N
F_{y2}	1st semitrailer's lateral tire force	N
F_{y3}	2nd semitrailer's lateral tire force	N
I_{xx1}	Roll moment of inertia of tractor sprung mass, measured form CG of sprung mass	6879 kgm^2
I_{xx2}	Roll moment of inertia of 1st semitrailer sprung mass, measured from CG of sprung mass	30416 kgm^2
I_{xx3}	Roll moment of inertia of 2nd semitrailer sprung mass, measured from CG of sprung mass	30416 kgm^2
I_{xz1}	Roll/yaw product of inertia of tractor sprung mass, measured from the CG of sprung mass	130 kgm^2
I_{xz2}	Roll/yaw product of inertia of 1st semitrailer sprung mass, measured from the CG of sprung mass	0

I_{xz3}	Roll/yaw product of inertia of 2nd semitrailer sprung mass, measured from the CG of sprung mass	0
I_{zz1}	Yaw moment of inertia of whole mass of the tractor	$19665\ kgm^2$
I_{zz2}	Yaw moment of inertia of whole mass of the 1st semitrailer	$439992\ kgm^2$
I_{zz3}	Yaw moment of inertia of whole mass of the 2nd semitrailer	$439992\ kgm^2$
$N_{\beta 1}$	Partial derivative of tractor's net tire yaw moment with respect to its side-slip angle	Nm/rad
$N_{\beta 2}$	Partial derivative of 1st semitrailer's net tire yaw moment with respect to its side-slip angle	Nm/rad
$N_{\beta 3}$	Partial derivative of 2nd semitrailer's net tire yaw moment with respect to its side-slip angle	Nm/rad
$N_{\dot{\psi} 1}$	Partial derivative of tractor's net tire yaw moment with respect to its yaw rate	Nms/rad
$N_{\dot{\psi} 2}$	Partial derivative of 1st semitrailer's net tire yaw moment with respect to its yaw rate	Nms/rad
$N_{\dot{\psi} 3}$	Partial derivative of 2nd semitrailer's net tire yaw moment with respect to its yaw rate	Nms/rad
$N_{\delta 1f}$	Partial derivative of tractor's net tire yaw moment with respect to its front wheel steering angle	Nm/rad

l_{c1}	Longitudinal distance between the whole mass CG of the tractor and the coupling point	4.251 m
l_{c21}	Longitudinal distance between the whole mass CG of the 1st semitrailer and the 1st coupling joint	5.500 m
l_{c22}	Longitudinal distance between the whole mass CG of the 1st semitrailer and the 2nd coupling joint	7.070 m
l_{c3}	Longitudinal distance between the whole mass CG of the 2nd semitrailer and the 2nd coupling joint	5.500 m
K_{f1}	Roll stiffness of front suspension of the tractor, adjusted with the tire vertical stiffness	700000 Nm/rad
K_{r1}	Roll stiffness of rear suspension of the tractor, adjusted with the tire vertical stiffness	1100000 Nm/rad
K_{r2}	Roll stiffness of rear suspension of the 1st semitrailer, adjusted with the tire vertical stiffness	2000000 Nm/rad
K_{r3}	Roll stiffness of rear suspension of the 2nd semitrailer, adjusted with the tire vertical stiffness	2200000 Nm/rad
K_{tf1}	Tire roll stiffness of front axle of tractor	900000 Nm
K_{tr1}	Tire roll stiffness of rear axle set of tractor	1500000 Nm
K_{tr2}	Tire roll stiffness of rear axle set of 1st semitrailer	6000000 Nm
K_{tr3}	Tire roll stiffness of rear axle set of 2nd semitrailer	5200000 Nm
K_{12}	Roll stiffness of coupling point of tractor and 1st semitrailer	550000 Nm
K_{23}	Roll stiffness of coupling point of tractor and 2nd semitrailer	550000 Nm

ϕ_{t1}	Roll angle of tractor's un-sprung mass	rad
ϕ_{t2}	Roll angle of 1st semitrailer's un-sprung mass	rad
ϕ_{t3}	Roll angle of 2nd semitrailer's un-sprung mass	rad
L_{f1}	Roll damping of front suspension of tractor	50000 Nms/rad
L_{r1}	Roll damping of rear suspension of tractor	80000 Nms/rad
L_{r2}	Roll damping of rear suspension of 1st semitrailer	120000 Nms/rad
L_{r3}	Roll damping of rear suspension of 2nd semitrailer	120000 Nms/rad
h_{cr1}	Height of the coupling point on the tractor, measured upwards from roll center of tractor sprung mass	0.625 m
h_{cr2}	Height of the coupling point on 1st semitrailer, measured upwards from roll center of semitrailer sprung mass	0.395 m
h_{cr3}	Height of the coupling point on 2nd semitrailer, measured upwards from roll center of semitrailer sprung mass	0.395 m

Appendix 2: System Matrices of DTAHV

$\mathbf{M} \in \mathbf{R}^{18\times18}$, $\mathbf{N} \in \mathbf{R}^{18\times18}$, $\mathbf{Q} \in \mathbf{R}^{18\times1}$, $\mathbf{T} \in \mathbf{R}^{18\times6}$. The nonzero entries of these matrices are given:

$M(1,2) = I_{xz1} - l_{c1}m_{s1}(h_{s1} - h_{r1})$

$M(1,3) = -l_{c1}m_1U_1$

$M(1,4) = -I_{zz1}$

$M(2,1) = L_{f1} + L_{r1}$

$M(2,2) = I_{xx1} + m_{s1}(h_{s1} - h_{r1})^2 - h_{cr1}m_{s1}(h_{s1} - h_{r1})$

$M(2,3) = m_{s1}U_1(h_{s1} - h_{r1}) - h_{cr1}m_1U_1$

$M(2,4) = -I_{xz1}$

$M(2,13) = -\left(L_{f1} + L_{r1}\right)$

$M(3,1) = L_{f1} + L_{r1}$

$M(3,3) = -m_{u1}U_1(h_{u1} - h_{r1})$

$M(3,4) = I_{xzt1}$

$M(3,13) = -\left(L_{f1} + L_{r1}\right)$

$M(3,14) = -I_{xxt1} - m_{u1}(h_{u1} - h_{r1})^2$

$M(4,2) = m_{s1}(h_{s1} - h_{r1})$

$M(4,3) = m_1U_1$

$$M(4,6) = m_{s2}(h_{s2} - h_{r2})$$

$$M(4,7) = m_2 U_2$$

$$M(4,10) = m_{s3}(h_{s3} - h_{r3})$$

$$M(4,11) = m_3 U_3$$

$$M(5,2) = l_{c21} m_{s1}(h_{s1} - h_{r1})$$

$$M(5,3) = l_{c21} m_1 U_1$$

$$M(5,6) = -I_{xz2}$$

$$M(5,8) = -I_{zz2}$$

$$M(5,10) = -l_{c22} m_{s3}(h_{s3} - h_{r3})$$

$$M(5,11) = -l_{c22} m_3 U_3$$

$$M(6,2) = h_{cr2} m_{s1}(h_{s1} - h_{r1})$$

$$M(6,3) = h_{cr2} m_1 U_1$$

$$M(6,5) = L_{r2}$$

$$M(6,6) = I_{xx2} + m_{s2}(h_{s2} - h_{r2})^2$$

$$M(6,7) = m_{s2} U_2 (h_{s2} - h_{r2})$$

$$M(6,8) = -I_{xz2}$$

$$M(6,10) = h_{cr3} m_{s3}(h_{s3} - h_{r3})$$

$$M(6,11) = h_{cr3} m_3 U_3$$

$$M(6,15) = -L_{r2}$$

$$M(7,5) = L_{r2}$$

$$M(7,7) = -m_{u2}U_2(h_{u2} - h_{r2})$$

$$M(7,8) = I_{xzt2}$$

$$M(7,15) = -L_{r2}$$

$$M(7,16) = -I_{xxt2} - m_{u2}(h_{u2} - h_{r2})^2$$

$$M(8,10) = l_{c3}m_{s3}(h_{s3} - h_{r3}) + I_{xz3}$$

$$M(8,11) = l_{c3}m_3U_3$$

$$M(8,12) = -I_{zz3}$$

$$M(9,9) = L_{r3}$$

$$M(9,10) = I_{xx3} + m_{s3}(h_{s3} - h_{r3})^2 - h_{cr3}m_{s3}(h_{s3} - h_{r3})$$

$$M(9,11) = m_{s3}U_3(h_{s3} - h_{r3}) - h_{cr3}m_3U_3$$

$$M(9,12) = -I_{xz3}$$

$$M(9,17) = -L_{r3}$$

$$M(10,9) = -L_{r3}$$

$$M(10,11) = m_{u3}U_3(h_{u3} - h_{r3})$$

$$M(10,12) = -I_{xzt3}$$

$$M(10,17) = L_{r3}$$

$$M(10,18) = I_{xxt3} + m_{u3}(h_{u3} - h_{r3})^2$$

$$M(11,2) = h_{cr1}$$

$$M(11,3) = U$$

$$M(11,4) = -l_{c1}$$

$$M(11,6) = -h_{cr2}$$

$$M(11,7) = -U$$

$$M(11,8) = -l_{c21}$$

$$M(12,6) = h_{cr2}$$

$$M(12,7) = U$$

$$M(12,8) = -l_{c22}$$

$$M(12,10) = -h_{cr3}$$

$$M(12,11) = -U$$

$$M(12,12) = -l_{c3}$$

$$N(1,3) = N_{\beta_1} + l_{c1}Y_{\beta_1}$$

$$N(1,4) = N_{\dot{\psi}_1} + l_{c1}Y_{\dot{\psi}_1} - l_{c1}m_1U_1$$

$$N(2,1) = \left(K_{f1} + K_{r1} + K_{12}\right) - m_{s1}g(h_{s1} - h_{r1})$$

$$M(2,3) = h_{cr1}Y_{\beta_1}$$

$$N(2,4) = m_{s1}U_1(h_{s1} - h_{r1}) + h_{cr1}Y_{\dot{\psi}_1} - h_{cr1}m_1U_1$$

$$N(2,5) = -K_{12}$$

$$N(2,13) = -\left(K_{f1} + K_{r1}\right)$$

$$N(3,1) = K_{f1} + K_{r1}$$

$$N(3,3) = -h_{r1}Y_{\beta_1}$$

$$N(3,4) = -h_{r1}Y_{\dot{\psi}_1} - m_{u1}U_1(h_{u1} - h_{r1})$$

$$N(3,13) = m_{u1}g(h_{u1} - h_{r1}) - \left(K_{f1} + K_{r1}\right) - \left(K_{tf1} + K_{tr1}\right)$$

$$N(4,3) = -Y_{\beta_1}$$

$$N(4,4) = m_1U_1 - Y_{\dot{\psi}_1}$$

$$N(4,7) = -Y_{\beta_2}$$

$$N(4,8) = m_2U_2 - Y_{\dot{\psi}_2}$$

$$N(4,11) = -Y_{\beta_3}$$

$$N(4,12) = m_3U_3 - Y_{\dot{\psi}_3}$$

$$N(5,3) = -l_{c21}Y_{\beta_1}$$

$$N(5,4) = l_{c21}m_1U_1 - l_{c21}Y_{\dot{\psi}_1}$$

$$N(5,7) = -N_{\beta_2}$$

$$N(5,8) = -N_{\dot{\psi}_2}$$

$$N(5,11) = l_{c22}Y_{\beta_3}$$

$$N(5,12) = l_{c22}Y_{\dot{\psi}_3} - l_{c22}m_3U_3$$

$$N(6,1) = -K_{12}$$

$$N(6,3) = -h_{cr2}Y_{\beta_1}$$

$$N(6,4) = h_{cr2}m_1U_1 - h_{cr2}Y_{\dot{\psi}_1}$$

$$N(6,5) = K_{r2} + K_{12} + K_{23} - m_{s2}g(h_{s2} - h_{r2})$$

$$N(6,8) = m_{s2}U_2(h_{s2} - h_{r2})$$

$$N(6,9) = -K_{23}$$

$$N(6,11) = -h_{cr3}Y_{\beta_3}$$

$$N(6,12) = h_{cr3}m_3U_3 - h_{cr3}Y_{\dot{\psi}_3}$$

$$N(6,15) = -K_{r2}$$

$$N(7,5) = K_{r2}$$

$$N(7,7) = -h_{r2}Y_{\beta_2}$$

$$N(7,8) = -m_{u2}U_2(h_{u2} - h_{r2}) - h_{r2}Y_{\dot{\psi}_2}$$

$$N(7,15) = m_{u2}g(h_{u2} - h_{r2}) - (K_{r2} + K_{tr2})$$

$$N(8,11) = N_{\beta_3} - l_{c3}Y_{\beta_3}$$

$$N(8,12) = l_{c3}m_3U_3 + N_{\dot{\psi}_3} - l_{c3}Y_{\dot{\psi}_3}$$

$$N(9,5) = -K_{23}$$

$$N(9,9) = K_{23} + K_{r3} - m_{s3}g(h_{s3} - h_{r3})$$

$$N(9,11) = h_{cr3}Y_{\beta_3}$$

$$N(9,12) = m_{s3}U_3(h_{s3} - h_{r3}) + h_{cr3}Y_{\dot{\psi}_3} - h_{cr3}m_3U_3$$

$$N(9,17) = -K_{r3}$$

$$N(10,9) = -K_{r3}$$

$$N(10,11) = h_{r3}Y_{\beta_3}$$

$$N(10,12) = m_{u3}U_3(h_{u3} - h_{r3}) + h_{r3}Y_{\dot{\psi}_3}$$

$$N(10,17) = K_{r3} + K_{tr3} - m_{u3}g(h_{u3} - h_{r3})$$

$$N(11,4) = U$$

$$N(11,8) = -U$$

$$N(12,8) = U$$

$$N(12,12) = -U$$

$$Q(1,1) = N_{\delta_{1f}} + l_{c1}Y_{\delta_{1f}}$$

$$Q(2,1) = h_{cr1}Y_{\delta_{1f}}$$

$$Q(3,1) = -h_{r1}Y_{\delta_{1f}}$$

$$Q(4,1) = -Y_{\delta_{1f}}$$

$$Q(5,1) = -l_{c21}Y_{\delta_{1f}}$$

$$Q(6,1) = -h_{cr2}Y_{\delta_{1f}}$$

$$T(4,1) = -Y_{\delta_{2f}}$$

$$T(4,2) = -Y_{\delta_{2m}}$$

$$T(4,3) = -Y_{\delta_{2r}}$$

$$T(4,4) = -Y_{\delta_{3f}}$$

$$T(4,5) = -Y_{\delta_{3m}}$$

$$T(4,6) = -Y_{\delta_{3r}}$$

$$T(5,1) = -N_{\delta_{2f}}$$

$$T(5,2) = -N_{\delta_{2m}}$$

$$T(5,3) = -N_{\delta_{2r}}$$

$$T(5,4) = l_{c22} Y_{\delta_{3f}}$$

$$T(5,5) = l_{c22} Y_{\delta_{3m}}$$

$$T(5,6) = l_{c22} Y_{\delta_{3r}}$$

$$T(6,4) = -h_{cr3} Y_{\delta_{3f}}$$

$$T(6,5) = -h_{cr3} Y_{\delta_{3m}}$$

$$T(6,6) = -h_{cr3} Y_{\delta_{3r}}$$

$$T(7,1) = -h_{r2} Y_{\delta_{2f}}$$

$$T(7,2) = -h_{r2} Y_{\delta_{2m}}$$

$$T(7,3) = -h_{r2} Y_{\delta_{2r}}$$

$$T(8,4) = N_{\delta_{3f}} - l_{c3} Y_{\delta_{3f}}$$

$$T(8,5) = N_{\delta_{3m}} - l_{c3} Y_{\delta_{3m}}$$

$$T(8,6) = N_{\delta_{3r}} - l_{c3} Y_{\delta_{3r}}$$

$$T(9,4) = h_{cr3} Y_{\delta_{3f}}$$

$$T(9,5) = h_{cr3} Y_{\delta_{3m}}$$

$$T(9,6) = h_{cr3} Y_{\delta_{3r}}$$

$$T(10,4) = h_{r3} Y_{\delta_{3f}}$$

$$T(10,5) = h_{r3} Y_{\delta_{3m}}$$

Appendix 3: Nomenclature and Parameter Values for STAHV

Parameter	Paraphrase	Value
α_1	Sideslip angle of tires on the 1st axle	rad
α_2	Sideslip angle of tires on the 2nd axle	rad
α_3	Sideslip angle of tires on the 3rd axle (group)	rad
β_1	Tractor CG sideslip angle	rad
β_2	Semitrailer CG sideslip angle	rad
δ_{1f}	Scaled tractor front wheel steering angle	rad
δ_3	Scaled semitrailer rear wheel steering angle	rad
ψ_1	Tractor CG yaw angle	rad/s
ψ_2	Semitrailer CG yaw angle	rad/s
U_1	Tractor's forward velocity	m/s
a_{11}	Longitudinal distance between tractor front axle and tractor total mass CG	$1.115\ m$
b_{12}	Longitudinal distance between tractor rear axle and tractor total mass CG	$2.585\ m$
b_{23}	Longitudinal distance between trailer total mass CG and trailer middle axle	$2.047\ m$
C_{f11}	Cornering stiffness of tractor front tire	$419950\ N/rad$
C_{r12}	Cornering stiffness of tractor rear tire	$1697450\ N/rad$

C_{r23}	Cornering stiffness of semitrailer tire	2302160 N/rad
I_{zz1}	Moment of inertia of tractor total mass	20616 kgm^2
I_{zz2}	Moment of inertia of trailer total mass	238270 kgm^2
l_{c1}	Longitudinal distance between tractor total mass CG and fifth wheel	1.959 m
l_{c21}	Longitudinal distance between trailer total mass CG and fifth wheel	5.653 m
m_1	Tractor total mass	6525 kg
m_2	Trailer total mass	33221 kg

Appendix 4: System Matrices of STAHV

The non-zero elements of matrices are listed below.

$$M(1,1) = -m_2(l_{c1} + l_{c21})$$

$$M(1,2) = -m_2 l_{c21}$$

$$M(1,3) = (m_1 + m_2)U_1$$

$$M(2,1) = I_{zz1} + m_2 l_{c1}(l_{c1} + l_{c21})$$

$$M(2,2) = m_2 l_{c1} l_{c21}$$

$$M(2,3) = -m_2 l_{c1} U_1$$

$$M(3,1) = I_{zz2} + m_2 l_{c1}(l_{c1} + l_{c21})$$

$$M(3,2) = I_{zz2} + m_2 l_{c21}^2$$

$$M(3,3) = -m_2 l_{c21} U_1$$

$$M(4,4) = 1$$

$$P(1,1) = \frac{(l_{c21} + b_{23} + l_{c1})C_{r23} - C_{f11}a_{11} + C_{r12}b_{12}}{U_1} - (m_1 + m_2)U_1$$

$$P(1,2) = \frac{(l_{c21} + b_{23})C_{r23}}{U_1}$$

$$P(1,3) = -\left(C_{f11} + C_{r12} + C_{r23}\right)$$

$$P(1,4) = C_{r23}$$

$$P(2,1) = m_2 l_{c1} U_1 - \frac{(l_{c1} + b_{23} + l_{c21})C_{r23} l_{c1} + C_{f11}a_{11}^2 + C_{r12}b_{12}^2}{U_1}$$

$$P(2,2) = -\frac{(l_{c21} + b_{23})C_{r23}l_{c1}}{U_1}$$

$$P(2,3) = C_{r12}b_{12} - C_{f11}a_{11} + C_{r23}l_{c1}$$

$$P(2,4) = -C_{r23}l_{c1}$$

$$P(3,1) = m_2 l_{c21}U_1 - \frac{(l_{c21} + b_{23} + l_{c1})C_{r23}(l_{c21} + b_{23})}{U_1}$$

$$P(3,2) = -\frac{(l_{c21} + b_{23})^2 C_{r23}}{U_1}$$

$$P(3,3) = (l_{c21} + b_{23})C_{r23}$$

$$P(3,4) = -(l_{c21} + b_{23})C_{r23}$$

$$P(4,2) = 1$$

$$H_1 = \begin{bmatrix} C_{r23} \\ -C_{r23}l_{c1} \\ -C_{r23}(l_{c21} + b_{23}) \\ 0 \end{bmatrix}$$

$$H_2 = \begin{bmatrix} C_{f11} \\ C_{f11}a_{11} \\ 0 \\ 0 \end{bmatrix}$$

$$C = \left[-(l_{c21} + l_{c1})A(1,:) - l_{c21}A(2,:) + U_1 A(3,:) + [U_1, 0, 0, 0]\right]$$

$$D_1 = [-(l_{c21} + l_{c1})B_1(1,:) - l_{c21}B_1(2,:) + U_1 B_1(3,:)]$$

$$D_2 = [-(l_{c21} + l_{c1})B_2(1,:) - l_{c21}B_2(2,:) + U_1 B_2(3,:)]$$

$$A_{mn}(1,1) = A_1 + B_1\theta_0^*(1 - D_1\theta_0^*)^{-1}D_1$$

$$A_{mn}(1,2) = B_1\theta_1^{*T} + B_1\theta_0^*(1 - D_1\theta_0^*)^{-1}D_1\theta_1^{*T}$$

$$A_{mn}(1,3) = B_1\theta_2^{*T} + B_1\theta_0^*(1 - D_1\theta_0^*)^{-1}D_1\theta_2^{*T}$$

$$A_{mn}(2,1) = \iota\theta_0^*(1 - D_1\theta_0^*)^{-1}C_1$$

$$A_{mn}(2,2) = \Lambda + \iota\theta_1^{*T} + \iota\theta_0^*(1 - D_1\theta_0^*)^{-1}D_1\theta_1^{*T}$$

$$A_{mn}(2,3) = \iota\theta_2^{*T} + \iota\theta_0^*(1 - D_1\theta_0^*)^{-1}D_1\theta_2^{*T}$$

$$A_{mn}(3,1) = \iota(1 - D_1\theta_0^*)^{-1}C_1$$

$$A_{mn}(3,2) = \iota(1 - D_1\theta_0^*)^{-1}D_1\theta_1^{*T}$$

$$A_{mn}(3,3) = \Lambda + \iota(1 - D_1\theta_0^*)^{-1}D_1\theta_2^{*T}$$

$$B_{mn1}(1,1) = B_1 + B_1\theta_0^*(1 - D_1\theta_0^*)^{-1}D_1$$

$$B_{mn1}(2,1) = \iota + \iota\theta_0^*(1 - D_1\theta_0^*)^{-1}D_1$$

$$B_{mn1}(3,1) = \iota(1 - D_1\theta_0^*)^{-1}D_1$$

$$B_{mn2}(1,1) = B_2 + B_1\theta_0^*(1 - D_1\theta_0^*)^{-1}D_2$$

$$B_{mn2}(2,1) = \iota\theta_0^*(1 - D_1\theta_0^*)^{-1}D_2$$

$$B_{mn2}(3,1) = \iota(1 - D_1\theta_0^*)^{-1}D_2$$

$$C_{mn}(1,1) = (1 - D_1\theta_0^*)^{-1}C_1$$

$$C_{mn}(1,2) = (1 - D_1\theta_0^*)^{-1}D_1\theta_1^{*T}$$

$$C_{mn}(1,3) = (1 - D_1\theta_0^*)^{-1}D_1\theta_2^{*T}$$

$$D_{mn1} = (1 - D_1\theta_0^*)^{-1}$$

$$D_{mn2} = (1 - D_1\theta_0^*)^{-1}D_2$$